

Alma Mater Studiorum - Università di Bologna

DEI - DIPARTIMENTO DI INGEGNERIA DELL'ENERGIA ELETTRICA E
DELL'INFORMAZIONE

Dottorato di Ricerca in Ingegneria Elettronica, delle Telecomunicazioni e
Tecnologie dell'Informazione

XXVIII Ciclo

Settore Concorsuale: 09/F2 - Telecomunicazioni

Settore Scientifico Disciplinare: ING-INF/03

**Wireless Techniques for Body-Centric Cooperative
Communications**

Tesi di:

Stefan Mijovic

Coordinatore:

Chiar.mo Prof. Ing. **Alessandro Vanelli-Coralli**

Relatori:

Chiar.mo Prof. Ing. **Roberto Verdone**

Dott. Ing. **Chiara Buratti**

Esame anno finale 2016

*"If we knew what it was we were doing,
it would not be called research, would it?"*

Albert Einstein

Table of Contents

Table of Contents	iii
Abstract	vii
List of Acronyms	ix
List of Figures	xv
List of Tables	xix
Introduction	1
Wireless Body Area Networks Concept	1
Cooperative Communications Paradigm	3
Structure and Contribution of the Thesis	4
1 Communication Protocols for Wireless Body Area Networks	7
1.1 Introduction	7
1.1.1 Related Works	9
1.1.2 Thesis Contribution	12
1.2 Standard Solutions for WBAN	13
1.2.1 IEEE 802.15.4 Standard	14
1.2.2 IEEE 802.15.6 Standard	18
1.3 Reference Scenario: WiserBAN Project	23
1.3.1 Use Cases and Requirements	25
1.3.2 System Architecture	26
1.4 MAC Design for WBANs	29
1.4.1 Superframe-based MAC	29

Contents

1.4.2	Low Power Listening MAC	35
1.5	Performance Evaluation	38
1.5.1	Study Methodology	38
1.5.2	Experimental Results	47
1.6	Conclusions	62
2	Cooperative Communications in Wireless Body Area Networks	63
2.1	Introduction	63
2.1.1	Related Works	65
2.1.2	Thesis Contribution	67
2.2	Reference Scenario and Channel Model	68
2.3	Communication Protocol	69
2.4	Problem Statement	73
2.5	B-MIMO	75
2.6	Scheduling algorithms	75
2.7	Numerical results	77
2.7.1	Performance Metrics	78
2.7.2	The Impact of the Threshold χ	79
2.7.3	B-MIMO versus non-cooperative system	81
2.7.4	B-MIMO versus Cooperative MIMO	81
2.8	Conclusions	86
3	Cooperative Communications in Wireless Sensor Networks	89
3.1	Introduction	89
3.1.1	Related Works	90
3.1.2	Thesis Contribution	91
3.2	Reference Scenario	93
3.2.1	Channel Model	93
3.2.2	Signal Model	95
3.2.3	Pilot-based Estimation of Precoding Coefficients	96
3.2.4	Synchronisation Error	98
3.3	Problem Statement	99
3.4	Single-cluster Scenario	101
3.4.1	Energy Efficiency	101
3.4.2	Analysis and Optimisation	102
3.4.3	Numerical Results	106
3.5	Multi-cluster Scenario	113
3.5.1	Wyner Model	113
3.5.2	Energy Efficiency	114

3.5.3	Analysis and Optimisation	116
3.5.4	Numerical Results	118
3.6	Conclusions	122
	Conclusions and Future Work	125
	Bibliography	129
	Publications	139
	Acknowledgements	143

Abstract

Body-centric and *cooperative* communications are new trends in telecommunications field. Being concerned with human behaviour, *body-centric* communication networks, also known as Wireless Body Area Networks (WBANs), are suitable for a wide variety of applications. The advances in the miniaturisation of embedded devices to be placed on or around the body, foster the diffusion of these systems, where the human body is the key element defining communication characteristics. *Cooperative* communications paradigm, on the other hand, is one of the emerging technologies that promises significantly higher reliability and spectral efficiency in wireless networks.

This thesis investigates possible applications of the *cooperative* communication paradigm to *body-centric* networks and, more generally, to Wireless Sensor Networks (WSNs). Firstly, communication protocols for WBANs are in the spotlight. Performance achieved by different approaches is evaluated and compared through experimentation providing guidelines for choosing appropriate protocol and setting protocol parameters to meet application requirements. Secondly, a cooperative Multiple Input Multiple Output (MIMO) scheme for WBANs is presented. The scheme, named B-MIMO, exploits the natural heterogeneity of the WBAN propagation channel to improve energy efficiency of the system. Finally, a WSN scenario is considered, where sensor nodes cooperate to establish a massive MIMO-like system. The analysis and subsequent optimisation show the advantages of cooperation in terms of energy efficiency and provide insights on how many nodes should be deployed in such a scenario.

List of Acronyms

ACK Acknowledgement

ADC Analot to Digital Converter

APP Application

BAN Body Area Network

BC Backoff Counter

BE Backoff Exponent

BER Bit Error Rate

BLER Block Error Rate

BO Backoff Interval

BP Backoff Period

BPSK Binary Phase Shift Keying

BSN Body Sensor Network

List of Acronyms

B-MIMO BAN Multiple Input Multiple Output

CAP Contention Access Period

CDF Cummulative Distribution Function

CFP Contention Free Period

CMOS Complementary Metal-Oxide Semiconductor

CSEM Centre Suisse d'Electronique et de Microtechnique

CSI Channel State Information

CSIR Channel State Information at the Receiver

CSIT Channel State Information at the Transmitter

CSMA Carrier Sensing Multiple Access

CSMA/CA Carrier Sensing Multiple Access with Collision Avoidance

CW Contention Window

DAC Digital to Analog Converter

DBPSK Differential Binary Phase Shift Keying

DC Direct Current

DQPSK Differential Quadrature Phase Shift Keying

DSP Digital Signal Processor

DS-SS Direct Sequence Spread Spectrum

- EAP** Exclusive Access Phase
- ED** End Device
- EE** Energy Efficiency
- FFD** Full Function Device
- GMSK** Gaussian Minimum Shift Keying
- GTS** Guaranteed Time Slot
- HBC** Human Body Communication
- IC** Integrated Circuit
- IEEE** Institute of Electrical and Electronics Engineers
- IETF** Internet Engineering Task Force
- IoT** Internet of Things
- ISM** Industrial Scientific Medical
- LE** Low Energy
- LLC** Logical Link Control
- LPL** Low Power Listening
- MAC** Medium Access Control
- MAP** Managed Access Phase
- MEMS** Micro Electro Mechanical Systems

List of Acronyms

MICS Medical Implant Communication Service

MIMO Multiple Input Multiple Output

MISO Multiple Input Single Output

MSK Minimum Shift Keying

NB Number of Backoffs

NC Network Coordinator

NET Network

OFDM Orthogonal Frequency Division Multiplexing

O-QPSK Offset Quadrature Phase Shift Keying

OSI Open System Interconnection

PAN Personal Area Network

PER Packet Error Rate

PHY Physical

PLR Packet Loss Rate

PSDU Physical layer Service Data Unit

pSIFS Short Inter Frame Space

P2P Point-to-Point

QoS Quality of Service

RAP	Random Access Phase
RC	Remote Control
RF	Radio Frequency
RFD	Reduced Function Device
RISC	Reduced Instruction Set Computing
RTX	Retransmission
RX	Receiver
SAR	Specific Absorption Rate
SC	Smart City
SF	Superframe
SIMO	Single Input Multiple Output
SINR	Signal to Interference and Noise Ratio
SiP	System in Package
SIR	Signal to Interference Ratio
SISO	Single Input Single Output
SNR	Signal to Noise Ratio
SoC	System on Chip
SPI	Serial Peripheral Interface

List of Acronyms

STBC Space-Time Block Code

STC Space-Time Code

TDD Time Division Duplex

TDMA Time Division Multiple Access

TX Transmitter

UP User Priority

UWB Ultra Wide Band

VAA Virtual Antenna Array

V-MIMO Virtual Multiple Input Multiple Output

WBAN Wireless Body Area Network

WBSN Wireless Body Sensor Network

WMTS Wireless Medical Telemetry Service

WPAN Wireless Personal Area Network

WSN Wireless Sensor Network

ZF Zero Forcing

List of Figures

1.1	OSI model.	8
1.2	Spectrum allocation IEEE 802.15.4 standard.	16
1.3	IEEE 802.15.4 superframe structure.	17
1.4	Spectrum allocation IEEE 802.15.6 standard.	19
1.5	IEEE 802.15.6 superframe structure for beacon mode access.	21
1.6	WiserBAN scenario.	25
1.7	WiserBAN protocol stack.	27
1.8	WiserBAN protocol frame format.	27
1.9	WiserBAN superframe structure	31
1.10	IEEE 802.15.4 CSMA/CA algorithm flowchart.	32
1.11	IEEE 802.15.6 CSMA/CA algorithm flowchart.	34
1.12	IEEE 802.15.6 Slotted ALOHA algorithm flowchart.	35
1.13	Low Power Listening protocol.	36
1.14	Traffic generation types.	41
1.15	Energy consumption measurement setup.	46
1.16	Average packet delay, 'on body' and 'on table' measurements.	48

List of Figures

1.17	Average energy consumed varying T_W	49
1.18	Average packet delay varying T_W	50
1.19	Average energy consumed varying T_{on}	51
1.20	Network throughput in different star topologies.	52
1.21	Average delay for a heterogeneous UP network.	54
1.22	Average delay for different network sizes, all the nodes with the same UP.	55
1.23	Average delay for a three nodes-network with the same UP.	56
1.24	PLR for a three nodes-network with the same UP.	56
1.25	Network throughput for different RTX.	57
1.26	Average energy consumption per hour for SF and LPL MAC.	59
1.27	Time spent in different radio states for SF-based and LPL MAC.	59
1.28	Node lifetime for SF-based and LPL MAC.	60
2.1	Scenario 3D.	69
2.2	Scenario 2D.	69
2.3	CDF of SNR for nodes placed in different positions on body.	74
2.4	Scheduling scheme - example of <i>round robin</i>	77
2.5	Energy efficiency as a function of the threshold χ	80
2.6	Energy efficiency of B-MIMO and the non-cooperative system.	82
2.7	Throughput of B-MIMO and the non-cooperative system.	82
2.8	BLER for different scheduling algorithms and cooperation schemes.	84
2.9	Energy efficiency of different scheduling algorithms and cooperation schemes.	84

2.10 BLER for different scheduling algorithms and cooperation schemes in interference-limited scenario.	86
3.1 Time division duplex protocol.	93
3.2 Scenario.	94
3.3 Symmetric scenario setting.	105
3.4 Energy efficiency as a function of N for $\tau = 5$	107
3.5 Energy efficiency as a function of τ for $N = 30$	108
3.6 Optimal number of sensor nodes, N^* as a function of K	111
3.7 Energy efficiency achieved by N_{sim}^* and N_{as}^* , as a function of K	112
3.8 Wyner model.	114
3.9 Energy efficiency vs. N for $K = 3$ and $\alpha = 0, 0.5$ and 1	119
3.10 EE-optimal value of sensor nodes N^* vs. α for $K = 1, 3$ and 5	120
3.11 Energy efficiency vs. N , for $\alpha = 0.5$ and different K and t_{max}	121

List of Tables

1.1	Radio states power	46
1.2	Average energy consumption of transmitter for 'on table' and 'on body' scenario	48
1.3	Average number of preambles sent before data packet.	51
1.4	Average and maximum packet delay.	53
1.5	Parameters of SF-based and LPL MAC	58
1.6	Delay of SF-based and LPL MAC.	61
2.1	Simulation parameters.	78
2.2	BLER for different values of parameter χ	80
3.1	Single-cluster scenario simulation parameters.	109
3.2	Multi-cluster scenario simulation parameters	118

Introduction

This thesis focuses on the paradigms of *body-centric* and *cooperative* communications, whose concepts are presented in next sections, along with the motivations supporting the study performed and the research approach followed. The PhD study was conducted at the Department of Electrical, Electronic and Information Engineering "Guglielmo Marconi" (DEI), University of Bologna, Italy. Part of the research (Chapter 3) reported in this thesis was done in collaboration with Prof. Mérouane Debbah and Prof. Luca Sanguinetti of CentraleSupélec, Gif-sur-Yvette, France. Most of the research activities were performed within frameworks of the European Commission-funded FP7 projects WiserBAN [1] and Newcom# [2].

Wireless Body Area Networks Concept

The increasing use of wireless networks and the constant miniaturisation of electrical devices have empowered the development of Wireless Body Area Networks (WBANs) [3]. WBANs (also called Body Area Network (BAN) and Body Sensor Networks (BSNs)) are composed of wearable and implantable sensors and/or actuators, capable of communicating among them and with external devices through radio

Introduction

interfaces, to monitor physiological signals collected from a human body. A WBAN can be defined as a collection of low-power, miniaturised, invasive or non-invasive, lightweight devices with wireless communication capabilities that operate in the proximity of a human body [4]. On one hand, WBANs enable new applications and thus new possible markets with respect to Wireless Personal Area Networks (WPANs) and WSNs, while, on the other hand, the design is affected by several constraints which call for new paradigms and protocols. With respect to WSNs, the presence of the human body affects the radio wave propagation, leading to a specific and peculiar radio channel, which has to be properly accounted for in the design of protocols [5]. The diversity of envisioned applications, which span from the medical field (vital signs monitoring, automatic drug delivery) to the entertainment, gaming and ambient intelligence sectors, creates a set of technical requirements with a wide variation in terms of expected performance metrics (e.g., throughput or delay). Therefore, scalable and flexible architectures and protocols are needed.

The requirements for achieving a nearly invisible WBAN radio microsystem are:

- *the sensor nodes must be ultra-miniature*, e.g. fit within very tiny/thin housings such as miniature hearing aids, cardiac implants, insulin pumps, cochlear implants,
- *the wireless link must be ultra low-power*, for use in lifestyle and biomedical applications, using tiny power sources,
- *the antenna and radio must adapt to around-the-body propagation losses* due to various node placements on or in the body, but also variable conditions due to moving parts,

- *the node must include high performance data-processing capability*, which is needed to process, fusion the sensor data coming from many sensors placed around the body, and extract the relevant features for further transmission,
- *the communication protocol must be very versatile* such that it can satisfy a wide range of application requirements corresponding to different application fields.

Current available solutions addressing the increasing demand for WBAN specific solutions are using non-specific WPAN solutions. These WPANs, which are typified by Bluetooth or ZigBee wireless solutions, enable the realisation of proto-WBAN solutions that allow basic WBAN system realisations, but present major limitations in terms of power consumption and size.

Since the introduction of the WBAN concept, there were several attempts to standardise various aspects of WBANs but no standard has managed to satisfy the ever-expanding application requirements. The novelty and the fast expansion of WBAN applications provide a perfect playground for researchers, offering them a wide set of degrees of freedom to play with.

Cooperative Communications Paradigm

Emerging classes of wireless networks, such as ad-hoc and sensor networks and cellular networks with multiple hops, often consist of a large number of nodes in different geometric locations. Compared with classical point-to-point systems, these new types of network are extremely difficult to analyse and optimise. Therefore, new theoretical and practical techniques are needed to augment classical communication and networking theory and practice.

Introduction

Cooperative communication and networking is one of the emerging technologies that promises significantly higher reliability and spectral efficiency in wireless networks. Unlike conventional point-to-point communications, cooperative communication is a new form of diversity that allows users or nodes to share resources to create collaboration via distributed transmission and processing of messages [6]. This cooperative diversity concept is similar to the MIMO system but is applied on a network level. As a result, it is often called a distributed MIMO or network MIMO. It represents a paradigm shift from a network of conventional point-to-point links to network cooperation.

Cooperative communication paradigm is envisaged in various application fields, ranging from cellular networks [7] to WSNs [8], and depending on the design, it can achieve different performance gains, such as achievable rate, energy efficiency, reliability, etc. A WSN can use cooperative relaying to reduce the energy consumption in sensor nodes, hence lifetime of sensor network increases. Due to the nature of the wireless medium, communication through weaker channels requires huge energy as compared to relatively stronger channels.

Cooperative communication schemes typically increase the complexity of the system drastically, both in terms of hardware and communication protocols. The main challenge research community is facing is to exploit the cooperative communication idea while keeping the system practically feasible.

Structure and Contribution of the Thesis

The topic of this thesis is the application of the cooperative communications paradigm to WBANs and WSNs in general. It is structurally divided into three parts.

- First part, Chapter 1, deals with design, implementation and performance evaluation of communication protocols for WBANs. Presented research was conducted through the European Commission-funded FP7 WiserBAN project, whose aim was creating an ultra-miniature and ultra low-power Radio Frequency (RF) microsystem for WBANs, targeting primarily wearable and implanted devices for healthcare, biomedical and lifestyle applications. The project required a customised communication protocol capable of achieving stringent application requirements. The protocol stack developed within the WiserBAN project was one of the first practical implementations of protocol stack for WBANs. In particular, the focus of Chapter 1 is mainly on Medium Access Control (MAC) protocols. Different approaches to the design of MAC protocols are presented and compared through experimentation on a hardware platform intended for WBAN applications. Conclusions drawn from this part provide guidelines to WBAN communication protocol designers about the performance and limitations of synchronous and asynchronous MAC protocols and how to tune protocol parameters to reach required performance.
- Second part, Chapter 2, presents a cooperative MIMO beamforming scheme for WBANs. The considered application scenario consists of sensor nodes, placed on a human body, which are transmitting data to sinks in an indoor environment. WBANs are known for the heterogeneous channel conditions experienced by nodes placed on different parts of the human body. This effect is due to body shadowing which dominates channel gain. The consequence is that some nodes cannot communicate while the body is in certain positions with respect to the receiver. Cooperation among nodes can greatly ameliorate this effect. The

proposed idea exploits the natural heterogeneity of the WBAN propagation medium in order to boost energy efficiency and Block Error Rate (BLER) in an interference-limited scenario. Numerical results, obtained through simulations, show the benefits of cooperation in a highly heterogeneous system as WBANs and shed some light on the problem of cooperating node selection problem in WBANs.

- Third part, Chapter 3, deals with cooperation among nodes in WSNs. This research was partially conducted through the European Commission-funded Newcom# (Network of Excellence in Wireless Communications) project. Considering the future mass deployment of sensor nodes, a simple cooperation mechanism is proposed which requires minimal overhead. The mechanism exploits the fact that sensor nodes are usually deployed to measure the same environmental parameters, such that the data they are transmitting is either the same or correlated. Having in mind a network of inexpensive devices, various realistic effects are modelled and taken into account, namely channel estimation error, hardware impairments, imperfect synchronisation, data correlation and external interference. Exploiting recent achievements in massive MIMO field, asymptotic regime, in which the number of sensor nodes grows without bounds, is considered to simplify analysis and optimisation of various design parameters. Simulations are used to validate the analysis and the results show that asymptotic analysis is sound even for relatively low number of sensor nodes. This research brings the massive MIMO toolkit from cellular networks world to WSNs and provides insights on the energy efficiency maximising number of cooperating nodes in WSNs under various realistic performance hindrances.

Chapter 1

Communication Protocols for Wireless Body Area Networks

In this chapter an important aspect of WBANs, the communication protocol, is discussed. A real implementation of a protocol stack, developed for the purposes of the European project WiserBAN, is presented with the focus on the performance evaluation of the MAC layer protocols.

1.1 Introduction

Communication devices have to agree on many aspects of the data to be exchanged before successful transmission can take place. Rules defining the set of message exchanges are called *communication protocols*. There are many properties of a transmission that a protocol can define. Common ones include: packet size, transmission speed, handshaking and synchronisation techniques, address formatting and mapping, flow control and routing.

The Open System Interconnection (OSI) model is a conceptual model that characterises and standardises the communication functions of a telecommunication or

Chapter 1. Communication Protocols for Wireless Body Area Networks

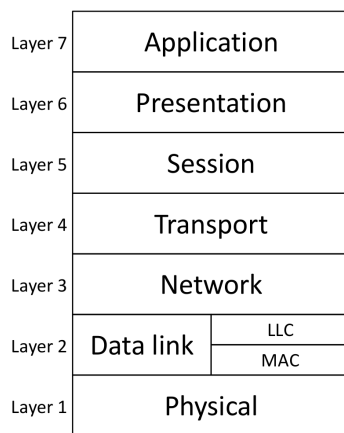


Figure 1.1: OSI model.

computing system regardless of their underlying internal structure and technology. Its goal is the interoperability of diverse communication systems with standard protocols. The model partitions a communication system into abstraction layers (see Fig. 1.1). The original version of the model defined seven layers, although a protocol stack can implement only a subset of these layers. A communication standard defines one or more layers in the OSI model.

Given a huge variety of applications of communication systems with very different requirements, each communication protocol is tailored for a specific application or a set of applications with similar requirements. Since WBANs target a very niche application field, custom communication protocols are typically employed. However, some standards for WBANs already exist. In Section 1.2, Institute of Electrical and Electronics Engineers (IEEE) standards used in WBANs will be presented. First, the overview of WBAN protocols literature is given.

1.1.1 Related Works

Many works dealing with WBAN application requirements can be found in literature. [9] presents the concept of BANs and gives an overview of the corresponding use cases and application scenarios. Authors propose a set of requirements referring to technical (radio interface) characteristics of WBANs. Work presented in [4] gives a comprehensive study of the proposed technologies for WBANs at Physical (PHY), MAC, and network layers. [10] also aims at reporting an overview of WBAN main applications, technologies and standards, issues in WBANs design, and evolution. The paper reports some case studies, based on both real implementation and experimentation on the field, and on simulations.

Many communication protocols meant for different WBAN applications are being developed and can be found in literature. For example, [11] and [12] present a comprehensive study of MAC protocols developed for WBANs, emphasising the importance of energy efficiency in such networks. Authors discuss design requirements for WBANs identifying major sources of energy dissipation and investigating the existing designed protocols focusing on their strengths and weaknesses. In [13], a comprehensive survey of recent MAC protocols for WBANs has been presented, highlighting and clarifying all the significant changes and improvements that each MAC protocol introduces.

MAC protocols can roughly be categorised into synchronous and asynchronous ones, along with hybrid combinations of the two.

Asynchronous MAC protocols generally employ mechanisms to keep duty-cycle of the radio low to achieve energy efficient operation. This is motivated by the fact

Chapter 1. Communication Protocols for Wireless Body Area Networks

that *idle listening*¹ is a major cause of energy wasting [3]. As a consequence, many approaches for duty-cycling in MAC protocols can be found in the literature. In S-MAC [14] nodes periodically wake up, receive and transmit data and then return to sleep. When a node wakes up, it exchanges synchronisation and schedule information with its neighbours and, once devices are synchronised, information is exchanged. T-MAC [15] improves S-MAC by shortening the active period if the channel is idle. B-MAC [16] is a Carrier Sensing Multiple Access (CSMA)-based protocol, where nodes wishing to transmit data to an intended receiver, first transmit a preamble that is slightly longer than the sleeping period of the receiver, to wake up the target node. WiseMAC [17] is ALOHA-based protocol, which uses a technique similar to B-MAC, but it reduces the length of the preamble. Another low power MAC protocol which is the most similar to the one proposed in this work is X-MAC [18]. The protocol works as follows: nodes in the networks exchange sleeping and awake phases. Transmitter wishing to send a packet starts transmitting a burst of short preambles until the receiver detects one of them. Once the receiver becomes aware that it is the destination of the data packet, it responds with an acknowledgement frame and then the data is exchanged. Whenever any non target receiver detects a preamble it goes back to sleep. Once the data is exchanged, the receiver stays awake for a given interval of time, until the awake period expires and then goes back to sleep.

As far as *synchronous* MAC protocols are concerned, many works dealing with performance estimation of standard WBAN protocols, based on simulations and mathematical modelling, can be found in literature. In [19] mathematical model is presented in order to determine the theoretical throughput and delay limits of WBAN using

¹Idle listening is a phenomenon when a device is keeping the radio in reception mode when no packets are being exchanged in the network.

the Carrier Sensing Multiple Access with Collision Avoidance (CSMA/CA) protocol defined in the IEEE 802.15.6 standard for an ideal channel with no transmission errors. The throughput and delay results are presented as a function of payload size and the limits are derived for different frequency bands and data rates. In [20] network performance of an IEEE 802.15.6 CSMA/CA-based WBAN is evaluated in terms of Packet Loss Rate (PLR), packet delay and throughput. The evaluation has been performed through simulation by considering two different channel models for on-body communication. In [21] PLR is estimated as a function of channel quality, diversity order, and Signal to Noise Ratio (SNR) values for all User Priority (UP) defined in the IEEE 802.15.6 standard. Performance is evaluated by means of analytical modelling and simulation considering a Rician fading channel as a reference model. Possible improvements of the IEEE 802.15.6 standard were proposed in several papers. In [22] it has been shown that choosing an appropriate length for Exclusive Access Phase (EAP) and Random Access Phase (RAP) period can have a great impact on MAC performances under non saturation condition. Analytic model was validated by simulation showing that a correct period length can minimise delays allowing more fair resource's assignment. Other possible improvements of the standard were proposed investigating the energy efficiency issues and the synchronisation mechanism has been identified as one of the main culprit for the energy consumption. The Med-MAC synchronisation algorithm proposed in [23] allows to keep synchronisation when devices are sleeping so to save from 25% to 87% of energy with respect the traditional IEEE 802.15.6 MAC standard.

1.1.2 Thesis Contribution

As it could be seen from the literature overview given in the previous section, most works rely on mathematical modelling and/or simulations to evaluate the performance of MAC protocols in WBANs. The work presented in this chapter is based on an actual practical implementation of a full protocol stack for WBAN. Conclusions are drawn from results of a comprehensive experimental campaign.

Performance is evaluated in terms of PLR, average packet delay, average energy consumption and throughput. Regarding the energy consumption measurements, a rigorous methodology is devised which allows for in-depth analysis of protocols behaviour. In particular, the overall energy consumption of the radio transceiver is broken-down to fraction corresponding to radio states, such as Transmitter (TX), Receiver (RX), standby, etc., which helps in understanding how protocols can be tuned to achieve required performance.

The protocol stack implements two MAC modes to cope with heterogeneous application requirements of different use cases, a Superframe (SF)-based MAC and Low Power Listening (LPL) MAC. The two MAC modes represent synchronous and asynchronous approach respectively. Modes are first examined separately and it is shown how to trade-off different performance metrics by setting protocol parameters. Moreover, considering different application scenarios (topology, traffic, node placement, etc.) showed strong and weak points of each mode. Secondly, the two modes are compared in order to determine their suitability in different settings.

The main contributions of this chapter can be summarised as follows:

- a real implementation of a protocol stack for WBANs on a hardware platform

intended for WBANs is presented;

- numerical results are achieved through experimentation, thus many aspects invisible to simulations and mathematical modelling are shown;
- implementation of two MAC modes, representing synchronous and asynchronous approach, allowed for a fair comparison between them. Even though results are obtained for a particular implementation, conclusions can be drawn about the two families of protocols;
- important guidelines are provided which allow proper parameter setting for satisfying specific application requirements.

The rest of this chapter is organised as follows. Section 1.2 summarises features of two IEEE standards used in WSNs and WBANs. In Section 1.3, WiserBAN project, through which this research was conducted, is presented. It describes application scenario and requirements and the overall implemented protocol stack. Section 1.4 deals with the MAC layer of WiserBAN stack and introduces the two MAC modes. Experimental setup and numerical results are presented in Section 1.5 and finally conclusions are drawn in Section 1.6.

1.2 Standard Solutions for WBAN

Starting in 2003, various IEEE and Internet Engineering Task Force (IETF) standardisation bodies started putting together a framework for the communication protocols of the emerging systems. IEEE 802.15 is a working group of the Institute of Electrical and Electronics Engineers IEEE 802 standards committee which specifies WPAN

Chapter 1. Communication Protocols for Wireless Body Area Networks

standards. Two standards most prominently in use in WBANs are IEEE 802.15.4 and lately IEEE 802.15.6. The overview of the two standards is given in the sequel.

1.2.1 IEEE 802.15.4 Standard

IEEE 802.15.4-2003 (Low Rate WPAN) deals with low data rate but very long battery life (months or even years) and very low complexity. The IEEE 802.15.4 Working Group² focuses on the standardisation of the bottom two layers of OSI protocol stack, physical (Layer 1) and data-link (Layer 2) layer. The higher layers are normally specified by industrial consortia such as the ZigBee Alliance³. The first edition of the 802.15.4 standard was released in May 2003. Several standardised and proprietary networks (or mesh) layer protocols run over 802.15.4-based networks, including IEEE 802.15.5, ZigBee, 6LoWPAN, WirelessHART, and ISA100.11a.

IEEE 802.15.4 wireless technology is a short-range communication system intended to provide applications with relaxed throughput and latency requirements in WPANs. The main field of application of this technology is the implementation of WSNs, that are key underlying technologies in the Internet of Things (IoT) and Smart City (SC) frameworks.

In the following some technical details related to the PHY layer and the MAC sublayer as defined in the standard, are reported.

The IEEE 802.15.4 PHY layer operates in three different unlicensed bands (and with different modalities) according to the geographical area where the system is deployed. However, Direct Sequence Spread Spectrum (DS-SS) is mandatory everywhere to reduce the interference level in shared unlicensed bands.

²See also the IEEE 802.15.4 web site: <http://www.ieee802.org/15/pub/TG4.html>

³See also the ZigBee Alliance web site: <http://www.zigbee.org>

PHY layer provides the interface with the physical medium. It is in charge of radio transceiver activation and deactivation, energy detection, link quality, clear channel assessment, channel selection, and transmission and reception of the message packets. Moreover, it is responsible for establishment of the RF link between two devices, bit modulation and demodulation, synchronization between the transmitter and the receiver, and, finally, for packet level synchronization.

IEEE 802.15.4 specifies a total of 27 half-duplex channels across the three frequency bands, whose channelisation is depicted in Fig. 1.2 and is organised as follows:

- 868 MHz band, used in the European area, implements a cosine-shaped Binary Phase Shift Keying (BPSK) modulation format, with DS-SS at chip-rate $300 \frac{\text{kchip}}{\text{s}}$ (a pseudo-random sequence of 15 chips transmitted in a $25 \mu\text{s}$ symbol period). Only a single channel with data rate $20 \frac{\text{kbit}}{\text{s}}$ is available and, with a required minimum -92 dBm RF sensitivity, the ideal transmission range (i.e., without considering wave reflection, diffraction and scattering) is approximately 1 km;
- 915 MHz band, ranging between 902 and 928 MHz and used in the North American and Pacific area, implements a raised-cosine-shaped BPSK modulation format, with DS-SS at chip-rate $600 \frac{\text{kchip}}{\text{s}}$ (a pseudo-random sequence of 15 chips is transmitted in a $50 \mu\text{s}$ symbol period). Ten channels with rate $50 \frac{\text{kbit}}{\text{s}}$ are available and, with a required minimum -92 dBm RF sensitivity, the ideal transmission range is approximately 1 km;
- 2.4 GHz Industrial Scientific Medical (ISM) band, which extends from 2400 to 2483.5 MHz and is used worldwide, implements a half-sine-shaped Offset

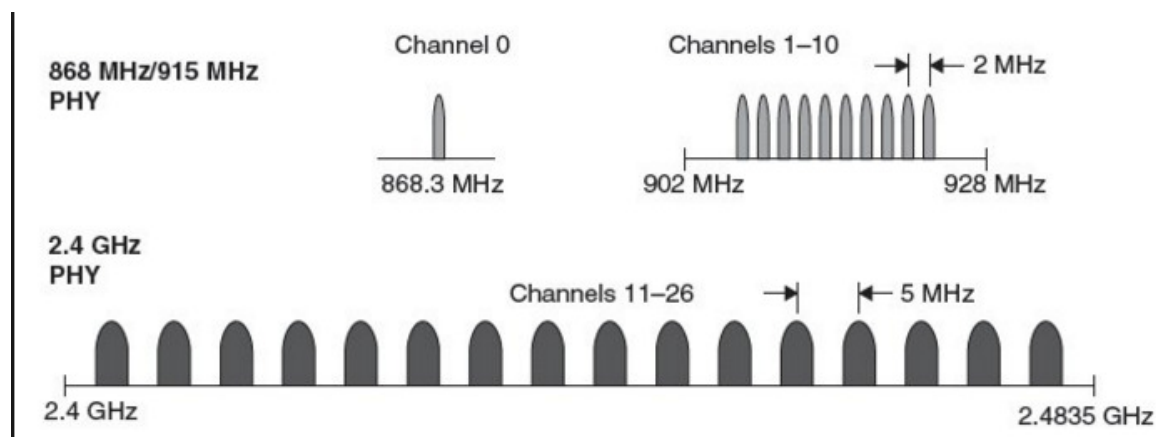


Figure 1.2: Spectrum allocation chart and channelisation for WPAN applications in IEEE 802.15.4 standard.

Quadrature Phase Shift Keying (O-QPSK) modulation format, with DS-SS at $2 \frac{\text{Mchip}}{\text{s}}$ (a pseudo-random sequence of 32 chips is transmitted in a $16 \mu\text{s}$ symbol period). Sixteen channels with data rate $250 \frac{\text{kbit}}{\text{s}}$ are available and, with minimum -85 dBm RF sensitivity required, the ideal transmission range is approximately 220 m.

The ideal transmission range is computed considering that (although any legally acceptable power is permitted) IEEE 802.15.4-compliant devices should be capable of transmitting at -3 dBm . Since the 2.4 GHz band is shared with many other services, the other two available bands can be used as an alternative.

Power consumption is a primary concern, so, to achieve long battery life the energy must be taken continuously at an extremely low rate, or in small amounts at a low power duty cycle: this means that IEEE 802.15.4-compliant devices are active only during a short time. The standard allows some devices to operate with both the transmitter and the receiver inactive for over 99% of time. So, the instantaneous link

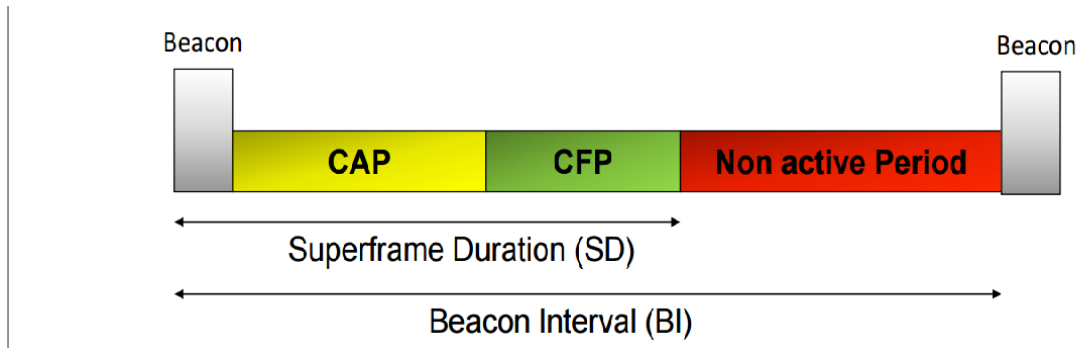


Figure 1.3: IEEE 802.15.4 SF structure.

data rates supported (i.e., $20 \frac{\text{kbit}}{\text{s}}$, $40 \frac{\text{kbit}}{\text{s}}$, and $250 \frac{\text{kbit}}{\text{s}}$) are high with respect to the data throughput in order to minimise device duty cycle.

IEEE 802.15.4 defines two different operational MAC modes, namely *beacon-enabled* and *non beacon-enabled*, which correspond to two different channel access mechanisms.

In the non beacon-enabled mode nodes use an unslotted CSMA/CA protocol to access the channel and transmit their packets [24].

In the beacon-enabled mode [24], instead, the access to the channel is managed through a Superframe (SF), starting with a packet, called *beacon*, transmitted by WPAN Network Coordinator (NC). The SF may contain an inactive part, allowing nodes to go in sleep mode, whereas the active part is divided into two parts: the Contention Access Period (CAP) and the Contention Free Period (CFP), composed by Guaranteed Time Slots (GTSs), that can be allocated by the NC to specific nodes (see Figure 1.3). The use of GTSs is optional.

In CAP, CSMA/CA channel access algorithm is employed. Description of this algorithm will be given later on in the chapter.

To overcome the limited transmission range, multihop self-organizing network

Chapter 1. Communication Protocols for Wireless Body Area Networks

topologies are required. These can be realised taking into account that IEEE 802.15.4 defines two type of devices: the Full Function Device (FFD) and the Reduced Function Device (RFD). The FFD contains the complete set of MAC services and can operate as either a NC or as a simple network device. The RFD contains a reduced set of MAC services and can operate only as a network device.

Two basic topologies are allowed, but not completely described by the standard since definition of higher layers functionalities are out of the scope of IEEE 802.15.4: the star topology, formed around an FFD acting as a NC, which is the only node allowed to form links with more than one device, and the peer-to-peer topology, where each device is able to form multiple direct links to other devices so that redundant paths are available.

1.2.2 IEEE 802.15.6 Standard

The latest international standard for WBANs is the IEEE 802.15.6 which aims at providing an international standard for low power, short range, and extremely reliable wireless communication within the surrounding area of the human body, supporting a vast range of data rates for different applications. Short-range, wireless communications in the vicinity of, or inside, a human body (but not limited to humans) are specified in this standard. It uses existing ISM bands as well as frequency bands approved by national medical and/or regulatory authorities. Support for Quality of Service (QoS), extremely low power, and data rates up to 10 Mbit/s is required while simultaneously complying with strict non-interference guidelines where needed. This standard considers effects on portable antennas due to the presence of a person (varying with male, female, skinny, heavy, etc.), radiation pattern shaping to minimise the

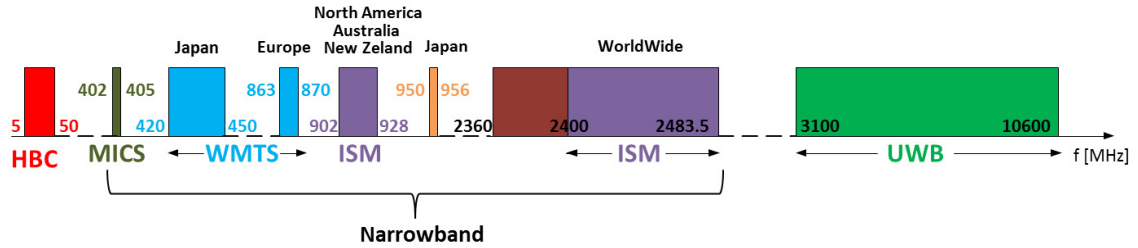


Figure 1.4: Spectrum allocation chart for WBAN applications in IEEE 802.15.6 standard.

Specific Absorption Rate (SAR) into the body, and changes in characteristics as a result of the user motions.

The first degree of flexibility introduced by this standard is related to the choice of the PHY layer. To meet the wide variety of system requirements coming from the different applications, a unique PHY solution does not seem a feasible option, and hence the proposal defines three possible alternatives (see Fig. 1.4):

a) **Narrowband PHY** (optional): a compliant device shall be able to support transmission and reception in at least one of the following frequency bands:

- 402-405 MHz: Medical Implant Communication Service (MICS) band; it is widely accepted although the available bandwidth is limited;
- 420-450 MHz: Wireless Medical Telemetry Service (WMTS) band; available in Japan;
- 863-870 MHz: WMTS band; available in Europe;
- 902-928 MHz: ISM band; it is available for use without license in North America, Australia and New Zealand;
- 950-956 MHz: available in Japan;

Chapter 1. Communication Protocols for Wireless Body Area Networks

- 2360-2400 MHz: this is a newly proposed frequency band to be adopted for WBAN applications;
 - 2400-2483.5 MHz: ISM band; it is available worldwide, but there could be coexistence issues with other standards using the same band.
- b) **Ultra Wide Band (UWB) PHY**: it is divided into a low (3.25-4.75 GHz) and a high (6.6-10.25 GHz) band, both consisting of operating channels of 500 MHz bandwidth each. UWB PHY is specifically designed to offer robust performance for high quality, low complexity and ultra low power operations, all primary aspects when dealing with WBANs, where human safety and coexistence issues are of utmost importance. Two types of UWB technology are considered: *impulse radio (IR-UWB)* and *frequency modulation (FM-UWB)*. Two operational modes are also defined: *default* for medical and non-medical applications, and *high quality of service* for high-priority medical applications. Both modes shall support IR-UWB as mandatory PHY, whereas the *default* one also supports FM-UWB as optional.
- c) **Human Body Communication (HBC) PHY**: this PHY solution uses the human body as a communication medium. The band of operation is centred at 21 MHz with a bandwidth of 5.25 MHz.

Interested reader can refer to [25] for the complete set of specifications of PHY layer.

Even if different PHY solutions are presented, just a single MAC protocol is proposed. In order to support different applications and data flow types (i.e., continuous, periodic, non-periodic, and burst), each one characterised by specific performance requirements, the MAC protocol should be as flexible as possible, combining both,

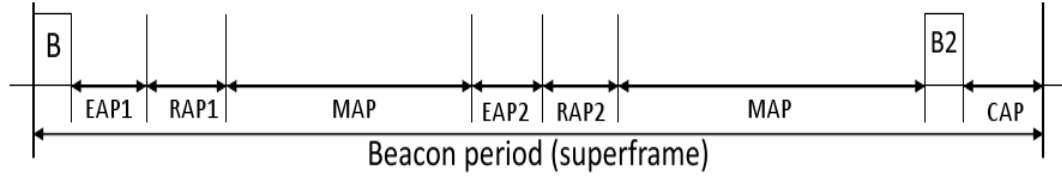


Figure 1.5: IEEE 802.15.6 SF structure for beacon mode access.

contention-based and contention-free, access techniques. The standard also provides several UP values in order to diversify and prioritise nodes channel access, according to the information they have to transmit (e.g., background data, video traffic, medical data, or emergency traffic). A WBAN coordinator could decide whether to operate in one of the following three access modes:

- a) **Beacon mode with SF**: the coordinator establishes a common time base by sending beacon packets that define the beginning of an active SF. It shall also divide each active SF into applicable access phases, ordering them as shown in Fig. 1.5 and defining their duration. The duration of any phase may be set to zero, except for the RAP 1, which must have a minimum guaranteed duration. The coordinator may also maintain inactive SFs, where it transmits no beacons and provides no access phases. In the Managed Access Phase (MAP), the coordinator may schedule intervals, or send poll or post packets to nodes. A poll is defined as a control frame used to grant nodes an immediate polled allocation (i.e., non-recurring time interval for uplink traffic), or to notify a node of a future poll or post. A post is a management or data type frame sent by the coordinator to inform a node of a posted allocation, which is a non recurring time interval that

Chapter 1. Communication Protocols for Wireless Body Area Networks

the coordinator grant to itself for downlink traffic exchange. Further details on polled and posted allocation techniques can be found in [25].

In the EAPs, used only for the transmission of emergency data, RAP, and CAP, nodes compete for the medium access using CSMA/CA or Slotted ALOHA techniques. IEEE 802.15.6 versions of CSMA/CA and Slotted ALOHA are explained in details in Sec. 1.4.1.

- b) **Non-beacon mode with superframes:** in this mode, a coordinator may have only a MAP in any SF, and it may organise the access to the medium as explained above for the MAP phase in the beacon enabled access mode.
- c) **Non-beacon mode without superframes:** a coordinator may provide unscheduled allocation intervals. After determining that the next frame exchange will take place in non-beacon mode without SF, a node shall treat any time interval as a portion of EAP or RAP, employing CSMA/CA-based random access to obtain a contended allocation [25].

As it could be seen, the huge variety of channel access techniques proposed in the standard gives a great flexibility to the protocol, but at the same time it is not so immediate for designers to choose the best option for the intended application, and to find the optimal solution.

Security aspects are also accounted for in the standard, and they are addressed with nodes choosing among three different security levels. *Level 0:* unsecured communications; it provides no measures for message authenticity and integrity validation, confidentiality, and privacy protection. *Level 1:* authentication but not encryption;

messages are transmitted in secured authenticated but not encrypted frames, providing measures for authentication and integrity validation, but not confidentiality and privacy protection. *Level 2*: authentication and encryption; it results in the most secure transmission conditions provided by the standard. The security selection sets off a security association between devices for activating a pre-shared master key, or generating a new one. As part of message security, replay protection is also provided.

1.3 Reference Scenario: WiserBAN Project

The WiserBAN project was a European project, aiming at creating an ultra-miniature and ultra-low-power radio frequency microsystem for WBANs [1]. WiserBAN dealt with WBANs and is about improving personal sensing capabilities by using miniature, unobtrusive, long-lifetime sensor nodes. WiserBAN delivered innovative wearable and implantable radio microsystems which enable concrete exploitation perspectives in a broad range of industrial segments such as healthcare, biomedical, wellness, and lifestyle. It generated high societal and market impact and enabled major technological breakthroughs.

WiserBAN developed a highly integrated "radio & antenna & data-processing" microsystem which reduces significantly the barriers in terms of size and power consumption of existing wireless solutions. The ambitiousness of the project can be recognised in its declared goals:

- develop a radio microsystem that fits in a $4\text{ mm} \times 4\text{ mm} \times 1\text{ mm}$ (16 mm^3), hence a factor nearly $50\times$ smaller in size than WPAN solutions ($\sim 1000\text{ mm}^3$ range);
- develop an ultra low-power radio targeting the mW power consumption level,

Chapter 1. Communication Protocols for Wireless Body Area Networks

hence a factor of $20\times$ to $50\times$ better in autonomy than Bluetooth, Bluetooth LE or ZigBee by combining Micro Electro Mechanical Systems (MEMS) and deep-submicron Complementary Metal-Oxide Semiconductor (CMOS) technologies;

- provide miniature antenna technologies that are optimised for $0.2 - 2\text{m}$ around-the-body propagation, and which will be tiny ($30 - 100\text{mm}^3$ range), hence a factor of at least $10\times$ smaller antennas than existing 2.4GHz solutions ($\sim 1000\text{mm}^3$ range);
- co-develop the antenna and radio microsystem and provide smart antenna adaptivity to various embodiments and varying environments around the body, for example owing to moving body parts, whereas existing solutions provide fixed and inflexible solutions that suffer from propagation losses and impedance shifts;
- embed a data processing unit within the microsystem, and achieve $10\times$ better sensor data processing efficiency compared to microprocessors used in today's WPAN radios, by integrating a high-performance low-power Digital Signal Processor (DSP) core on the same chip as the radio, and therefore without impacting on the size of the microsystem;
- develop a flexible/reconfigurable and low-power radio baseband and protocol, for enabling long autonomy, interference-robust and reliable WBAN communication, and compliance with existing and emerging WBAN standards;
- develop a heterogeneous System-in-Package System in Package (SiP) platform that addresses the miniaturised assembly of the wireless microsystem components: the RF and DSP System on Chip (SoC), the antenna interface, the RF and low-frequency MEMS devices, and applicative ASICs of the end-users;

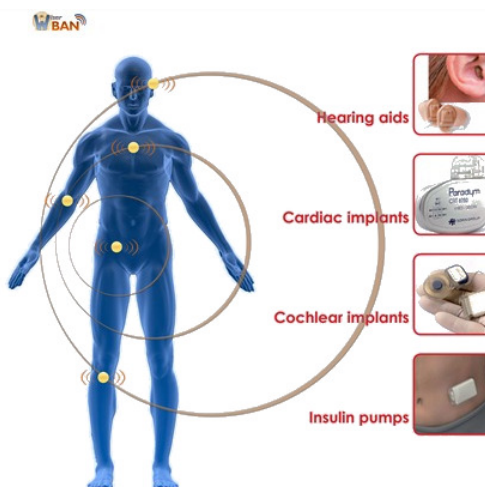


Figure 1.6: WiserBAN scenario.

- demonstrate industry-driven wearable and implanted WBAN prototypes, showing that MEMS and RF Integrated Circuit (IC) technologies can create a ultra-miniature and low-power microsystems.

1.3.1 Use Cases and Requirements

The WiserBAN project addressed primarily the following wearable and implantable use cases: hearing instruments, cardiac implants, insulin pumps and cochlear implants (see Fig. 1.6). In such applications where miniaturisation and unobtrusiveness are a must, only limited wireless connectivity and autonomy can be achieved using today's wireless solutions because of their excessive size and power consumption. WiserBAN pushed wireless microsystem technology beyond the state of the art by delivering an ultra-tiny and ultra-low-energy radio that enable WBAN capability and novel product perspectives for wearable and implanted devices for use in lifestyle and bio-medical

applications. WiserBAN also aimed at developing a dedicated communication protocol stack, able to cover considered use cases, shown in Fig. 1.6. In all the use cases nodes have to communicate with a Remote Control (RC), that is the smart phone of the user, embedding a μ SD card with the WiserBAN chip. To give a flavour of application requirements diversity some examples follow. Monitoring application has a periodic bidirectional traffic and requires a PLR below 10^{-2} and a maximum delay below 100 ms. For an application where devices are remotely controlled, the traffic is aperiodic, unidirectional and has the same requirements as monitoring application. In the case of audio streaming the requirements are much stricter. Target PLR and maximum delay are 10^{-5} and 50 ms respectively, while the required throughput is 160 kbit/s.

1.3.2 System Architecture

One of the aims of WiserBAN project is to develop a dedicated protocol stack, targeting some specific use cases, as shown in Fig. 1.7. In particular, at the PHY layer, three different modulation schemes are implemented:

- **PHY 1:** IEEE 802.15.4-compliant PHY; it adopts a Minimum Shift Keying (MSK) modulation with spreading, resulting in a bit-rate of 250 kbit/s;
- **PHY 2:** it is derived from **PHY 1** removing the spreading; just MSK modulation is used with a bit-rate of 2 Mbit/s;
- **PHY 3:** Bluetooth Low Energy-compliant PHY, which uses a Gaussian Minimum Shift Keying (GMSK) modulation, with a bit-rate of 1 Mbit/s.

1.3 Reference Scenario: WisserBAN Project

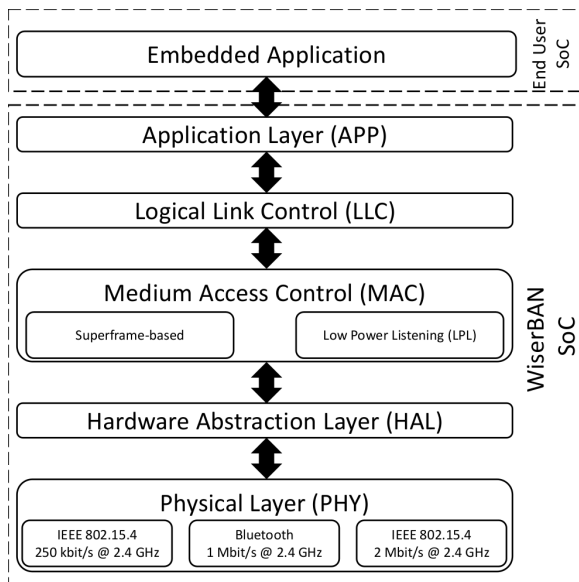


Figure 1.7: WisserBAN protocol stack.

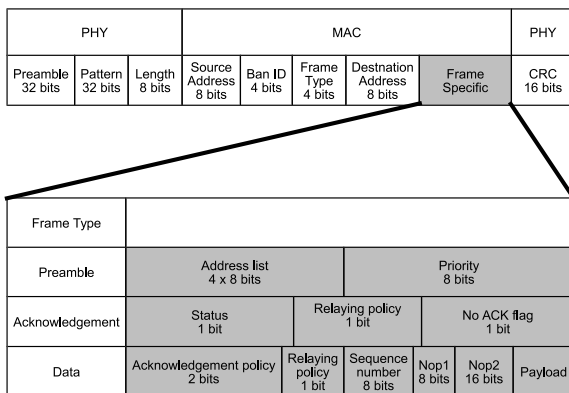


Figure 1.8: WisserBAN protocol frame format.

Chapter 1. Communication Protocols for Wireless Body Area Networks

As for the MAC layer, one of its main functions consists in the management of access to the radio resource, when more than one device (other than the NC) are part of the network. WiserBAN stack implements two MAC modes:

- **SF based MAC:** a synchronous MAC mode intended to handle high traffic with multiple nodes in the network, i.e., audio streaming to hearing aids. It can adapt to the application requirements by changing the structure of the SF. Major limitation is the necessity for maintaining the synchronisation in the network which introduces an energy consumption floor;
- **LPL MAC:** an asynchronous MAC mode intended primarily for use in low traffic setting and energy constrained devices, i.e., implanted devices. Performance can be tuned up to a certain level by setting the parameters. Its lack of proper collision avoidance technique makes this mode unsuitable for networks with high number of nodes.

The two MAC modes will be presented in details in Sections 1.4.

For what concerns higher layers, Logical Link Control (LLC) provides an interface between upper layers (e.g., Application (APP)) and MAC, managing the data flow toward the MAC. Data coming from APP is sorted into *flows* according to performance requirements. LLC is monitoring QoS, based on feedback from MAC, and is capable of changing MAC parameters in order to meet the requirements. It is also in charge of reporting to higher layers about the actual QoS achieved. WiserBAN, being a simple network with only few nodes, does not have a proper network layer. Some network layer capabilities are handled by MAC layer directly, such as relaying which is basically a rudimentary form of routing. APP layer is an interface between

the transceiver SoC (Icycom, WiserBAN) and the end user SoC. The communication between the two is established through an Serial Peripheral Interface (SPI) bus.

The fact that the WiserBAN project is an actual implementation of WBAN concept implies that some features are project-specific, most prominently hardware platform which has a great impact on the overall performance. However, all the experiments are done on the same platform allowing for the generalisation of conclusions. Another project-specific aspect of the presented work are the use cases which determine application requirements. Luckily use cases range from low-power low-traffic implanted device to high-throughput audio streaming equipment, representing a wide spectrum of nowadays WBAN applications.

In the following, the focus is going to be on MAC layer protocols and their performance.

1.4 MAC Design for WBANs

1.4.1 Superframe-based MAC

In SF mode, channel access control is practically realised by the NC through the establishment and the maintenance of SFs, whose length, T_{SF} is defined as the time interval between two consecutive beacon packets (see Fig. 1.9). The SF may consist of *active* and *inactive* portions. During the latter nodes can go into stand-by state to reduce their power consumption. As shown in Fig. 1.9, the WiserBAN SF active portion is divided into several parts, inspired by IEEE 802.15.4 [24] and IEEE 802.15.6 [25] standards:

Chapter 1. Communication Protocols for Wireless Body Area Networks

- **Beacon period:** reserved for the transmission of the beacon by the NC. It contains network management information;
- **Poll period:** where nodes have reserved mini-slots to send an Acknowledgement (ACK) to the NC in case the beacon is correctly received;
- **Relaying period:** used for multi-hop transmissions⁴;
- **CFP:** where nodes access the radio channel through a Time Division Multiple Access (TDMA)-based scheme, where a certain number of time slots is allocated to nodes with more stringent application requirements;
- **CAP:** where nodes compete for the access to the channel according to the CSMA/CA or Slotted ALOHA algorithms;
- **ACK portion:** mini-slots are assigned to the nodes to communicate if data exchange during the current SF were successful or not.

Information about T_{SF} , as well as the durations of periods constituting the SF, is contained in the beacon packet and can be tuned in real-time according to the requirement demanded by the application, through the LLC layer. CAP must be always present in the SF since control packets (e.g., CFP slot requests) are exchanged in it. If no other traffic needs to be managed in it, its duration, T_{CAP} , is set to the minimum possible value.

WiseBAN MAC adopts three channel access protocol solutions for CAP: the CSMA/CA in the two versions proposed in the IEEE 802.15.4 and IEEE 802.15.6 standards, and the Slotted ALOHA algorithm as defined in IEEE 802.15.6 (see Fig. 1.9).

⁴Although the protocol stack does not implement a proper network layer, some of its features are present including multi-hop transmission which greatly improves the performance in a highly variable WBAN channel

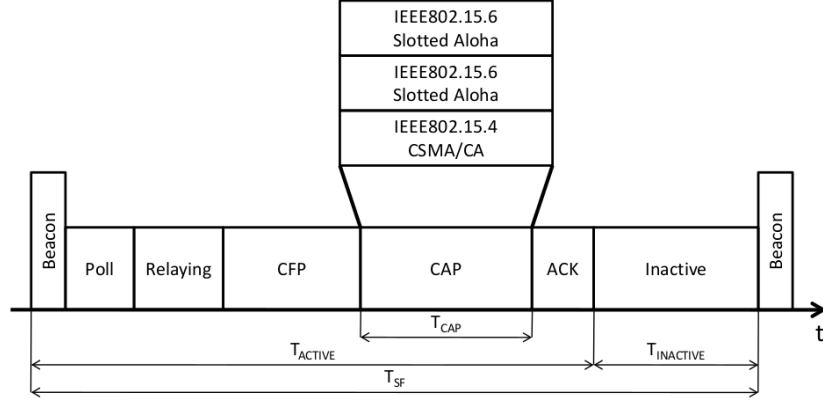


Figure 1.9: WiserBAN SF structure.

1. **IEEE 802.15.4 CSMA/CA Algorithm** (Fig. 1.10): it is implemented using units of time called Backoff Periods (BPs) with a duration of $320\ \mu\text{s}$. For each transmission attempt, every node in the network should maintain three variables, namely Number of Backoffs (NB), Contention Window (CW), and Backoff Exponent (BE). NB is the number of times the algorithm is required to backoff while attempting the current transmission. It is initialised to 0 and it can assume a maximum value of NB_{max} . CW is the contention window length, whose initial value is equal to 2. It defines the number of BPs where no activity on the channel should be detected before a new transmission can start. BE is the backoff exponent related to the number of BPs a node shall wait before attempting again to sense the channel. It varies between BE_{min} (initial value) and BE_{max} . Once CAP starts, a node with a packet to transmit will first delay any activity (backoff state) for a number of BPs randomly drawn in the range $[0, 2^{\text{BE}-1}]$. After this delay, channel sensing is performed for one BP. If the

Chapter 1. Communication Protocols for Wireless Body Area Networks

channel is sensed as busy, CW is reset to 2, while NB and BE are increased by 1, ensuring that $BE \leq BE_{\max}$. If $NB \leq NB_{\max}$ the node should return in backoff state and wait for another random interval of time. If the channel is assessed as idle, CW is decremented by 1 instead. If $CW > 0$, the node waits for another BP and then it sounds the channel again, acting as described before (busy or idle state). The algorithm ends either with the data transmission for $CW = 0$ or with a failure, when $NB \geq NB_{\max}$, meaning that the node did not succeed in accessing the channel in a maximum number of attempts.

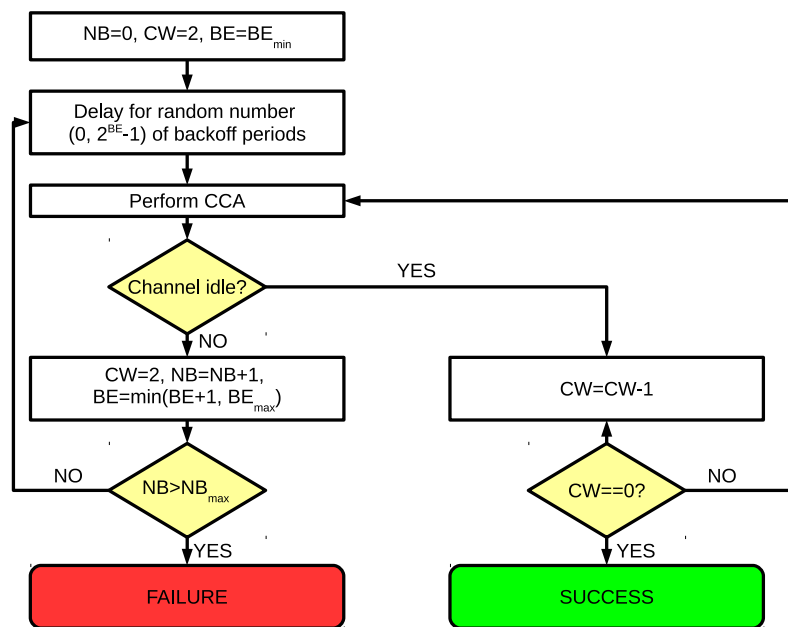


Figure 1.10: IEEE 802.15.4 CSMA/CA algorithm flowchart.

2. **IEEE 802.15.6 CSMA/CA Algorithm** (Fig. 1.11): in this case the time is divided into slots of $125 \mu\text{s}$. When a node has data to be sent, it randomly chooses a Backoff Counter (BC) in the interval $[1, CW(UP)]$, where $CW(UP) \in$

$[CW_{\min}(\text{UP}), CW_{\max}(\text{UP})]$. The values of $CW_{\min}(\text{UP})$ and $CW_{\max}(\text{UP})$ depend on the user priority (UP), larger CW values for data with less stringent requirements. If the channel has been sensed as idle for a Short Inter Frame Space (pSIFS)= $50 \mu\text{s}$, the node decrements its BC by one for each idle slot that follows. Once the BC has reached zero, the node can transmit its frame. The CW is doubled every two failures, ensuring that it does not become larger than $CW_{\max}(\text{UP})$. If the channel is found busy, the BC is locked until the channel becomes idle again for pSIFS.

3. **IEEE 802.15.6 Slotted ALOHA Algorithm**(Fig. 1.12): time is divided into slots, whose duration depends on the length of the frames that have to be transmitted. Each node wishing to perform a transmission obtains a contended allocation in the current ALOHA slot if $z \leq \text{CP}(\text{UP})$, where z is a random value in the interval $[0, 1]$, drawn for every attempt. $\text{CP}(\text{UP})$ is the Contention Probability set according to the result of the last contended allocation, and whose value depends on the UP (smaller for lower priority data). If the node did not previously obtain any contended allocation or succeeded in the last contended allocation it had obtained, it shall set the $\text{CP}(\text{UP})$ to its maximum value, which depends on the user priority. If the node transmitted a frame requiring no ACK, or the ACK was received at the end of its last contended allocation, it shall keep the CP unchanged. If the node failed in the last contended allocation it had obtained, it shall halve the $\text{CP}(\text{UP})$ value every two failed attempts, ensuring that it does not become smaller than $\text{CP}_{\min}(\text{UP})$.

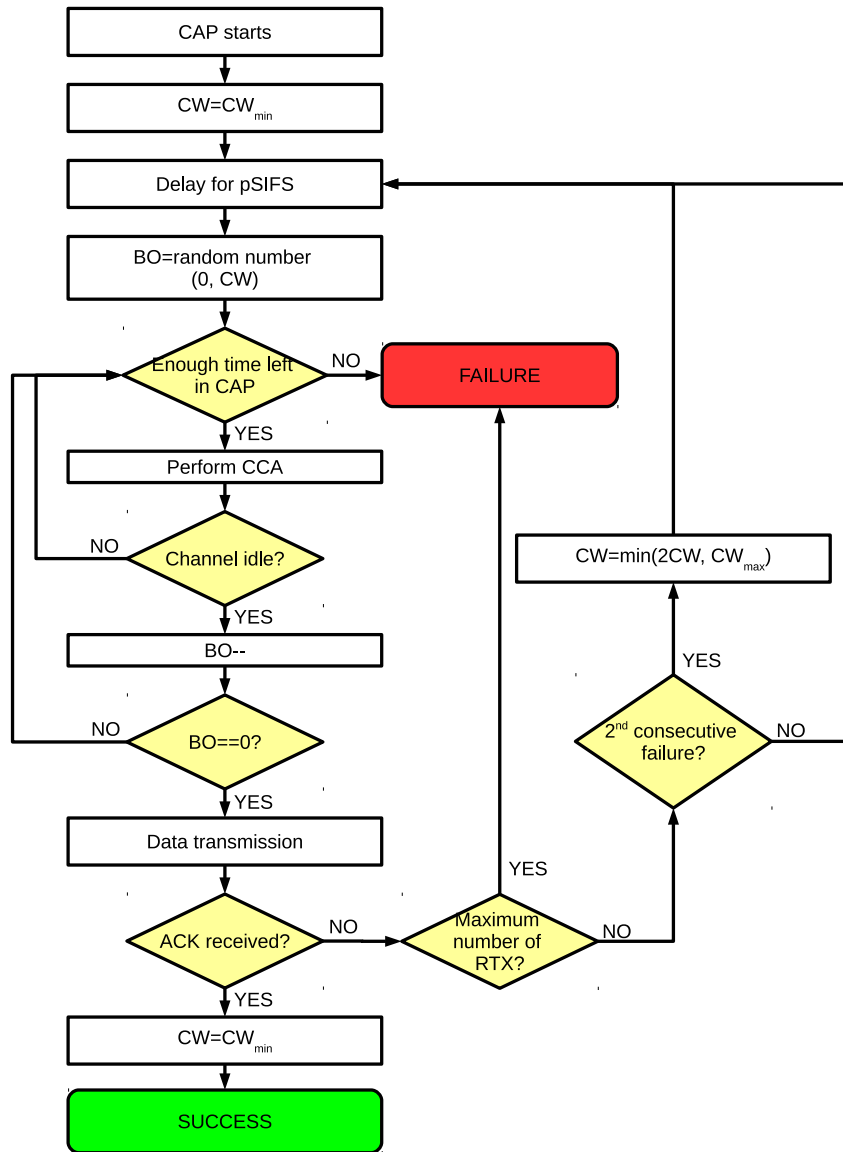


Figure 1.11: IEEE 802.15.6 CSMA/CA algorithm flowchart.

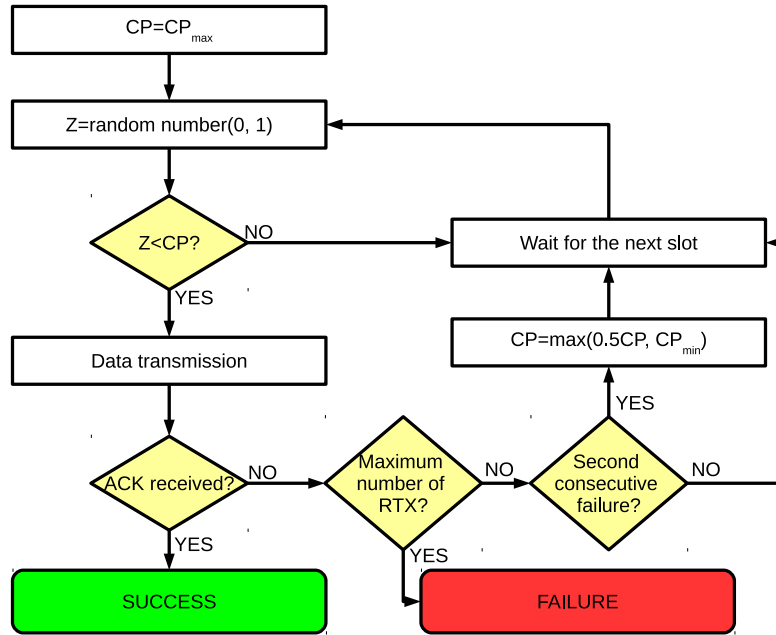


Figure 1.12: IEEE 802.15.6 Slotted ALOHA algorithm flowchart.

1.4.2 Low Power Listening MAC

LPL is an asynchronous MAC protocol. In LPL, nodes alternate sleeping and listening periods. The duration of the sleeping period is denoted as T_s , while the duration of the listening period is denoted as T_{on} (see Fig. 1.13). A node, having data to be transmitted to a given receiver, or a set of receivers, transmits a burst of short preambles, in order to get synchronised with the receiver(s). Preambles are separated by a short interval of time reserved for a potential reception of an ACK. The period between the transmission of two consecutive preambles is denoted as T_p . Preambles contain the addresses of all the intended receivers and the transmitter waits for the ACK from all these nodes. Before the transmission of the first preamble the node listens the channel for a given interval of time (T_{on}), in order to avoid collision with an

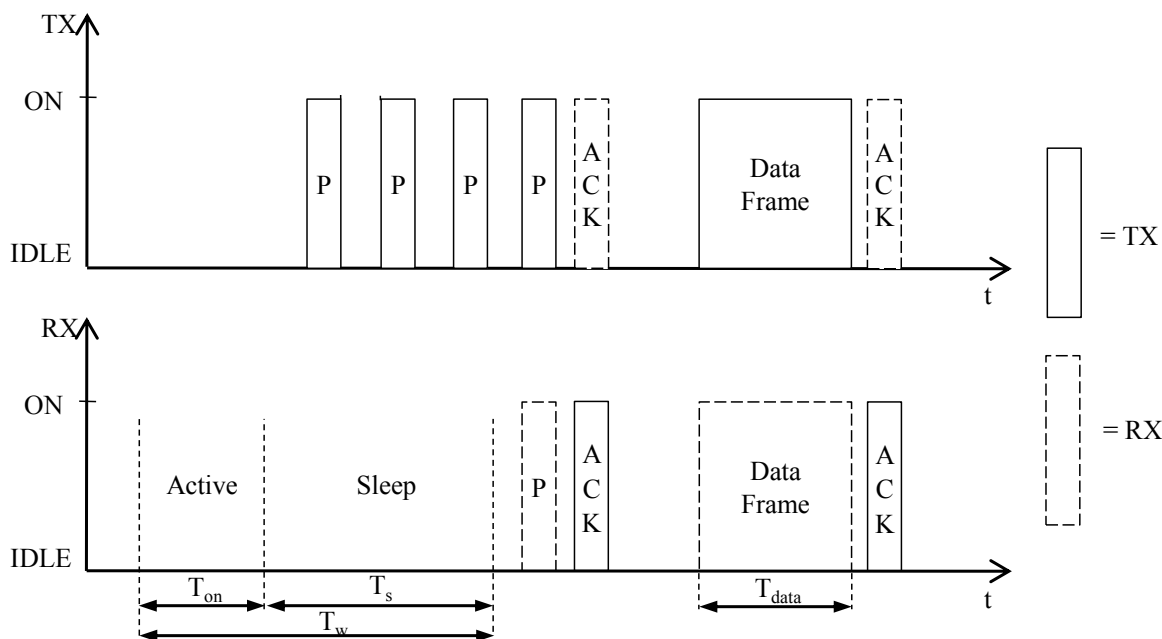


Figure 1.13: LPL protocol.

ongoing packet transmission. To be sure that the intended destination node receives at least one preamble, the transmitter needs to send preambles for at least T_S . When the transmitter receives all the ACKs coming from the intended receivers, it stops sending preambles and transmits the data packet. The value of T_S depends on the application requirements in terms of maximum tolerable delay. The interval T_P accounts for time needed for transmission of preamble, turn-around time and ACK wait time. As for the duration T_{on} , its minimum is hardware dependent and has to be in such way that it guarantees the reception of the preamble frame, while its maximum is related to energy consumption requirements.

The protocol includes a strategy to manage different levels of UP assigned to nodes. During the listening phase which precedes the preamble burst transmission, the transmitter may receive a preamble coming from another node in the network.

If the received preamble has been sent by a node having a lower UP (see Priority field in Fig. 1.8), an ACK with a flag (No ACK flag in Fig. 1.8) is sent in order to stop the ongoing preamble burst coming from the other node. At this point the node having the highest UP will send its own preamble burst. On the other hand, if the received preamble has a higher UP, the node will check whether it is one of its intended destinations. In the case it is, the node sends an ACK and data transfer occurs, otherwise the node will perform random back-off uniformly distributed within an interval of time, denoted as T_{BO} , and it will repeat the procedure starting from channel listening. The priority mechanism is very important in a WBAN application scenario since some packets (i.e., emergency packets) need to be transmitted with the lowest possible delay.

If the transmitter has more than one packet for the same node, it will indicate this by setting a parameter contained in the data frame properly (Pending Packet Indicator field shown in Fig. 1.8). Therefore, if such parameter is set to 1, the receiving node will not go to sleep mode as it usually does, but it will wait for the packet. As a consequence, the transmitter does not send preambles for any of the subsequent packets but only for the first packet in the chain, as it is aware of the fact that the targeted node is waiting for the data packet. Depending on the scenario, this mechanism can greatly increase the energy efficiency of the protocol.

The key point of LPL is that if there are no packets to be transmitted in the network, the nodes spend most of the time in sleep mode, thus maintaining low duty cycle, expressed as $\frac{T_{on}}{T_W}$. This implies that LPL is suitable for applications where the network traffic is low and irregular. On the other hand, LPL lacks proper collision avoidance techniques which limits its performance in a network with multiple nodes

and moderate to high traffic.

1.5 Performance Evaluation

For the sake of performance analysis, WiserBAN stack has been implemented and tested on the Icycom platform provided by WiserBAN project partner Centre Suisse d'Electronique et de Microtechnique (CSEM).

1.5.1 Study Methodology

1.5.1.1 Experimental Platform

Icycom is a radio frequency SoC integrating a 868 – 915 MHz low power RF transceiver, MSK modulation and data rate of $200 \frac{\text{kbit}}{\text{s}}$, a 32 bit $120 \frac{\mu\text{A}}{\text{MHz}}$ dual-MAC DSP Reduced Instruction Set Computing (RISC) core with 96 kB of SRAM. The SoC runs off a 1 V supply, compatible with a single alkaline cell, and is optimised for long battery life, consuming less than 2.5 mA in active receiving mode, 40 mA for 10 dBm transmission and 1 μA in standby with real time clock running. Additional peripherals such as a voltage-divider to address lithium batteries, ADC, SPI, I2C, UART, I2S, etc., are all included on the same chip, resulting in a compact system solution. Icycom targets portable industrial, scientific and medical band applications, in particular those that need long battery life and/or signal processing, such as WSN and medical. More details about Icycom SoC can be found in [26, 27].

1.5.1.2 Scenarios

In the measurements, two settings were considered, both in an indoor environment:

- **'on table'**: devices located on a table at the same distance from each other, appositely chosen larger than two wavelengths⁵ ($\lambda \sim 35$ cm) in order to avoid near field propagation problem. Transmit power set to 10 dBm, such that connectivity issues are avoided and only the MAC performance is evaluated;
- **'on body'**: devices located on a human subject, in the right hand and on the chest, simulating cardiac implant use case. Transmit power set to -20 dBm (to simulate the attenuation experienced by an in-body implant), such that a more realistic environment is accounted for. The subject was walking back and forth in a room 5×3 m on a straight path 3 m long, keeping the 1 m distance from the walls.

'On body' setting was used only for evaluating the impact of propagation medium on performance. Difference in current draw when transmitting 10 dBm and -20 dBm is compensated⁶ for in the reported energy consumption measurements such that performance is only affected by MAC layer aspects of connectivity issues and not hardware itself.

Regarding the network topology, two were considered:

- **Point-to-Point (P2P)**: the data exchange occurs between two devices of the same hierarchical level;
- **Star**: several End Device (ED) are connected to a NC. A Star topology with n EDs is denoted as Star- n topology.

⁵For antennas shorter than half of the wavelength of the radiation they emit (i.e., "electromagnetically short" antennas), the near field is the region within a radius ($d \ll \lambda$), while the far-field is the region for which $d \gg 2\lambda$.

⁶The same level of current is considered in both cases.

Chapter 1. Communication Protocols for Wireless Body Area Networks

Given the heterogeneity of the WiserBAN use cases, protocol performance was measured considering various traffic types. They can be categorised based on:

- **Application types:**

- *Query-based application:* communication is initiated by a short query packet from the NC to an ED(s) which then responds with a data packet;
- *Monitoring application:* EDs are periodically or randomly generating data, which is then sent towards the NC.

- **Traffic generation types:**

- *Periodic traffic:* a data packet or a query is generated every T_{PG} seconds (Fig. 1.14 a));
- *Random traffic:* a data packet or a query is generated at a random instance within an interval of duration T_{PG} seconds (Fig. 1.14 b)).

T_{PG} determines the traffic intensity. It can be also expressed as packet generation rate $f_{PG} = \frac{1}{T_{PG}}$.

1.5.1.3 Metrics

In the subsequent performance analysis the following metrics are considered:

- PLR is the ratio between the number of lost packets (packets not correctly received by the intended receiver, NC) and the overall number of packets generated by transmitter(s). Packets get lost due to the following reasons:
 - collisions, i.e., simultaneous transmissions from two or more nodes;

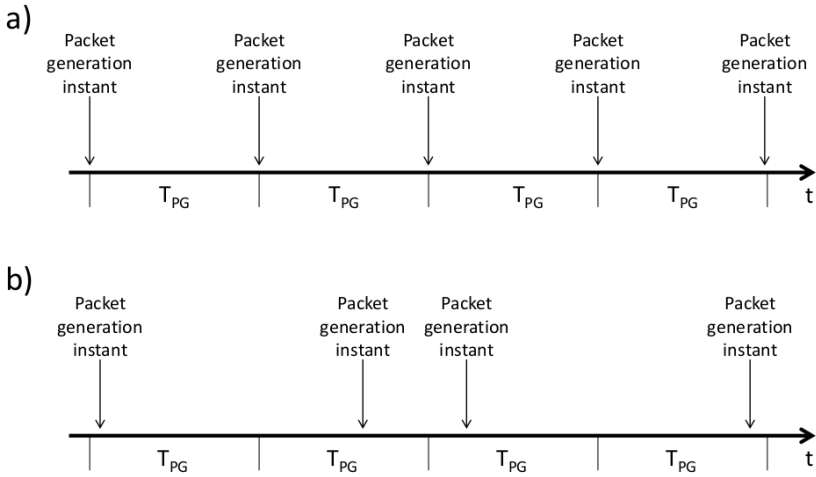


Figure 1.14: Traffic generation types.

- bad channel conditions caused by the link between the transmitter and the receiver being shadowed by body parts, a sudden deep fade, etc.;
- bad synchronisation, for example the intended receiver is not in reception mode when the transmitter starts transmitting the packet.

PLR is computed by simply counting the number of correctly received packets and the total number of generated packets during the experiment;

- Average delay [ms] measures the average amount of time elapsed between the generation instant of a packet at the APP layer of transmitter and its reception at the APP layer of the receiver. In a *query-based* application, average delay represents the average amount of time elapsed between the generation instant of query at the APP layer of the NC and the reception of reply at the APP layer of the NC. Major part of packet delay is due to channel access mechanisms as well as Retransmissions (RTXs), but packet delay also includes actual

Chapter 1. Communication Protocols for Wireless Body Area Networks

transmission time, processing time, etc. Packet delay is computed by means of timestamps. The average is then taken over all the successfully received packets in the experiment;

- Throughput $\left[\frac{\text{kbit}}{\text{s}}\right]$ represents the amount of useful information, consisting only of APP layer payload, i.e, excluding all the headers, correctly received by the NC in a unit of time. As such, it measures the efficiency of a network expressed as the transfer rate of useful and non-redundant information. APP payload will be denoted simply as payload in the following. In an ideal protocol, throughput would be equal to PHY layer bitrate, however the necessary presence of PHY and MAC headers introduces overhead which is not negligible. Collisions make a great impact on throughput, especially in a high traffic multi-terminal network. Network throughput is typically plotted against the offered traffic in order to show the protocol capabilities of handling traffic generated in the network. The analytical expressions for evaluating the offered traffic $G \left[\frac{\text{bit}}{\text{s}}\right]$ and the throughput $S \left[\frac{\text{bit}}{\text{s}}\right]$ is hereafter reported:

$$G = \frac{N(\text{Payload [bit]} + \text{Header [bit]})}{T \text{ [s]}} \quad (1.5.1)$$

$$S = \frac{N_{\text{RX}}\text{Payload}}{T} \quad (1.5.2)$$

where:

- N is the number of nodes in the network. it is used to evaluate the amount of traffic generated in the period of time T by the whole network (assuming each of N nodes generates on average 1 packet every T seconds);
- T is the average period of time between two subsequent packet generations;

- N_{rx} is the average number of successfully received packets in a period of duration T , given by $N_{RX} = N(1 - PLR)$;
- Payload is variable payload size and Header is total header size, including PHY and MAC header, equal to 19 bytes.

Network throughput is measured by simply counting the amount of useful information successfully received by NC during the experiment and dividing it by the total duration of the experiment;

- Average energy consumption $\left[\frac{J}{h}\right]$ or $\left[\frac{mJ}{\text{packet}}\right]$ measures the energy efficiency of a protocol. The energy consumption of a device can be expressed as a sum of the energy consumed by all its parts (processor, peripherals, etc.). In WBAN devices, and even more generally WSN devices, the energy consumption is mostly determined by the radio transceiver activities. Having this in mind, the first step is to characterise the energy consumption of the radio interface. Icycom platform (see Section 1.5.1.1) is powered by a Direct Current (DC) power supply with a $10\ \Omega$ resistor connected in series. The voltage drop across the resistor, observed on the oscilloscope, is proportional to the current drawn by the platform. Knowing the current and the voltage supplied to the platform, the power is simply calculated as a product of the two. The scheme of this measurement and oscilloscope screenshots are presented in Fig. 1.15. The radio interface of Icycom platform is realised as a state machine. The defined states are:

- OFF, which corresponds to radio interface turned off and other parts of the platform, such as processor, timers, etc., running. It represents the energy consumption floor;

Chapter 1. Communication Protocols for Wireless Body Area Networks

- ON, which corresponds to initialised radio interface;
- PM0, the radio interface in power mode zero;
- STANDBY, when the radio interface is in stand-by mode, that is the radio is ready to switch to either RX or TX state;
- RX, where the radio is ready for reception;
- RXR, during an ongoing reception or listening;
- TX, when the radio is ready for transmission;
- TXT, during an ongoing transmission.

The state machine has such a complex structure because Icycom platform allows for different power consumption states in which different parts of the platform are switched off, such that a trade-off between energy consumption and wake-up time can be found. In the experiments this feature was not used for the focus was on the effects of the MAC protocols rather than hardware platform. By going through all the states sequentially the power of each of them is measured. The result of this measurement is presented in Table 1.1.

Once this was done, the time spent in each state during the measurements needed to be determined. For this purpose a software module was built. The main idea is to compute the time spent in each state by using an on-board timer. A timer was used in the free run mode, meaning that it will increment the value of its counter with a given frequency. This frequency was set to 1 MHz such that the time resolution of a measurement is 1 μ s. Whenever the radio changes state, a callback function is invoked. The callback function adds the value of the counter to the total time spent in the last radio state and resets the counter.

For example, let us suppose that the radio changes its state from state A to state B . When the radio entered state A , the counter was reset, i.e., its value set to zero. When the radio switches from state A to state B , the value of the counter represents the amount of time, in μs , spent in state A . Once this value is added to the overall time spent in state A , the counter is reset, such that when the next change occurs it will contain the time spent in state B . The results are displayed at the end of the measurement. This mechanism is very precise for monitoring activities of the radio interface.

If we denote the set of states as S , the energy consumption of the platform can be expressed as

$$E = \sum_{s \in S} P_s T_s \quad (1.5.3)$$

where P_s and T_s are power and time spent in state s , respectively.

In the following we are going to group states with similar purpose to facilitate the analysis of the results.

The above described methodology allows for a very precise measurements which can be used to verify the models used in simulators. Although the actual numerical results are hardware dependent, the general behaviour and trends are general since they are based on common features of all the platforms.

To tune the performance of the system, certain trade-offs between these metrics need to be made. For example, if the energy consumption is not constrained, by employing sophisticated synchronisation and scheduling mechanisms collisions can be avoided, thus boosting PLR and throughput. Some of this trade-offs will be discussed in the following sections.

Chapter 1. Communication Protocols for Wireless Body Area Networks

Table 1.1: Radio states power

State	Power [mW]	State	Power [mW]
OFF	1.98	RX	4.59
ON	1.98	RXR	8.25
PM0	1.98	TX	4.59
STANDBY	4.59	TXT	9.99

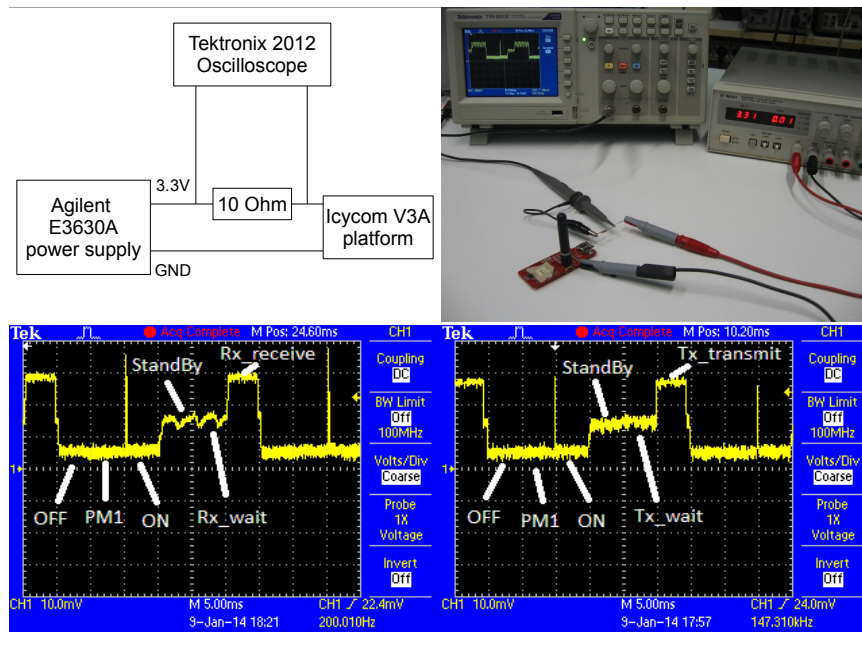


Figure 1.15: Energy consumption measurement setup.

1.5.2 Experimental Results

1.5.2.1 Low Power Listening

In the following experiments *monitoring application* and *random traffic* were considered, with $T_{PG} = 200$ ms, in a P2P topology. Payload size in range [20 and 100 byte] was used. Numerical results were achieved by averaging over 10.000 packets generated by EDs and transmitted towards the NC. The protocol performance was evaluated in terms of PLR, average delay, average energy consumed per data packet transmitted or received at transmitter and receiver side, respectively.

Regarding the comparison between '**on body**' and '**on table**' measurements, results are reported below. Fig. 1.16 reports the average packet delay as a function of the payload size in these two settings, while Table 1.2 reports comparison between energy consumed. It is clear that in case of '**on body**' measurements the transmitter will spend more energy, since the connectivity issues on the body make it harder to establish a communication with the receiver. The latter leads to a higher number of transmitted preambles. The average packet delay increases for the same reason.

Given that the performance trends of the two settings are the same, apart from the offset, and practical complications related to '**on body**' measurements, in the following only '**on table**' setting will be considered.

In order to understand how the performance can be tuned, several measurements with different parameters were performed. During the first set of measurements the value of T_W was varying while keeping T_{on} and T_P fixed, while in the second set of measurements, values of T_{on} and T_P were varying, keeping the value of T_W fixed.

Fig. 1.17 reports the average energy consumed per packet by the transmitter and

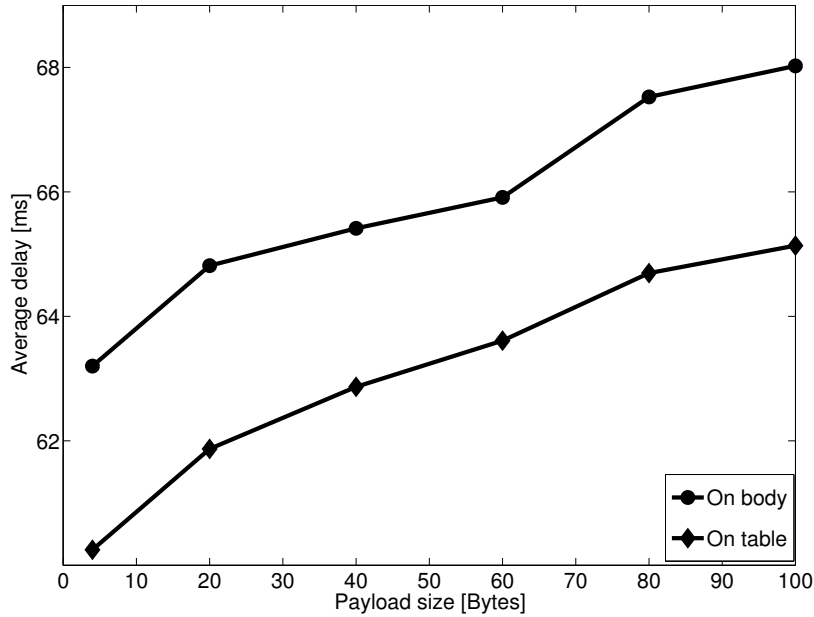


Figure 1.16: Average packet delay, 'on body' and 'on table' measurements.

Table 1.2: Average energy consumption of transmitter for 'on table' and 'on body' scenario

Payload size B	'On table' $\frac{\text{mJ}}{\text{packet}}$	'On body' $\frac{\text{mJ}}{\text{packet}}$
20	0.4600	0.4940
40	0.4740	0.5060
60	0.4800	0.5120
80	0.4890	0.5200
100	0.4930	0.5260

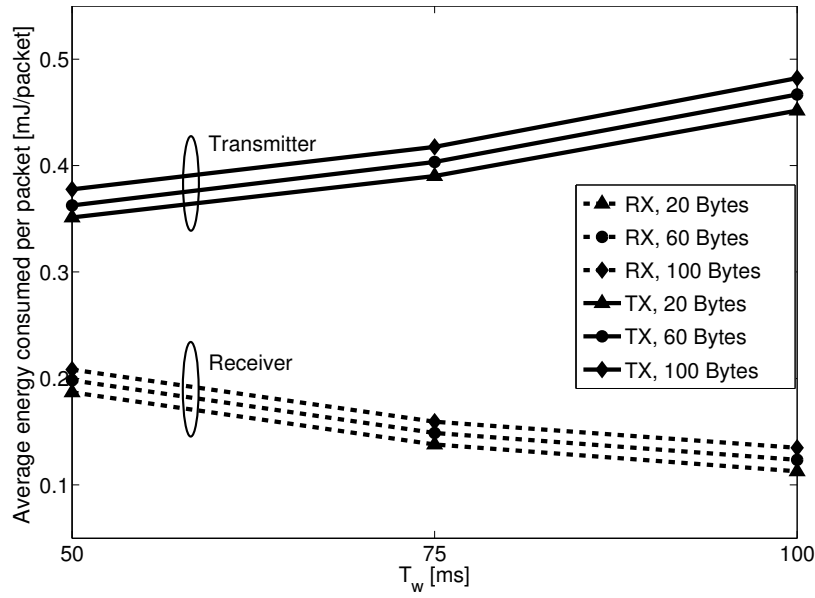


Figure 1.17: Average energy consumed varying T_w .

receiver, as a function of T_w , for different payload sizes and parameters T_{on} and T_P set to 5 and 3.5 ms respectively. Fig. 1.18 reports the average packet delay as a function of T_w for the same set of parameters. Energy consumed at the transmitter side increases with T_w , as expected, since the transmitter spends more time in the awake phase. On the other hand, the energy at the receiver side decreases with T_w , as the energy spent by the receiver does not depend on the number of preambles sent before the packet and since the duty cycle decreases with T_w . Regarding the delay, both average and maximum delay increase with T_w , because the transmitter finds the receiver in sleep state for longer intervals of time.

Fig. 1.19 reports the average energy consumed per packet by the transmitter and receiver as a function of T_{on} , having set $T_w = 100$ ms and payload size equal to 20 B. Theoretically, optimal performance is when T_P and T_{on} have the same value, but due to hardware constraints, an offset between them had to be introduced, in order

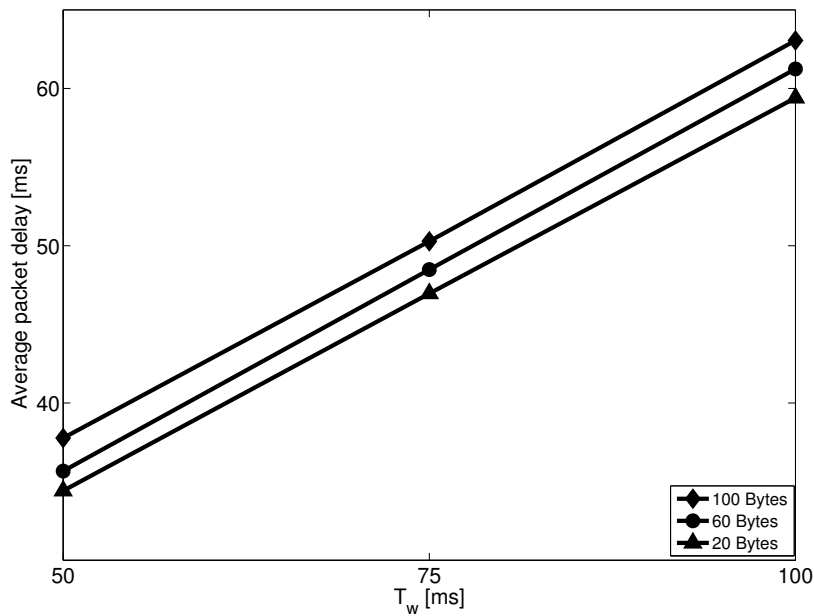


Figure 1.18: Average packet delay varying T_w .

to guarantee correct preamble reception. This offset is empirically determined to be 1.5 ms. Apart from the total energy consumed by the transmitter and the receiver, behaviour of different contributions of transmitter energy consumption is presented. TX_{random} is the random part of energy consumption, the one that accounts for all the preambles sent before data packet (Fig. 1.13, while $TX_{\text{deterministic}}$ accounts for the rest of the energy consumption. The deterministic part is increasing with T_{on} , because the listening duration increases both before the first preamble and during idle listening. The same is true for the total receiver energy. It can be seen that the random part decreases when increasing T_{on} because the average number of preambles sent before data packet (N_{mean}) decreases. However this dependence is not linear like the one for the deterministic part due to the fact that average number of preambles does not decrease linearly with T_{on} , as it is reported in Table 1.3. This implies the existence

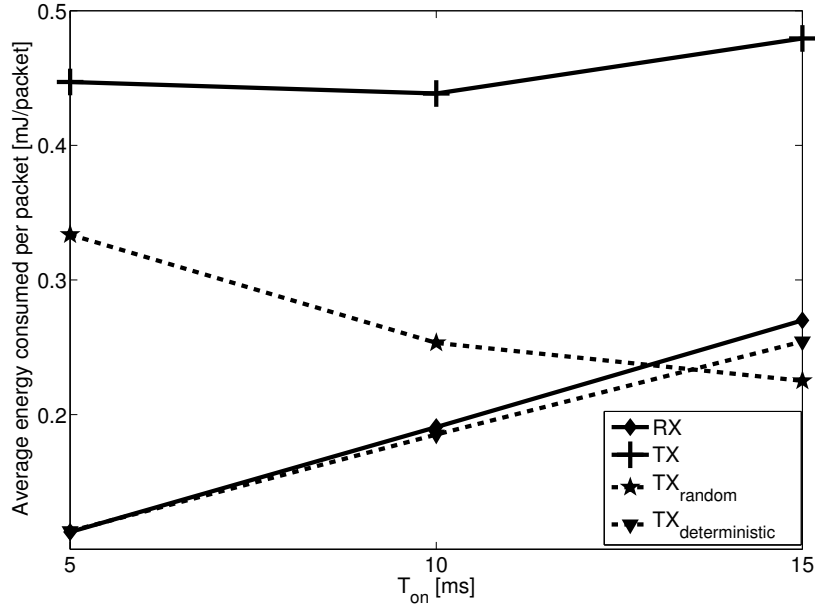


Figure 1.19: Average energy consumed varying T_{on}.

Table 1.3: Average number of preambles sent before data packet.

T _{on} [ms]	5	10	15
N _{mean}	15.11	6.39	4.27

of the minimum in the curve representing the total energy spent by the transmitter.

The delay is barely affected by the variation of these parameters, since it is primarily dependent on T_w.

Apart from P2P, star topology was investigated as well. The considered star topology network consisted of two or three EDs and a NC. In this network the node having a packet to be transmitted may find the channel busy, in which case it will backoff for a random interval of time uniformly distributed within the interval T_{BO}=[0-16]ms. Once this interval expires, the node will repeat the procedure as in

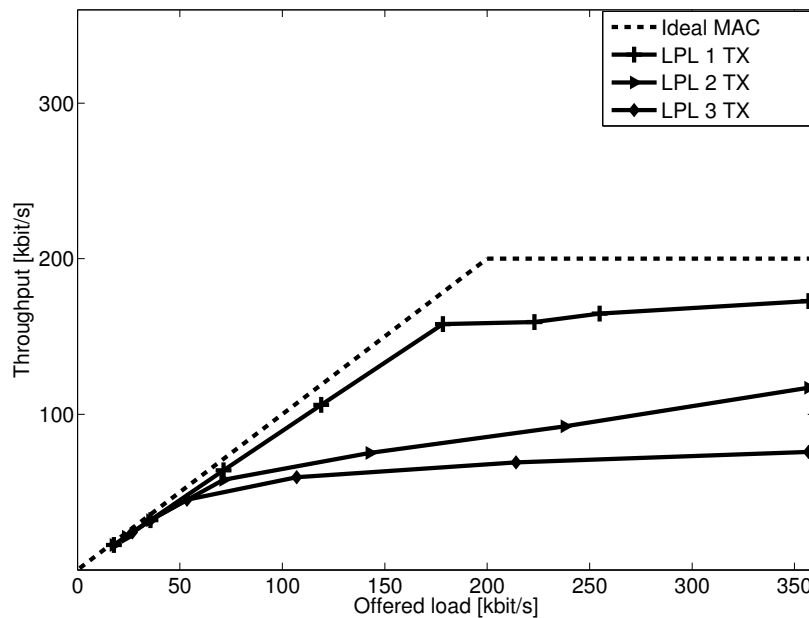


Figure 1.20: Network throughput in different star topologies.

the case of the first transmission attempt of the same packet. Due to this fact, both the average and the maximum packet delay increase with the number of transmitters, as it is reported in Table 1.4. The impact of the collision avoidance algorithm can be observed in the network throughput curves.

Fig. 1.20 reports the throughput, S , as a function of the offered load, G , in the scenarios with one receiver and one/two/three transmitters. We can see that for the low offered load three scenarios show similar performance. This is due to the fact that when the traffic is low nodes find the channel idle with high probability, which further implies that channel access mechanism will rarely be invoked. On the other hand, when the offered load is high, there is significant difference between the curves due to the back-off mechanism, which introduces intervals of time in which the resources, i.e., time, are not being used.

Table 1.4: Average and maximum packet delay.

	Point-to-Point	Star 2 TX	Star 3 TX
Average delay ms	60.97	103.96	179.56
Maximum delay ms	111.78	311.12	576.34

In all of the described experiments PLR was investigated as well. Since in all cases it was below 1%, no conclusions could be derived.

1.5.2.2 CSMA/CA IEEE 802.15.6

The setup for the following measurements is 'on table' setting and Star-3 network topology. *Monitoring application* was considered where *Periodic traffic* is used to evaluate the average packet delay and the PLR, while *random traffic* is used to evaluate the network throughput. In the case of *periodic traffic*, T_{PG} is equal to T_{SF} while in the case of *random traffic* different traffic intensities (T_{PG}) are considered.

Another important parameter is the superframe duration, T_{SF} , which is set to 200 ms. SF is composed of beacon period (5 ms), CFP (10 ms), CAP (60 ms) and inactive period (135 ms).

In the following figures, first the average delay is shown as a function of the payload size by considering different values of UP and number of RTXs.

Fig. 1.21 shows the average delay delay of each node, each one transmitting with a different user priority; the curves are related to the number of RTXs. Node 3, being the one with the highest UP, experiences the lowest average delay independently on the number of RTXs. Due to the lowest CW, it is always the first to successfully

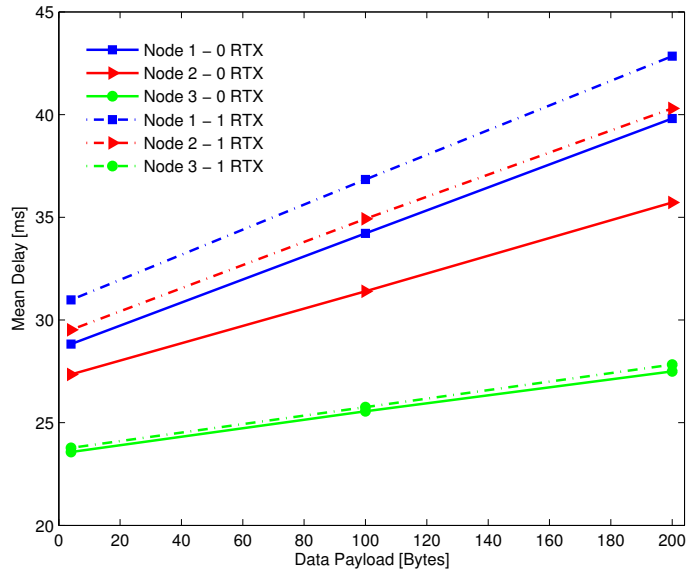


Figure 1.21: Average delay for a heterogeneous UP network.

access the channel. On the other hand Node 2 and Node 3 compete strongly to access the channel; therefore their mean delay significantly increase, with number of RTXs.

CW strongly impacts the performance, a larger CW will decrease the number of collisions but each node will wait on average longer to access the channel. This starts to be evident with a larger network, as it is shown in Fig. 1.22.

In order to see clearly how the CW value impacts the delay, it is useful to fix the number of devices in the network and show, in the same graph (see Fig. 1.23), the curves obtained with different values of the CW.

From the Fig. 1.23 we can see that, at 48 B payload size, the average delay coincides for each curve. It means that the value of the CW exactly counterbalances the effect of the average delay introduced by the backoff procedure and the delay introduced by collisions, meaning RTX. For a packet of a lower size, a higher CW value will result in

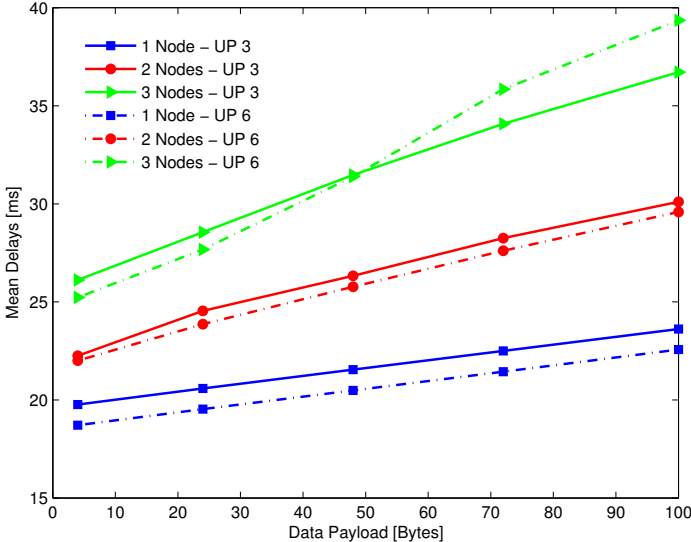


Figure 1.22: Average delay for different network sizes, all the nodes with the same UP.

an increasing waiting time before accessing the channel. In this case the probability to have a collision is lower and therefore also the delay introduced by RTXs will be lower. On the other hand this argument applies inversely when packets have a bigger size.

In Fig. 1.24 it is possible to analyse the impact that the number of RTXs and the CW has on the PLR behaviour as a function of the payload size. In particular an interesting result is that the PLR get worst for a number of RTXs lower than 2, being not possible to double the CW. Moreover the PLR has an almost flat behaviour: when the CAP is big enough to fit all the RTXs, the PLR coincides with the probability that at least two devices choose the same random back off value, and this is clearly independent from the payload size.

In the Fig. 1.25 the obtained results of throughput measurements are reported. It

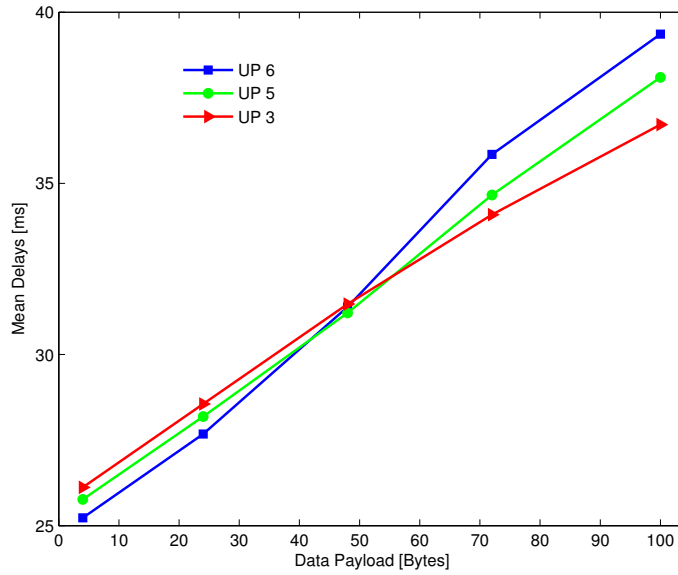


Figure 1.23: Average delay for a three nodes-network with the same UP.

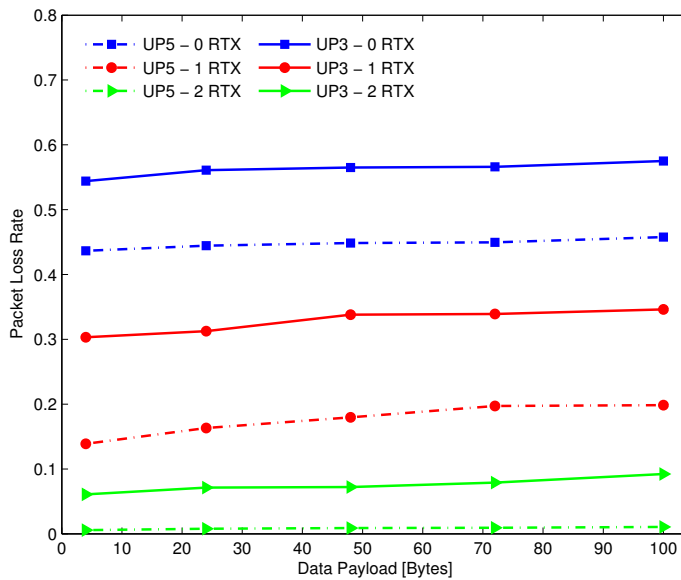


Figure 1.24: PLR for a three nodes-network with the same UP.

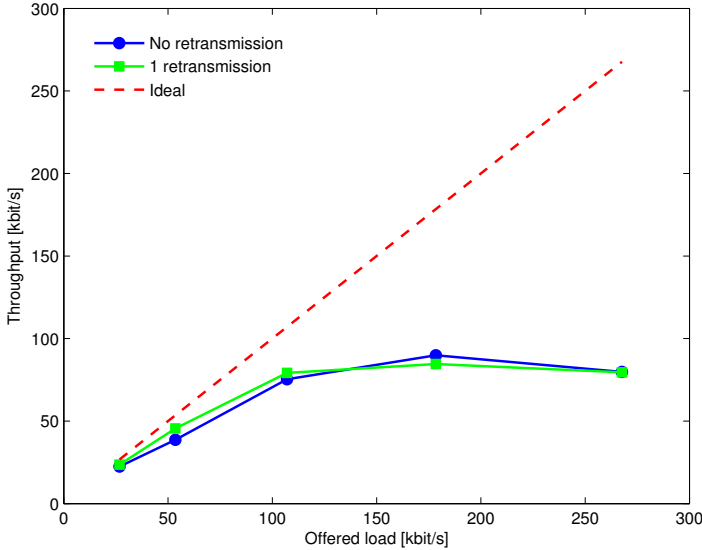


Figure 1.25: Network throughput for different RTX.

is possible to note that increasing the offered traffic above certain value ($\sim 170 \frac{\text{kbit}}{\text{s}}$) the achieved throughput distances itself considerably from the ideal MAC throughput. This is the effect of the saturation of throughput, thus the inability of network to handle a certain amount of traffic. In particular, when the offered load is very high, the resources are wasted in collisions and backoffs, such that the channel is successfully used only a fraction of time. In extreme cases, the channel might get 'congested' by a huge number of unsuccessful attempts, and the throughput gets lower with the offered load.

1.5.2.3 Comparison Between Protocols

In this section SF-based and LPL MAC are compared. The most important parameters of the two protocols are summarised in the Table 1.5. They were chosen such

Table 1.5: Parameters of SF-based and LPL MAC

SF-based		LPL	
Superframe duration	100 ms	T_S	95 ms
Beacon period	5 ms	T_{on}	5 ms
CAP duration	50 ms	T_P	3 ms
Inactive period	45 ms		

that the typical delay requirement (~ 100 ms) is met in both cases.

For these experiments **'on table'** setting is considered and a P2P network. The traffic is *query-based* and *random*. Packets sent by ED have a 100 B payload.

Fig. 1.26 presents the average energy consumption per hour as a function of a packet generation interval, T_{PG} , for the two considered protocols. Behaviour of the two protocols can now clearly be observed. In the case of SF-based MAC with CSMA/CA-based CAP the average energy consumption per hour is almost constant because vast majority of the energy is consumed in idle listening⁷ during CAP which is independent from packet generation interval and flattens the curve. On the other hand LPL suffers much less from idle listening. This makes T_{PG} significantly affect the energy consumption: the lower the traffic intensity, the lower the energy consumption. Namely, in the case of LPL, when there are no packets to transmit, duty cycle is only 5%, while in the case of IEEE 802.15.6 CSMA/CA it is 55%. This makes the increase in idle listening more significant in the case of IEEE 802.15.6 CSMA/CA.

To better illustrate the cause of different curve behaviour in Fig. 1.26, we report in

⁷Idle listening occurs when the device keeps the receiver on even if there is nothing to be received.

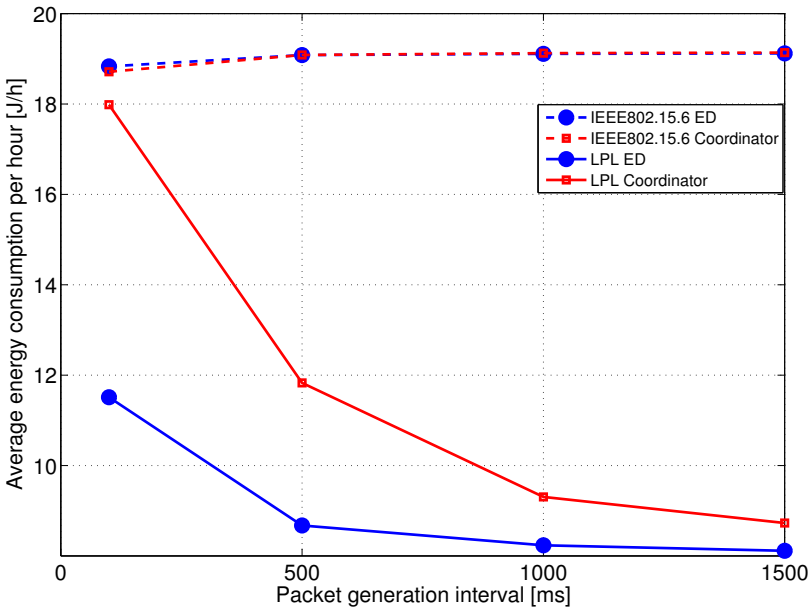


Figure 1.26: Average energy consumption per hour for SF and LPL MAC.
 [Average energy consumption per hour for SF-based and LPL MAC.]

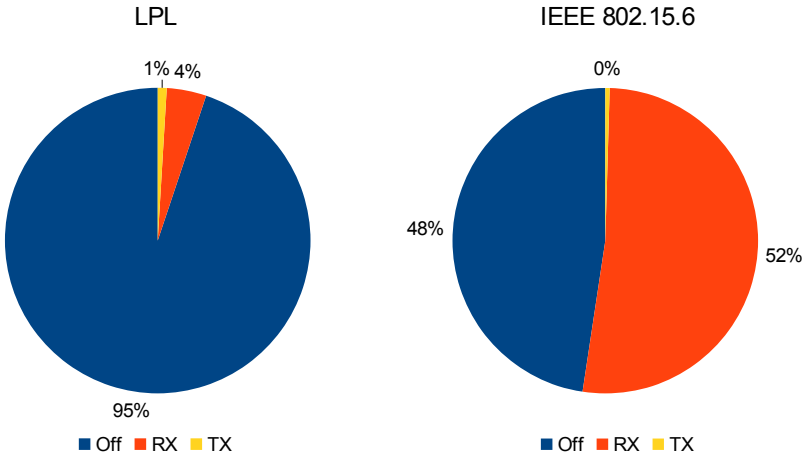


Figure 1.27: Time spent in different radio states for SF-based and LPL MAC.
 [Time spent in different radio states for SF-based and LPL MAC]

Fig. 1.27 the distribution of time the device spent in different radio states for the two protocols. For simplicity we grouped similar states into one more generic state. More specifically states OFF, PM0, and STANDBY become state OFF, states RX, RXR become state RX and states TX, TXT become state TX. The pie-charts clearly show the ability of LPL to mitigate idle listening with respect to IEEE 802.15.6 CSMA/CA. This quality is very appreciated when the traffic intensity is low, like in the case of many WBAN applications used for monitoring body parameters.

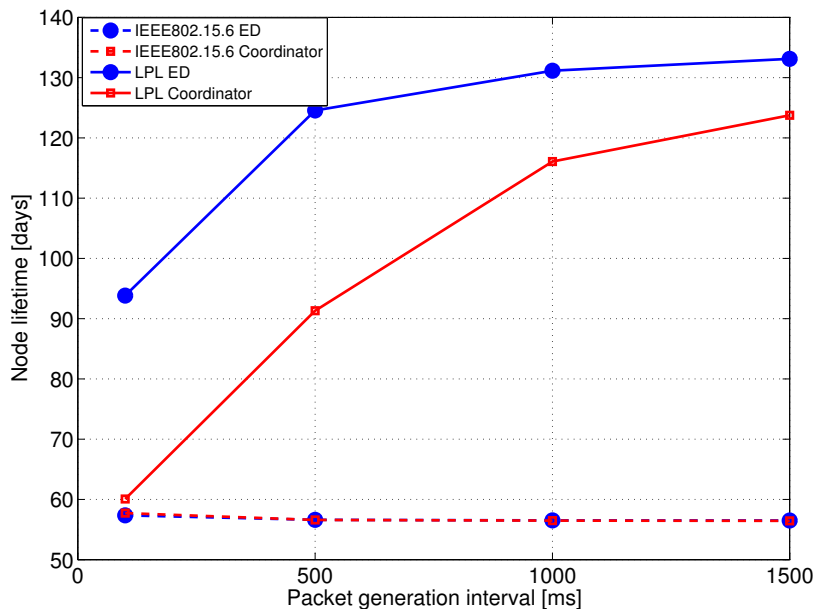


Figure 1.28: Node lifetime for SF-based and LPL MAC.

[Node lifetime for SF-based and LPL MAC.]

Starting from Fig. 1.26 and considering a battery with a given capacity we can estimate the node lifetime. In Fig. 1.28 we report the node lifetime as a function of the T_{PG} for the two considered protocols. It is derived from Fig. 1.26 considering a commercially available battery of 2.4 Ah capacity. We can see that with LPL

Table 1.6: Delay of SF-based and LPL MAC.

Protocol	Average delay ms	Maximum delay ms
LPL	61.0	111.8
SF	27.2	91.9

it is possible to achieve a lifetime double of the one achieved with IEEE 802.15.6 CSMA/CA. More precisely with the considered value for T_S and battery capacity, the lifetime is 130 days, this value can be further increased to meet the cardiac implant requirement by using a large battery and increasing T_S . In fact, it is the value of T_S that determines the magnitude of the latency. Moreover the fact that the cardiac implant is continuously polled by the coordinator every 1500 ms, is quite far from the reality. In a more realistic scenario the implanted device uses a larger value of T_S for most of the time, then, when waken-up by the coordinator, it can decrease T_S to a lower value imposed by the coordinator.

To show the low energy consumption does not come without consequences, performance in terms of packet delay is evaluated. Table 1.6 shows the average and maximum delay for the LPL and SF-based MAC. It can be seen that the SF-based MAC fulfils the requirement of 100 ms imposed on the packet delay from the the audio streaming application, while the maximum value obtained by the LPL MAC is grater than 100 ms. The average value of the latency is much smaller for the SF-based MAC than for the LPL MAC, this is mainly because of the transmission of preambles.

1.6 Conclusions

Communication protocols for WBANs need to satisfy a wide range of requirements, based on the specific use case. An IEEE standard, 802.15.6, is introduced to cope with this task, however most systems today are still using proprietary protocols. In the scope of a European project WiserBAN, a custom protocol stack was implemented. Particular attention was on its MAC and LLC layers. Given heterogeneous use cases, such as multimedia and implanted devices, the MAC modes were implemented, SF-based and LPL MAC. SF-based MAC is a synchronous protocol intended for use primarily in a high traffic scenario with multiple EDs. On the other hand, LPL MAC is an asynchronous protocol which offers great energy efficiency in a low traffic setting, but suffers from the lack of proper collision avoidance techniques.

In order to validate that the developed protocol satisfies the application requirements, a series of measurements were performed. First, results of the experimental campaign aimed at evaluating the two MAC modes separately was reported. The lessons learned are on how to tune the performance by setting protocol parameters. Trade-offs, such as average delay vs. average energy consumption in case of LPL or PLR vs. average delay in case of SF-based MAC are discussed and clear guidelines are given about what performance can be achieved and in which way. Second part was related to the comparison between the two MAC modes. Based on experimental results we can understand the expected lifetime of each mode, thus helping us understand the suitability of different protocols for different applications.

Chapter 2

Cooperative Communications in Wireless Body Area Networks

The previous chapter presented different approaches to the design of MAC protocols for WBANs. Although they have a big impact on the system performance, MAC protocols have their limits. To further improve the performance, novel paradigms are required. This chapter discusses the concept of *cooperative communications* in WBANs.

2.1 Introduction

MIMO systems are communication systems where terminals use multiple transmit and receive antennas to exploit multipath propagation. Systems with multiple antennas can exploit, besides the usual time and frequency, the spatial dimension, with large improvements in terms of diversity, interference mitigation and throughput. For this reason they are among the key technologies in modern wireless transmission systems.

The advantages of multiple antennas can be summarised in the following.

- Array gain; This is the increase in the average SNR at the receiver due to

Chapter 2. Cooperative Communications in Wireless Body Area Networks

coherent combination of signals. It can be obtained for both multiple transmit or multiple receive antennas, requiring Channel State Information at the Transmitter (CSIT) and Channel State Information at the Receiver (CSIR), respectively;

- Diversity gain; In the presence of fading, the received power level can present large variations. Diversity is used to reduce the variations of the SNR level due to fading, by sending each information symbol through different channels with independent fading levels, and then combining the outputs. In a $N_T \times N_R$ MIMO channel there are potentially $N_T \times N_R$ links. Spatial diversity can be obtained with multiple receiving antennas with CSIR (receive diversity), and with multiple transmit antennas (transmit diversity). Transmit diversity is possible both with CSIT (beamforming) and even in the absence of CSIT (Alamouti code [28], Space-Time Codes (STCs) [29]);
- Interference mitigation; Multiple antennas can be used as a spatial filter to reduce the power received from co-channel interfering sources. The enhanced robustness to co-channel interference increases the number of served users per unit area in wireless cellular systems;
- Spatial multiplexing; In MIMO channels with multipath it is possible to transmit up to $N_{\min} = \min\{N_T, N_R\}$ parallel streams over the same band, with an increase of the link throughput. Multipath multiplexing, also called spatial multiplexing, is not possible for Single Input Multiple Output (SIMO) or Multiple Input Single Output (MISO) channels.

Depending on the available Channel State Information (CSI), different combinations of the above mentioned advantages can be obtained. This is achieved through *weight vectors*. Weight vectors are complex vectors which are applied to the signal before transmission (in case of multiple transmit antennas) and/or after reception and before combining (in case of multiple receive antennas).

When communication terminals cannot be equipped with multiple antennas (as is the case with WBANs), cooperative MIMO technique (also known as virtual MIMO) could be exploited. Cooperative MIMO inherits most of the advantages of MIMO systems, with the difference that antenna elements are independent devices forming Virtual Antenna Arrays (VAAs). On one hand, this fact imposes additional overhead needed for establishing and maintaining VAAs. On the other hand, channel correlation, an issue often experienced by collocated MIMO systems, is almost surely absent, thus boosting diversity¹. Cooperative MIMO concept can be applied on WBANs, where devices on a body are equipped with a single antenna and where requirements in terms of reliability and energy efficiency are very stringent.

2.1.1 Related Works

Pioneer works in the field show that even though it introduces some communication overhead, cooperation among nodes increases reliability and reduces the total energy consumption [30]. To the author's knowledge, the first work suggesting the application of the MIMO concept on WBAN is [31], where it is shown that the use of MIMO significantly improves the channel capacity with respect to conventional systems. In this work cooperating nodes, deployed on the body, are assumed to be

¹Diversity gain can be limited by power imbalance, i.e., the fact that not all the links have the same power.

Chapter 2. Cooperative Communications in Wireless Body Area Networks

connected through wired links. Wireless communication among cooperative nodes is considered in [32], where results show that, apart from the increase of capacity, significant advantage can be obtained in terms of interference rejection. The application of cooperative MIMO on WBANs is further investigated in [33] where the authors develop a simple but effective cooperative diversity scheme for UWB-based WBAN.

As far as the study of MAC protocols for cooperative MIMO systems is concerned, [34] presents NetEigen, a protocol which does not only mitigate interference, but also maximises the desired received signal power. The latter effect is achieved by properly setting both transmitter and receiver weight vectors. Most recently, a cooperative scheduling framework that closely relies on NetEigen MAC has been proposed in [35]. Partner selection protocol for cooperative indoor-to-outdoor wireless access is presented in [36]. The protocol proposed in that work takes into account both pathloss and Rician K-factor as link quality metric and achieves a great increase in network lifetime. A network-coding-based cooperative ARQ MAC protocol is presented in [37]. The scheme proposed in that work achieves better energy efficiency with respect to state of the art protocols without compromising the offered QoS. A good overview of MAC protocols for cooperative communication systems is given in [38].

It is worth noting that cooperative beamforming implies additional transmit power constraints with respect to standard beamforming. Since each element is an actual device with its own power amplifier, a constraint on transmit power of each element needs to be imposed. It is well known that this limits the performance gain achieved by the standard beamforming, but still provides great advantage over Single Input Single Output (SISO) case [39].

2.1.2 Thesis Contribution

In contrast with the previous works, this thesis presents BAN Multiple Input Multiple Output (B-MIMO), a cooperative MIMO scheme envisaged for WBANs. B-MIMO applies cooperative beamforming to WBANs, by optimising the number of cooperating nodes according to their channel conditions. Due to the heterogeneity of the WBAN channel, nodes experience very different behaviours. Nodes shadowed by the body need to cooperate to reach the requested SNR, while nodes in good channel condition may not benefit from the cooperation with nodes that suffer from bad channel quality. B-MIMO reduces the number of cooperating nodes, depending on channel status, with the objective of reducing the energy consumption as well as the level of interference.

B-MIMO is applied to an indoor scenario where different bodies have data to transmit to a selected sink. Realistic settings, including nodes distribution and channel model, are considered. The proposed solution is compared to a non-cooperative system and a cooperative MIMO solution, where all nodes in the WBAN cooperate and no selection is applied. Results show that the proposed technique improves the performance in terms of energy efficiency, and also in terms of BLER when the system is interference-limited. Performance is evaluated by considering different well-known scheduling strategies: *maximum throughput*, *proportional fairness* and *round robin*. The design of a novel scheduling strategy is out of the scope of this thesis.

The rest of this chapter is organised as follows. Sec. 2.2 introduces the reference scenario and the channel model. The communication protocol and the cooperative MIMO scheme based on beamforming are described in Sec. 2.3. Sec. 2.4 motivates the need for new cooperation schemes and formalises the problems to be solved. Sec. 2.5

describes the proposed B-MIMO scheme while Sec. 2.6 briefly presents the well-known scheduling algorithms considered in the paper. Numerical results and conclusions are reported in Sec.s 2.7 and 2.8, respectively.

2.2 Reference Scenario and Channel Model

An indoor environment is considered (i.e., a hospital room) with several people (patients) inside (see Fig. 2.1). Each patient is equipped with a WBAN consisting of three nodes placed on left hip, heart and right ear. The nodes located on the body have data to transmit towards the sinks. Cooperative beamforming is used to transmit data towards a sink. Sinks, with multiple antennas, are placed on the walls of the room. Bodies, represented by elliptical cylinders in 3D, are located in random positions and with random orientations in the area.

Human body is a very specific propagation environment where body shadowing plays a major role. In order to properly account for the propagation environment, the channel model based on an extensive measurement campaign presented in [40] is used. In [40] measurements are performed in an indoor laboratory furnished with tables, chairs and some general equipment such that the model captures the effects of a real environment. The identified model is the most suitable for our scenario, since it is based on measurements performed by locating nodes exactly in the same positions considered in this work.

According to [40] the channel attenuation can be modelled as:

$$P(d, \alpha)|_{dB} = G_0(d)|_{dB} + S(\alpha)|_{dB} + F|_{dB} , \quad (2.2.1)$$

where d is the distance between the transmit node on body and the sink, α is the

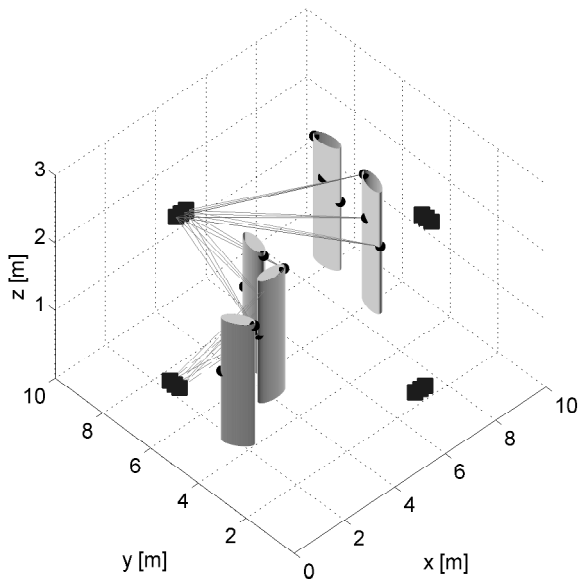


Figure 2.1: Scenario 3D.

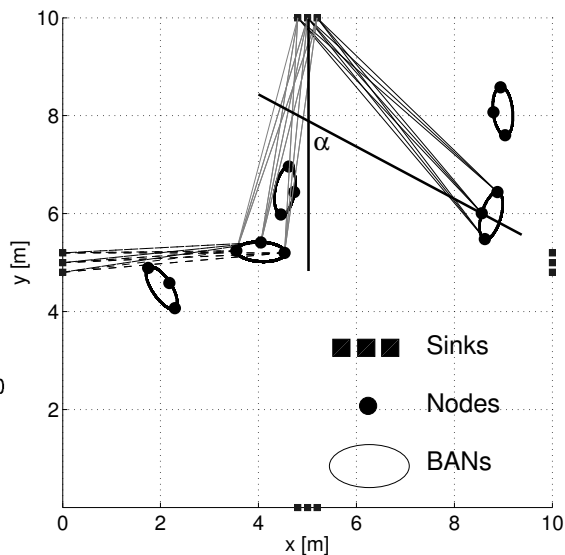


Figure 2.2: Scenario 2D.

relative angle between the body and the sink (see Fig. 2.2), $G_0(d)$ is the mean channel gain, $S(\alpha)$ is the body shadowing component of the channel transfer function, F is its fading component. For more information on the channel model and the relevant parameters, refer to [40]. A fixed 20 dB loss is applied when the signal passes through a body. As for the on-body communication, it is assumed that all nodes may communicate among them without losses by employing techniques presented in [41] and [42].

2.3 Communication Protocol

It is assumed that:

- a wired connection among sinks is present, such that they can maintain synchronisation;

Chapter 2. Cooperative Communications in Wireless Body Area Networks

- time is divided into frames, starting with a query sent by the sink(s).

Upon reception of queries each WBAN will associate to the strongest sink and the association is announced by short packets transmitted by each node in the WBAN. Considering that a CSMA-based protocol is used and the small size of packets, it is safe to consider lossless communication in this phase. The importance of this step is twofold:

- each sink will know how many WBANs are associated to it;
- each sink can estimate the uplink channel for each WBAN associated to it.

Frames are divided into time slots, assigned by each sink to the WBANs associated to it. Once a sink defines the schedule, at the beginning of each time slot, it will poll the WBAN which is scheduled to transmit in that time slot. Poll packets include previously computed channel estimation and the target source (one out of the three nodes, randomly selected by the sink). Once the source node receives the poll, it computes the beamforming weight vector (based on the full channel estimated by the sink) and it transmits a broadcast packet, containing the beamforming weights and the data to be transmitted, to the cooperating nodes. This packet is also used for synchronisation, and it is followed by the cooperative data transmission towards the sink.

Let's consider a cooperative MIMO scheme and take into account the fact that each antenna element has its own transmit power limitations. In the following, the number of antennas at the useful transmitter is denoted by $N_T^{(0)}$, the number of antennas at the receiver is denoted by N_R and the number of antennas of interferer i

is $N_T^{(i)}$. Received signal, when affected by N_{int} interferers, can be expressed as²:

$$\mathbf{y} = \mathbf{H}^{(0)} \boldsymbol{\alpha}^{(0)} x^{(0)} + \sum_{i=1}^{N_{\text{int}}} \mathbf{H}^{(i)} \boldsymbol{\alpha}^{(i)} x^{(i)} + \mathbf{n} \quad (2.3.1)$$

where $\mathbf{y} \in \mathcal{C}^{N_R \times 1}$ is a vector, $x^{(i)} \in \mathcal{C}$ is the input symbol of transmitter i , $\mathbf{H}^{(i)} \in \mathcal{C}^{N_R \times N_T}$ is the channel gain matrix between transmitter i and the receiver, $\boldsymbol{\alpha}^{(i)} \in \mathcal{C}^{N_T \times 1}$ is the weight vector of transmitter i , and $\mathbf{n} \in \mathcal{C}^{N_T \times 1}$ is the thermal noise vector. It is assumed that $\mathbb{E}\{\mathbf{n} \cdot \mathbf{n}^H\} = \sigma_n^2 \mathbf{I}$, where σ_n^2 is the thermal noise power per antenna element. The output symbol after the linear combiner at the sink can be expressed as

$$z = \mathbf{w}^H \mathbf{H}^{(0)} \boldsymbol{\alpha}^{(0)} x^{(0)} + \sum_{i=1}^{N_{\text{int}}} \mathbf{w}^H \mathbf{H}^{(i)} \boldsymbol{\alpha}^{(i)} x^{(i)} + \mathbf{w}^H \mathbf{n} \quad (2.3.2)$$

where $\mathbf{w} \in \mathcal{C}^{N_T \times 1}$ is the weight vector of the receiver. Consequently, SNR and Signal to Interference Ratio (SIR) are given by

$$SNR = \frac{P_t^{(0)} |\mathbf{w}^H \mathbf{H}^{(0)} \boldsymbol{\alpha}^{(0)}|^2}{\sigma_n^2} \quad (2.3.3)$$

$$SIR = \frac{P_t^{(0)} |\mathbf{w}^H \mathbf{H}^{(0)} \boldsymbol{\alpha}^{(0)}|^2}{\sum_{i=1}^{N_{\text{int}}} P_t^{(i)} |\mathbf{w}^H \mathbf{H}^{(i)} \boldsymbol{\alpha}^{(i)}|^2}, \quad (2.3.4)$$

where $P_t^{(0)}$ and $P_t^{(i)}$ are the total transmit power of the useful transmitter and interferer i respectively. In the case of collocated MIMO beamforming, the method for computing the transmit weight vector which optimises SNR is well known and presented in [43]. In order to properly account for the fact that antennas are distributed and not collocated, the following constraint on the transmit power of each element is imposed

$$|\alpha_j^{(i)}|^2 = \frac{1}{N_T^{(i)}}, \quad i = 1, 2, \dots, N_{\text{int}}, \quad j = 1, 2, \dots, N_T^{(i)} \quad (2.3.5)$$

²The following notation is used: $\mathbf{I} \in \mathcal{C}^{N_T \times N_T}$ is the identity matrix, $\mathbb{E}\{\cdot\}$ denotes expectation, and $\{\cdot\}^H$ denotes the conjugate transpose.

Chapter 2. Cooperative Communications in Wireless Body Area Networks

which means that all cooperating devices, equipped with their own power amplifiers, have the same transmitted power, i.e., power allocation strategies cannot be applied. Transmit weight coefficients can thus only affect the signal phase, ensuring constructive summing at the receiver.

Unfortunately, the presence of the constraint (2.3.5) makes the problem of the optimisation of vectors \mathbf{w} and $\boldsymbol{\alpha}^{(i)}$ very cumbersome. As a consequence, some sub-optimal techniques are generally applied. In particular, the algorithm for the evaluation of the transmit and receive weight vectors presented in [39] is used.

In order to make a comparison between the previously described cooperative system and a non-cooperative one, the following scheme is considered. A single sink is present in the area under observation with antennas placed in the same positions as in multi-sink case (all antennas in Fig. 2.2 belong to the same sink). As in the previously described system, at the beginning of each frame, the sink sends a query to which each node of each WBAN responds with a short packet. Upon reception of query responses, the sink estimates the uplink channel of all nodes in the scenario. Source nodes, one per WBAN per slot, transmit data towards the sink without cooperation. This means that the number of transmitted packets in a slot is equal to the number of WBANs in scenario, denoted as N_{WBAN} . It is assumed that the schedule of transmissions is known at the sink, e.g., nodes of a WBAN transmit in ascending order of their addresses. Since the sink knows the uplink channel, it can employ Zero Forcing (ZF) to separate transmissions of different nodes. Considering $\mathbf{x}^{N_{\text{WBAN}} \times 1}$ to be the vector of transmitted data, received signal vector in each slot can be expressed as

$$\mathbf{y} = \mathbf{H}\mathbf{x} + \mathbf{n} \quad (2.3.6)$$

where \mathbf{H} represents the channel matrix between all the sink antennas and all the nodes transmitting in the current slot. ZF implies

$$\mathbf{z} = (\mathbf{H}^H \mathbf{H})^{-1} \mathbf{H}^H \mathbf{y} = \mathbf{x} + (\mathbf{H}^H \mathbf{H})^{-1} \mathbf{H}^H \mathbf{n} \quad (2.3.7)$$

where $\mathbf{z}^{\text{NBAN} \times 1}$ is the vector of combined signals. As it can be seen, the interference is cancelled out, but the system performance still depends on channel conditions of each node. On one hand, this scheme introduces less overhead with respect to the cooperative MIMO, since there is no signalling within WBANs. On the other hand, there is no transmit diversity.

The analysis of MIMO ZF-based system performance is out of the scope of this thesis and it is introduced merely for benchmarking against cooperative system.

2.4 Problem Statement

Due to the heterogeneity of the channel, nodes of the same WBAN can achieve very different performance. To illustrate the previous consideration, Fig. 2.3 presents the Cumulative Distribution Function (CDF) of SNR achieved by nodes placed in the three different on-body positions considered in this thesis. It can be seen that performance strongly depends on the position of a node. Moreover, if a channel model typical for WSNs would be considered, the nodes would achieve not only similar performance but also the SNR at the considered distances would be much higher, both of the effects originating from the lack of the dominating shadowing component. The latter motivates the need for analysing WBAN scenario separately from the WSN scenario.

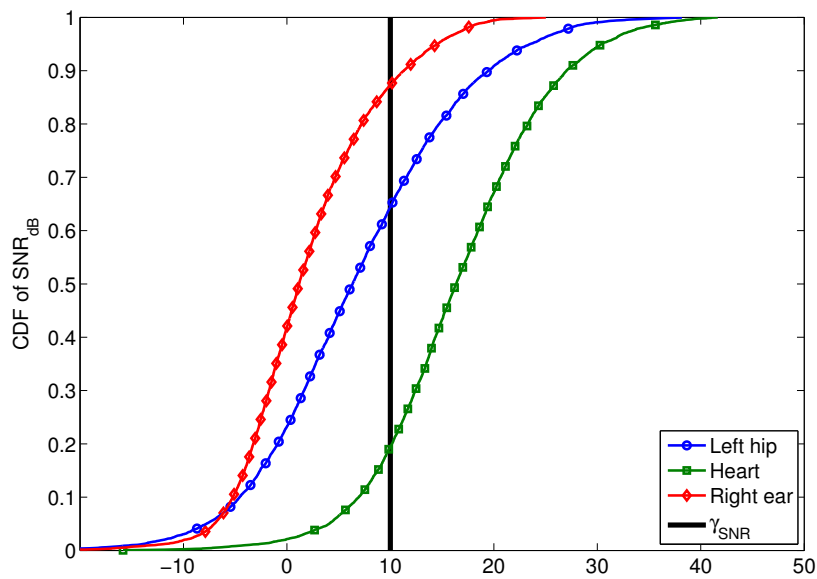


Figure 2.3: CDF of SNR for nodes placed in different positions on body.

A solution of the problem of performance heterogeneity can be solved by cooperation among nodes: nodes experiencing bad channel conditions can cooperate with other nodes, to reach the requested QoS. On the other hand, when the source has good channel conditions, cooperation with nodes having a bad channel could be useless. In fact, nodes experiencing a bad channel do not contribute significantly to the power received by the destination sink, while they may cause significant interference towards other sinks. The other drawback is that energy is wasted for a transmission which makes a negligible positive or even negative impact on the overall performance. Questions on which this thesis sheds some lights are:

- *how to select cooperating nodes?*
- *how much can the system benefit from proper node selection?*

2.5 B-MIMO

As an answer to the node selection problem, B-MIMO is introduced. B-MIMO is a cooperation scheme where each node will participate in the cooperative transmission only if its contribution to the overall power received by the intended destination is above a given threshold, denoted as χ . Each node can compute its contribution once the poll packet, containing the channel estimation, is received. According to [39], in order to compute its transmit weight, each node needs to compute also the receive weight vector of the sink. Given the channel estimation and the receiver weight vector, an 'equivalent' MISO channel, $\tilde{\mathbf{h}}^{(0)}$, can be estimated

$$\tilde{\mathbf{h}}^{(0)} = \mathbf{w}^H \mathbf{H}^{(0)}. \quad (2.5.1)$$

In order to quantify the individual contribution to the overall received power of each node, we define the ratio ψ_i as

$$\psi_i = \frac{\tilde{h}_i^{(0)} \alpha_i^{(0)}}{\tilde{\mathbf{h}}^{(0)} \boldsymbol{\alpha}^{(0)}}, \quad i = 1, 2, \dots, N_T^{(0)} \quad (2.5.2)$$

Therefore, if ψ_i is larger than χ , node i will cooperate with the source, otherwise it will not participate in the transmission towards the sink.

The method for selecting the value of parameter χ will be described in section 2.7.

2.6 Scheduling algorithms

The proposal of a new scheduling algorithm is out of the scope of this thesis and three well-known algorithms are considered to schedule transmissions from WBANs connected to the same sink: *maximum throughput*, *proportional fair* and *round robin*.

Chapter 2. Cooperative Communications in Wireless Body Area Networks

The goal of the first one is to maximise the overall network throughput, disregarding the fairness. *Proportional fair*, on the other hand, tends to equalise the throughput among all the WBANs associated to the same sink, thus maximising Jain index, which represents a measure of fairness [44]. *Round robin* is the most simple scheduling algorithm in which all WBANs get the same number of time slots, disregarding any performance or fairness metric. All three algorithms can be modelled using the same mathematical formula. Suppose that in each time slot weight coefficient can be assigned to each WBAN. Each sink will assign the next time slot to the WBAN having the highest weight. Weight of user i in slot k is given by:

$$W_{i,k} = \frac{x_{i,k}^\alpha}{\left(\sum_{j=1}^k x_{i,j}\right)^\beta} \quad (2.6.1)$$

where $x_{i,k}$ is the estimation of performance achieved by user i if slot k is assigned to it, and α, β are coefficients defining the behaviour of the scheduling algorithm.

Achievable rate, given by $R = \log_2(1 + \text{SNR}) \left[\frac{\text{bit}}{\text{s Hz}}\right]$, is chosen as the performance metric to be used by the scheduling algorithm. The achievable rate is estimated by sinks without taking interference into account since sinks can estimate SNR but cannot predict the interference. By setting $\alpha = 1$ and $\beta = 0$, the weight coefficient depends only on the nominator. This means that the slot will be assigned to the user that might achieve the best performance, which leads to *maximum throughput* algorithm. On the other hand, if $\alpha = 0$ and $\beta = 1$, the slot will be assigned to the user achieving the least throughput in the current frame, thus leading to *proportional fair* algorithm. By setting both $\alpha = 1$ and $\beta = 1$, equal importance is given to the numerator and denominator. In the considered scenario, where channel is fixed during a frame, the latter brings to *round robin* scheduling algorithm. Fine tuning

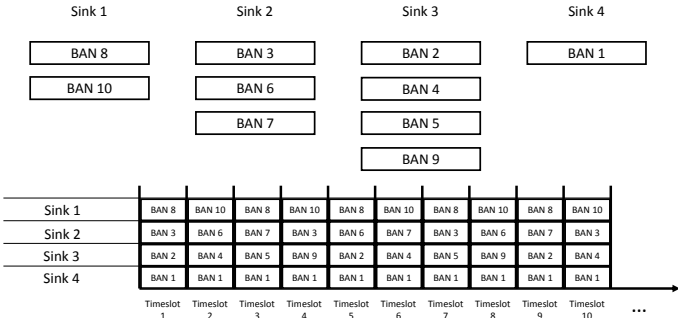


Figure 2.4: Scheduling scheme - example of *round robin*.

can be done by making different combinations of values of α and β .

Each sink schedules transmissions disregarding the schedule of other sinks. Consequently, there might be interference among WBANs associated to different sinks. The communication among sinks is limited to synchronisation maintenance.

An example of *round robin* is shown in Fig. 2.4.

2.7 Numerical results

In this section, first, metrics for performance evaluation are introduced, then some guidelines for setting parameter χ are provided and finally system performance, when different scheduling algorithms and cooperation schemes are employed, are compared.

Results have been obtained through a proprietary simulator, written in C++. A simulation round represents one frame which consists of one hundred time slots. In each round WBANs position and orientation are randomly and uniformly distributed in the observed area. Results are obtained averaging over 10000 rounds. Unless stated

Chapter 2. Cooperative Communications in Wireless Body Area Networks

Table 2.1: Simulation parameters.

Parameter	Value	Parameter	Value
P_T	0 dBm	Slot duration	8 ms
σ_n^2	-110 dBm	Frame duration	800 ms
γ_{SNR}	10 dBm	Packet size	1 kB
γ_{SIR}	3 dBm	Bitrate	1 $\frac{\text{Mbit}}{\text{s}}$
N_T	3	Square room side	10 m
N_R	3	Body height	180 cm
χ	5%	Sink height	120 cm

otherwise, parameters used in simulations are given in Table 2.1.

2.7.1 Performance Metrics

Performance is evaluated in terms of BLER, that is the percentage of packets (i.e., blocks of bits) generated by the different WBANs which are not received correctly by the destination sink. BLER is determined based on SNR and SIR: if during transmission both, SNR and SIR, are above two given thresholds γ_{SNR} and γ_{SIR} , respectively, the packet is considered to be successfully received, otherwise the packet is lost.

Energy efficiency, η [$\frac{\text{bit}}{\text{sJ}}$], is also evaluated. Energy efficiency can be defined as the average number of bits per second received by the sinks, per Joule of energy spent. Since the overhead generated in the network in order to establish the VAAs and to

perform the beamforming transmission is the same for all the cooperative strategies and scheduling algorithms, only the energy spent in cooperative data transmission is considered.

Another considered metric is network throughput S [$\frac{\text{bit}}{\text{s}}$], defined as the amount of useful and non-redundant information successfully received by sinks per unit of time. It is a metric proportional to BLER and the amount of generated traffic in the network.

2.7.2 The Impact of the Threshold χ

In section 2.5 parameter χ , representing the threshold for the individual contribution of each node to overall received power at the sink, is introduced. Increasing χ lowers the number of nodes participating in cooperative transmission, meaning lower transmit power per WBAN. The effect of the reduction of transmitting nodes is twofold: the number of packets lost due to low SNR increases but the number of packets lost due to low SIR decreases, because the interference power is lower as well. Since the considered scenario is mostly noise-limited, the overall effect is that the BLER value is slowly growing with χ (see Table 2.2). On the other hand, the energy consumption per WBAN decreases since the transmit power is lower. Energy efficiency takes into account both BLER and energy consumption. The latter is the dominant factor as it can be seen in Fig. 2.5 which shows the energy efficiency as a function of χ .

In the following, χ is set to 5%, since further increasing χ keeps energy efficiency almost constant, while causing BLER to rise.

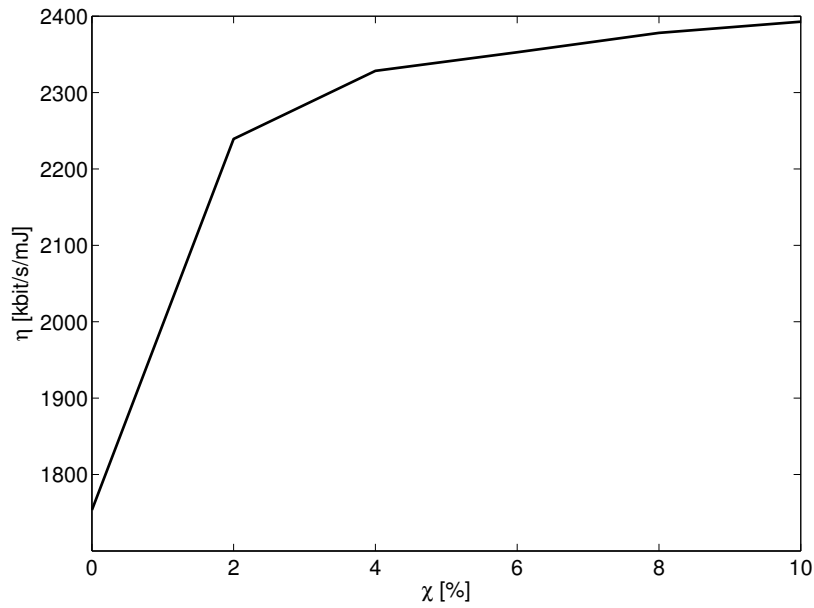


Figure 2.5: Energy efficiency as a function of the threshold χ .

Table 2.2: BLER for different values of parameter χ .

χ	0	2%	4%	6%	8%	10%
BLER	0.2817	0.2950	0.3025	0.3108	0.3148	0.3193

2.7.3 B-MIMO versus non-cooperative system

Following results were obtained considering *round robin* scheduling algorithm.

Fig. 2.6 reports the energy efficiency achieved by B-MIMO and a non-cooperative ZF-based system as a function of number of WBANs in the scenario, denoted as N_{BAN} , and two levels of transmit power. Since the increasing number of bodies in the room decreases the probability that there is a line of sight link between the transmitting node and the sink, BLER increases with N_{BAN} . This effect is more evident when the transmit power is low ($P_T = 1 \text{ mW}$) because in that case, line of sight connection is required for successful communication. Transmit diversity, introduced by cooperation, prevents BLER from increasing rapidly with N_{BAN} , thus making B-MIMO more energy efficient than the non-cooperative solution. In both cases, using lower levels of transmit power is more energy efficient since improvement in terms of BLER is not sufficient to counter-balance the increase in power consumption.

However, the fact that the number of simultaneous transmissions is limited by the number of sinks makes throughput achieved by B-MIMO saturate fast (see Fig. 2.7). On the other hand, the number of simultaneous transmissions in ZF-based system is limited by the number of sink antennas. If the transmit power is high enough, such that few packets are lost, this system is capable of achieving high throughput.

2.7.4 B-MIMO versus Cooperative MIMO

Fig. 2.8 shows BLER as a function of number of WBANs in the scenario, denoted as N_{BAN} . Both cooperative MIMO and B-MIMO schemes are considered when the three previously described scheduling algorithms are employed. The *maximum throughput*

Chapter 2. Cooperative Communications in Wireless Body Area Networks

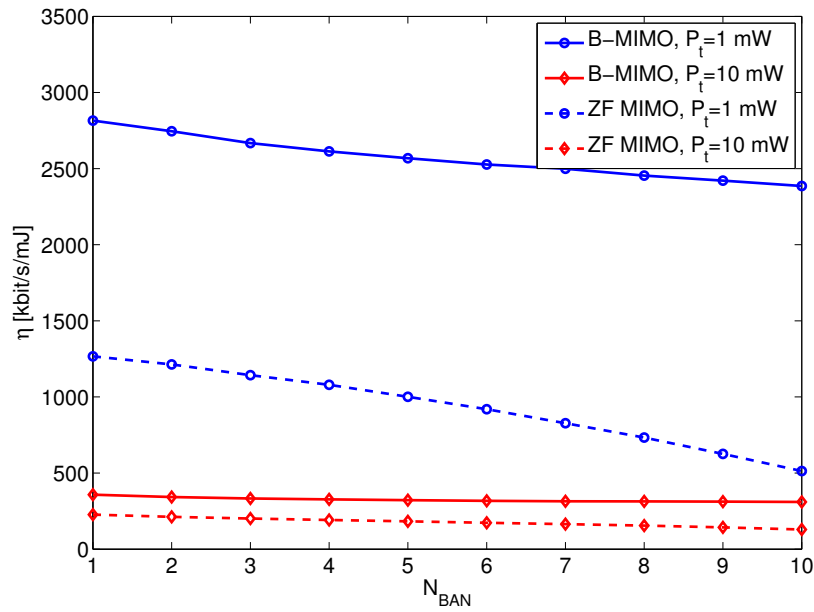


Figure 2.6: Energy efficiency of B-MIMO and the non-cooperative system.

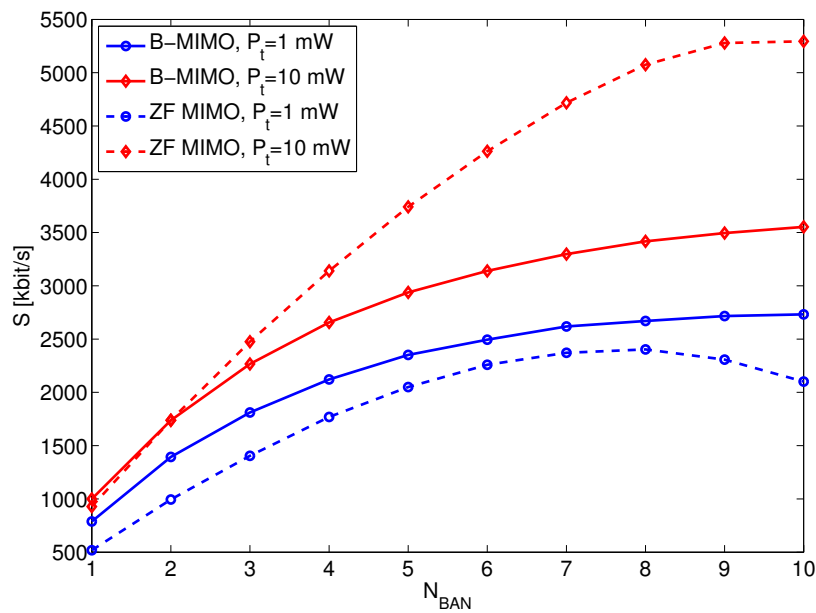


Figure 2.7: Throughput of B-MIMO and the non-cooperative system.

algorithm offers the best performance in terms of BLER, which is expected since sinks will assign all the slots to the WBAN having the best link quality, thus overall BLER of the system will be equal to the one of the best performing WBAN. As the number of WBANs increases, the variety of link qualities increases, meaning that the probability that at least one WBAN has a good connection with its sink is higher. The latter justifies the decreasing trend of BLER with N_{BAN} . In the case of *proportional fair* if a WBAN is performing badly, it will be assigned more slots in order to 'catch up' with other WBANs. The latter implies that if there is at least one WBAN with a bad link to its sink, it will be assigned most of the slots in the frame, thus causing an increase in BLER. *Round robin* represents an intermediate solution, where BLER slightly increases with N_{BAN} due to the increasing level of interference. In such scenario, cooperative MIMO outperforms B-MIMO in terms of BLER, since less power is transmitted in the B-MIMO and the system is mostly noise-limited, therefore the advantage of B-MIMO over conventional cooperative MIMO vanishes.

On the other hand, B-MIMO outperforms cooperative MIMO in terms of energy efficiency because the energy saved due to lower transmit power is more significant than performance loss in terms of BLER. The latter is presented in Fig. 2.9, where energy efficiency is shown as a function of N_{BAN} .

Since the energy consumption is independent on scheduling algorithm, the energy efficiency of different scheduling algorithms depends only on the BLER. Having taken into account the previous statement, the best performance is achieved by *maximum throughput* algorithm since it achieves the lowest BLER. On the other hand BLER of *round robin* and *proportional fair* is increasing with the number of WBANs in scenario, which brings to the inverse behaviour of the energy efficiency curves.

Chapter 2. Cooperative Communications in Wireless Body Area Networks

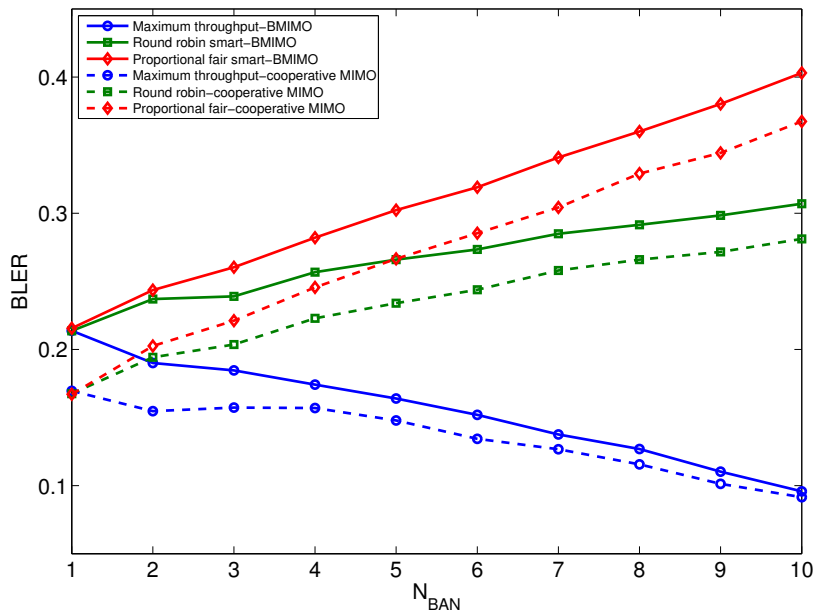


Figure 2.8: BLER for different scheduling algorithms and cooperation schemes.

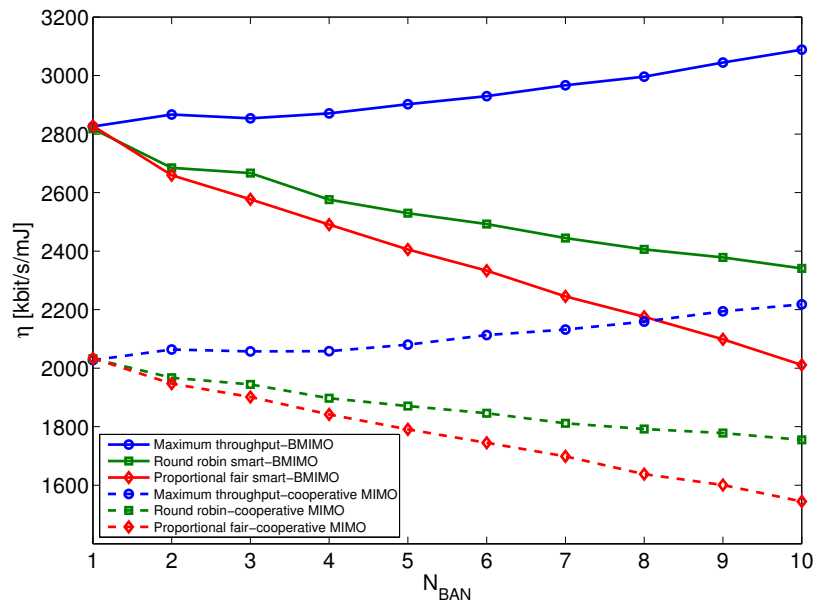


Figure 2.9: Energy efficiency of different scheduling algorithms and cooperation schemes.

It is worth noting that even though maximum throughput offers the best performance in terms of both BLER and energy efficiency, it is the least fair scheduling algorithm: its Jain index is the minimum possible. On the other hand, proportional fair maximises this metric at the cost of higher BLER and lower energy efficiency.

In order to consider an interference-limited system, the transmit power is set to 10 *dBm* and the noise power to -120 *dBm*, such that no packets are lost due to low SNR, i.e., losses are only due to low levels of SIR. Note that in the presence of more sinks (i.e., more WBANs transmitting at the same time), the scenario can become interference-limited, even if the receiver is characterised by a larger noise power.

Fig. 2.10 presents BLER as a function of the number of WBANs in an interference-limited scenario. First we can note that all the three scheduling algorithms have similar behaviour. This is explained by the fact that the scheduling is based on SNR which is not the dominant metric for BLER performance in an interference-limited scenario. *Maximum throughput* is still performing the best, since WBAN with the highest useful signal power has higher probability of having good SIR, while *proportional fair* and *round robin* achieve almost the same performance.

An interesting fact is that by employing B-MIMO we achieve not only better energy efficiency, but also a noticeable performance gain in terms of BLER over cooperative MIMO, due to lower generated interference. The conclusion is that apart from energy savings, B-MIMO systems can achieve performance improvement in interference-limited scenarios.

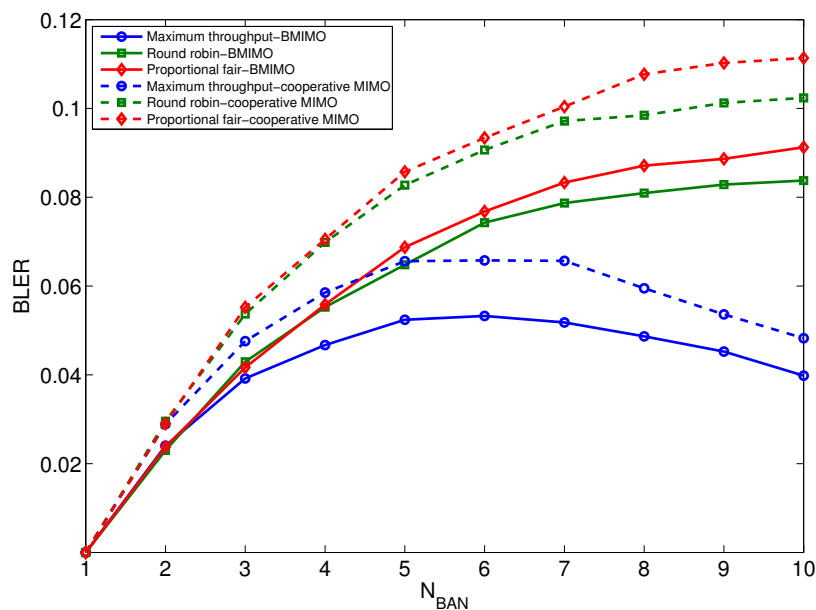


Figure 2.10: BLER for different scheduling algorithms and cooperation schemes in interference-limited scenario.

2.8 Conclusions

Owing to the particular propagation environment, WBANs require special attention. Body shadowing, dominating channel conditions, introduces great performance variations among nodes located at different positions on body. To ameliorate this problem, the cooperation paradigm appears to be a promising solution. Nodes, experiencing unfavourable channel conditions, rely on other nodes of the same WBAN to transmit their data. However, not all of the other nodes have to be in good channel conditions themselves. If cooperating nodes are not properly selected, cooperation can lead to excessive interference and energy consumption.

This chapter presented B-MIMO, a cooperative beamforming scheme thought for WBANs. An indoor scenario is considered where multiple WBANs are present and

nodes of the same WBAN establish a VAA to transmit data towards a sink. In B-MIMO, cooperating nodes are selected according to the channel conditions thus avoiding transmissions which do not contribute sufficiently to the overall power received by sinks. Comparing B-MIMO with a non-cooperative system shows clear advantages of cooperation, most important being transmit diversity which greatly boosts performance in terms of BLER thus achieving better energy efficiency. Comparison between B-MIMO and a cooperative solution where all nodes in the BAN belong to the VAA demonstrates the advantage of the novel solution in terms of energy efficiency and also in terms of BLER, in interference-limited scenarios. The decreasing of the number of cooperating nodes, in fact, decreases the energy consumption and the level of interference generated by WBANs.

Chapter 3

Cooperative Communications in Wireless Sensor Networks

This chapter extends the work presented in the previous chapter by considering a more general scenario, WSNs. WSNs and WBANs share certain features, such as the need for energy efficiency and hardware simplicity. Consequently, the cooperative communications concept is considered as a way to improve performance of WSNs as well.

3.1 Introduction

WSNs have recently gained increasing attention as a practical technology being introduced to different applications. A considerable number of these applications require transmission of the acquired data over long distances using transmission resources available only at sensor nodes. In this situation, direct transmission from a source node to a sink over a fading channel often presents difficulties mainly due to the large amount of energy required to establish a reliable transmission, fostering an inefficient use of batteries. MIMO systems are well known for their capability of achieving high

Chapter 3. Cooperative Communications in Wireless Sensor Networks

spectral efficiency in the presence of fading channels [45]. However, the need to install multiple antennas in sensor nodes can be problematic for economic and practical reasons. To extend the advantages of MIMO systems to single antenna devices, the idea of deploying a Virtual Multiple Input Multiple Output (V-MIMO) architecture appears to be very promising.

The advantages of MIMO and V-MIMO systems were already introduced in Chapter 2. While Chapter 2 was dealing with the application of cooperation paradigm on WBANs, this chapter is focused on cooperation in WSNs in general. WSNs have different characteristics from WBANs not only in terms of propagation medium and network sizes and topologies, but also in terms of application requirements. This motivates the need for analysing cooperative schemes in WSNs separately from WBANs.

3.1.1 Related Works

Many works in the literature deal with cooperative schemes for WSNs. One of the first studies was presented in [46], where an extended form of multi-hop communication systems is introduced which allows the application of MIMO capacity enhancement techniques over spatially separated relaying mobile terminals to drastically increase end-to-end capacity. The authors deduce an explicit resource allocation strategy in terms of fractional bandwidth and power allocation to each relaying hop over ergodic Rayleigh flat fading channels. [47] presents a multi-hop cooperative WSN, with nodes grouped in cooperative clusters that exploits transmit and receive cooperation among cluster nodes. It is shown that the proposed scheme achieves diversity equal to the equivalent MIMO system and significantly reduces energy consumption with respect

to the non-cooperative channel. In [48], the importance of time and phase synchronisation in distributed beamforming systems is shown and a distributed algorithm is proposed to deal with this issue. [49] presents a close-to-optimal node selection mechanism for distributed beamforming in cognitive radio networks. Results of this work showed that using the proposed method it is possible to save a big fraction of the total required energy per transmission and thus enhance the greenness of the network.

Regarding the optimisation of cluster size in non-cooperative WSNs, [50] proposes a new technique to determine the number of clusters and choose the best cluster heads based on the energy level of sensor nodes. The authors claim an increase in network lifetime with respect to the original cluster-tree network. Some works address this issue considering cooperative schemes: [49] derives a close-to-optimal number of nodes and a selection method for distributed beamforming. In [51], the optimal cluster size minimising the outage probability under a Rayleigh fading channel is derived for a cooperative WSN.

3.1.2 Thesis Contribution

Despite its promises, the deployment of a cooperative MIMO architecture in WSNs poses several technical challenges mainly because of the large amount of signalling required to enable cooperation among sensor nodes. To overcome this issue, this chapter presents a simple mechanism characterised by low overhead and suitable for cheap sensor nodes with limited hardware capabilities. Consider that WSN is organised in clusters, wherein nodes of each cluster cooperate to transmit data to one or more sinks located in the same cluster [52]. This multi-cluster scenario is analysed by employing the Wyner model [53], which simplifies the analysis and allows

Chapter 3. Cooperative Communications in Wireless Sensor Networks

for intuitive interpretation of results. Communication between sensor nodes and sinks is established through a Time Division Duplex (TDD) scheme and exploits channel reciprocity. The proposed precoding scheme is based on beamforming and it is suitable for WSNs where nodes are measuring the same parameter.

The aforementioned works, as many others in the literature, do not account for many realistic aspects of WSNs, such as hardware limitation and imperfect synchronisation. To fulfil this lack and move towards a practical scenario, the WSN under investigation is considered to be affected by inter-cluster interference, imperfect synchronisation, hardware impairments, channel estimation errors and data correlation within clusters. Having in mind future dense deployment of sensor nodes and inspired by recent achievements in massive MIMO field, the asymptotic regime, where the number of sensor nodes grows without bound, is considered. Under asymptotic assumption the analysis gets tractable and allows for optimisation of different network parameters. The main focus is on finding the number of sensor nodes which maximises the Energy Efficiency (EE) and how this parameter changes with various network settings, such as the number of sinks per cluster and the level of external interference. Comparison between the optimisation results and Monte Carlo simulations proves that it is sound to consider the asymptotic regime even for relatively low number of sensor nodes.

The remainder of this chapter is organised as follows. Section 3.2 describes channel and signal models and introduces the notation whereas the problem formulation is illustrated in Section 3.3. A simplified single-cluster scenario is analysed in Section 3.4 in order to introduce basic intuition about the problem under consideration.

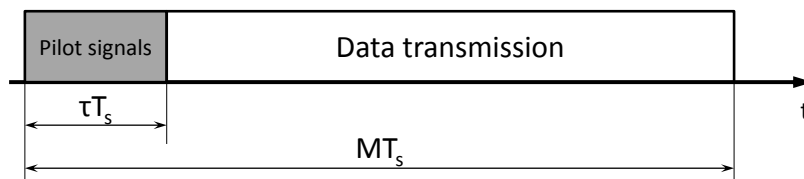


Figure 3.1: Time division duplex protocol.

Section 3.5 presents the analysis of a multi-cluster scenario with more realistic assumptions. Conclusions are drawn in Section 3.6.

3.2 Reference Scenario

Consider a WSN composed of L clusters, each consisting of N sensor nodes and K sinks (see Fig. 3.2). All sensor nodes and sinks are equipped with a single antenna and operate over a bandwidth B . A double index notation is used to refer to each node or sink in a given cluster. Under this convention, "node n in cluster i " is denoted as node ni and "sink k in cluster l " is denoted as sink kl .¹

3.2.1 Channel Model

In this work, a block flat-fading channel with coherence time T is considered. The transmission is assumed to take place according to the TDD protocol shown in Fig. 3.1, with T_s being the time required to transmit a symbol and M being the number of symbols transmitted within a frame. As presented in the figure, the transmission phase is preceded by a training phase during which pilots, of length τ symbols,

¹Matrices and vectors are denoted by upper-case boldface and lower-case boldface letters respectively. $(\cdot)^H$ is used to denote the Hermitian operator and $\text{tr}\{\cdot\}$ to denote the trace of a matrix. Diagonal matrix with entries a_n is denoted by $\text{diag}\{a_1 \dots a_N\}$ and \mathbb{Z}_+ indicates all strictly positive integer numbers.

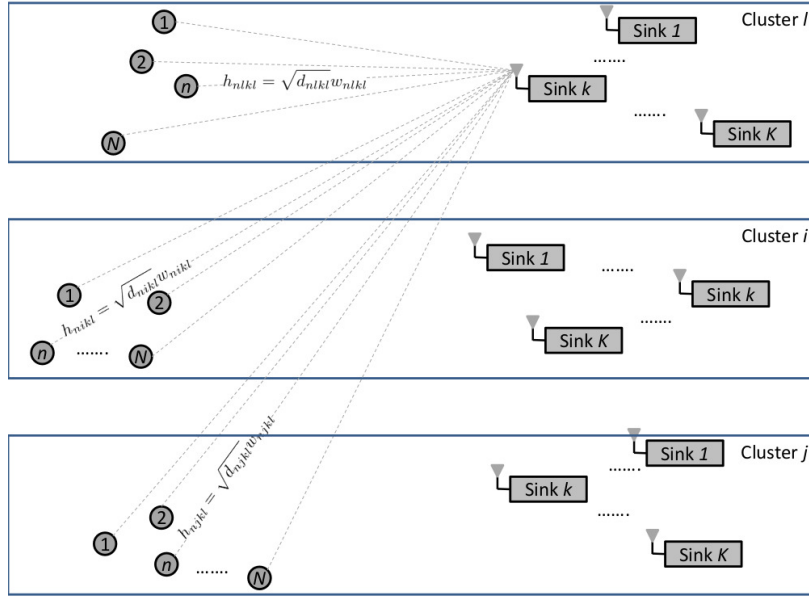


Figure 3.2: Scenario.

are sent by sinks with $0 \leq \tau \leq M$. Pilots enable sensors to estimate the channels. The TDD protocol is assumed to be matched to the coherence time (i.e., $MT_s \leq T$). Therefore, the channel can be considered as reciprocal and the sensors can make use of pilot-based estimates for data transmission. Let's denote as h_{nikl} the channel coefficient between node ni and sink kl and assume that

$$h_{nikl} = \sqrt{d_{nikl}} w_{nikl} \quad (3.2.1)$$

where $w_{nikl} \sim \mathcal{CN}(0, 1)$ is the small-scale fading channel and d_{nikl} accounts for the pathloss. For the sake of compactness, the following notation is used $\mathbf{h}_{ikl} = [h_{1ikl} \dots h_{Nikl}]^T$, $\mathbf{H}_{ikl} = \text{diag}\{h_{1ikl} \dots h_{Nikl}\}$, $\mathbf{w}_{ikl} = [w_{1ikl} \dots w_{Nikl}]^T$ and $\mathbf{W}_{ikl} = \text{diag}\{w_{1ikl} \dots w_{Nikl}\}$ to denote the channel/fading vector/matrix between all nodes in cluster i and sink kl .

3.2.2 Signal Model

It is assumed that sensors within a cluster l measure the same parameter such that the transmit data vector $\mathbf{s}_l = [s_{1l}, \dots, s_{Nl}]^T$ has correlation matrix $\mathbf{C} = \mathbb{E}[\mathbf{s}_l \mathbf{s}_l^H]$, with $C_{n,n} = \mathbb{E}[|s_{nl}|^2] = 1 \ \forall n$ and $C_{n,m} = \mathbb{E}[s_{nl}^* s_{ml}] = c \ \forall n \neq m$, where c defines the level of correlation between data of different nodes within the same cluster. On the other hand, data from different clusters are assumed to be uncorrelated.

Let us denote by v_{nl} the precoding coefficient used by node nl and assume that it is computed as:

$$v_{nl} = \frac{1}{\sqrt{\lambda_{nl}}} \sum_{k=1}^K h_{nlkl} \quad (3.2.2)$$

where λ_{nl} is chosen such that the following constraint $\mathbb{E}\{|v_{nl}|^2\} = 1$ is satisfied.

Therefore, from (3.2.1) it follows that

$$\lambda_{nl} = \sum_{k=1}^K d_{nlkl}. \quad (3.2.3)$$

In a more compact form, $\mathbf{V}_l = \text{diag}\{v_{1l}, \dots, v_{Nl}\}$ may be written as

$$\mathbf{V}_l = \mathbf{\Lambda}_l^{-1/2} \sum_{k=1}^K \mathbf{H}_{lkl} \quad (3.2.4)$$

with $\mathbf{\Lambda}_l^{-1/2} = \text{diag}\{\lambda_{1l}^{-1/2}, \dots, \lambda_{Nl}^{-1/2}\}$. Let $\hat{\mathbf{V}}_l$ be an estimate of \mathbf{V}_l and assume that hardware impairments (such as non-linearities in amplifiers, clock drifts, I/Q imbalance in mixers, finite-precision Analot to Digital Converters (ADCs) and so forth) affect transmission. Similar to [54–56], hardware impairments are modelled as a reduction of the original signal by a factor $\sqrt{(1 - \epsilon^2)}$ (where ϵ is related to error vector magnitude) and replacement of such a loss with Gaussian distortion noise with the same power. Let $\mathbf{\Phi}_l$ be the matrix that describes imperfect synchronisation among

nodes of cluster l . Then, the signal received at sink kl takes the form

$$y_{kl} = \mathbf{h}_{lkl}^H \Phi_l \left(\sqrt{p(1-\epsilon^2)} \hat{\mathbf{V}}_l \mathbf{s}_l + \boldsymbol{\eta}_l \right) + \sum_{i=1, i \neq l}^L y_{ikl} + n_{kl} \quad (3.2.5)$$

where p is the transmit power and $n_{kl} \sim \mathcal{CN}(0, \sigma^2)$ is the thermal noise. The term y_{ikl} accounts for the interference generated by cluster i at sink kl given by

$$y_{ikl} = \mathbf{h}_{ikl}^H \Phi_i \left(\sqrt{p(1-\epsilon^2)} \hat{\mathbf{V}}_i \mathbf{s}_i + \boldsymbol{\eta}_i \right) \quad (3.2.6)$$

with

$$\boldsymbol{\eta}_l = \sqrt{p\epsilon} \hat{\mathbf{V}}_l \boldsymbol{\xi}_l \quad (3.2.7)$$

accounting for non-ideal hardware. In (3.2.7), it is assumed that $\boldsymbol{\xi}_l \sim \mathcal{CN}(0, \mathbf{I}_N)$, such that the distortion noise at sensor nl is distributed as $\eta_{nl} \sim \mathcal{CN}(0, p\epsilon^2 |\hat{v}_{nl}|^2)$.

3.2.3 Pilot-based Estimation of Precoding Coefficients

Observe that d_{nlkl} corresponds to the long-term average channel attenuation, which changes in time some orders of magnitude slower than the fast fading component w_{nikl} . In practice, this means that d_{nlkl} is constant for a sufficiently large number of reception phases to be accurately estimated at the sensor. For this reason, in all subsequent discussions it is assumed that quantities $\{d_{nlkl}; \forall k, l\}$ are known at sensor nl . Therefore, only the estimation of $\sum_{k=1}^K h_{nlkl}$ is left.

In the training phase, sinks of the same cluster are assumed to be perfectly synchronised. This can be justified by the fact that sinks can be complex devices employing sophisticated synchronisation mechanisms. Moreover, relatively low number of sinks per cluster guarantees the feasibility of the procedure and limits the overhead.

3.2 Reference Scenario

The pilot signal transmitted by sinks in cluster l can be represented by a deterministic vector $\mathbf{u}_l \in \mathbb{C}^{\tau \times 1}$ with elements of power p_τ . Therefore, the power of the channel estimation phase can be expressed as

$$P_{CE} = K \frac{p_\tau}{\mu_{SINK}} \quad (3.2.8)$$

where $0 < \mu_{SINK} \leq 1$ accounts for the transceiver efficiency of sinks. It is assumed that pilot sequences used in different clusters are mutually orthogonal and that the pilot reuse factor is such that the so-called pilot contamination effect is negligible.

The collective received signal $\mathbf{x}_{nl} \in \mathbb{C}^{\tau \times 1}$ at sensor nl is given by

$$\mathbf{x}_{nl} = \sum_{k=1}^K h_{nlkl} \mathbf{u}_l + \mathbf{n}_{nl} = \nu_{nl} \mathbf{u}_l + \mathbf{n}_{nl} \quad (3.2.9)$$

where $\mathbf{n}_{nl} \sim \mathcal{CN}(0, \varsigma^2 \mathbf{I}_N)$ represents the additive noise at node nl during the pilot signalling. To keep the complexity of nodes at a tolerable level, the least-squares estimator of ν_{nl} is employed, defined by

$$\hat{\nu}_{nl} = \frac{1}{\tau p_\tau} \mathbf{u}_l^H \mathbf{x}_{nl}. \quad (3.2.10)$$

The variance of the estimation error is given by $\mathbb{E}\{|\nu_{nl} - \hat{\nu}_{nl}|^2\} = \frac{\varsigma^2}{\tau p_\tau}$. Plugging (3.2.9) into (3.2.10) and using (3.2.2) yields

$$\hat{\mathbf{V}}_l = \mathbf{V}_l + \mathbf{E}_l \quad (3.2.11)$$

where $\mathbf{E}_l \sim \mathcal{CN}\left(0, \frac{1}{\lambda_{nl}} \frac{\varsigma^2}{\tau p_\tau} \mathbf{I}_N\right)$ is the diagonal estimation error matrix.

Observe that a single pilot signal (i.e., $\tau = 1$) from all sinks would be sufficient to estimate the precoding coefficients at all sensors. This is a consequence of the adoption of the precoding scheme in (3.2.2), which requires sensor nl to have only knowledge of the composite channel $\sum_{k=1}^K h_{nlkl}$. Different precoding schemes based on knowledge of $\{h_{nlkl}; k = 1, \dots, K\}$ would require $\tau \geq K$. This might not be feasible when K is relatively large.

3.2.4 Synchronisation Error

In any distributed system (such as the one considered in this work), nodes within a cluster cannot be assumed to be perfectly synchronised in time. The cause for imperfect synchronisation ranges from hardware to communication protocol limitations. The transmissions of nodes are dispersed in time. Considering as a reference time the target time instant of transmission, t_0 , the actual transmission instants of each node can be modelled as a random variable t_{nl} , uniformly distributed in range $[-\frac{t_{\max}}{2}, \frac{t_{\max}}{2}]$, where t_{\max} is the maximum synchronisation error represented as a fraction of symbol time T_s . Assuming an Orthogonal Frequency Division Multiplexing (OFDM)-based system, i.e., WiFi-based WSN, the dispersion in time domain can be represented by phase shift in frequency domain $\phi_{nl} = e^{j2\pi t_{nl}}$ [57]. The overall effect of synchronisation error is expressed as a complex diagonal matrix $\mathbf{\Phi}_l = \text{diag}\{\phi_{1l}, \dots, \phi_{Nl}\}$ which multiplies the channel matrix \mathbf{H}_l^H ² from left. Synchronisation error only introduces phase shift implying that the elements of matrix $\mathbf{\Phi}_l$ are complex numbers with unit modulus. Matrix $\mathbf{\Phi}_l$ is unknown to the transmitters, as is the channel estimation error, therefore these effects cannot be compensated.

In the subsequent analysis, real and imaginary part of ϕ_{nl} , $\mathcal{R}\{\phi_{nl}\} = \cos(2\pi t_{nl})$ and $\mathcal{I}\{\phi_{nl}\} = \sin(2\pi t_{nl})$ respectively, are to be examined separately. First and second order moments of the two random variables are given by

$$\mathbb{E}[\mathcal{R}\{\phi_{nl}\}] = \text{sinc}(t_{\max}) \quad (3.2.12)$$

$$\mathbb{E}[|\mathcal{R}\{\phi_{nl}\}|^2] = \frac{1}{2}(1 + \text{sinc}(2t_{\max})) \quad (3.2.13)$$

²Matrix $\mathbf{H}_l^{K \times N}$ is the channel gain matrix between all sinks and all nodes in cluster l

and

$$\mathbb{E}[\mathcal{I}\{\phi_{nl}\}] = 0 \quad (3.2.14)$$

$$\mathbb{E}[|\mathcal{I}\{\phi_{nl}\}|^2] = \frac{1}{2} (1 - \text{sinc}(2t_{\max})). \quad (3.2.15)$$

where $\text{sinc}(x) = \frac{\sin(\pi x)}{\pi x}$. The effect of imperfect synchronisation is twofold: it reduces the useful received signal and introduces an interference-like term due to unmatched phases of the received signal components.

3.3 Problem Statement

One of the most common way to define the EE is as a benefit-cost ratio, where the service quality is compared with the associated energy costs. In this chapter, the EE $\left[\frac{\text{bit}}{\text{J}}\right]$ of cluster l is defined as

$$\text{EE}_l = \frac{\left(1 - \frac{\tau}{M}\right) \sum_{k=1}^K r_{kl}}{P_{T_l}} \quad (3.3.1)$$

where $r_{kl} \left[\frac{\text{bit}}{\text{s}}\right]$ denotes the achievable rate at sink k in cluster l and $P_{T_l} \left[\frac{\text{J}}{\text{s}}\right]$ accounts for the total consumed power. The factor $\left(1 - \frac{\tau}{M}\right)$ accounts for pilot overhead. The total consumed power is computed as

$$P_{T_l} = \left(1 - \frac{\tau}{M}\right) P_{TX_l} + \frac{\tau}{M} P_{CE} + N P_{SEN} + K P_{SINK} \quad (3.3.2)$$

where P_{TX_l} accounts for the power consumption of the sensor nodes in transmission state, P_{CE} of the pilot transmission phase whereas P_{SEN} and P_{SINK} are constant quantities accounting for the fixed power consumption required by each sensor and sink, respectively, for running the circuitry. The objective of this chapter is to examine

Chapter 3. Cooperative Communications in Wireless Sensor Networks

the solution of the following problem

$$\max_{N \in \mathbb{Z}_+} \text{EE}_l = \frac{(1 - \frac{\tau}{M}) \sum_{k=1}^K r_{kl}}{(1 - \frac{\tau}{M}) P_{TX_l} + \frac{\tau}{M} P_{CE} + N P_{SEN} + K P_{SINK}}. \quad (3.3.3)$$

In the sequel, two types of scenarios are considered.

- *single-cluster* scenario; this simplified scenario is investigated to gain some intuition about the structure of the problem. By "simplified scenario" it is meant that perfect synchronisation among nodes of the same cluster is considered and data transmitted by nodes of the same cluster is the same, not just correlated. Apart from the analysis of the EE-maximising number of nodes in the cluster, similar analysis is conducted on the EE-maximising training sequence duration.
- *multi-cluster* scenario; more elaborate scenario where the communication is hindered by inter-cluster interference as well as all the above mentioned realistic impairments. In this case, Wyner model [53] for interference is employed to facilitate the analysis. EE-maximising number of nodes in the cluster is examined as a function of level of interference. It is also shown how different impairments, such as imperfect synchronisation, affect system performance.

In both cases analysis and optimisation are performed considering the asymptotic regime in which the number of nodes per cluster grows without bound. It is then proven that the analysis is valid even for a relatively low number of nodes per cluster. This assumption is inspired by future mass deployment of WSNs (IoT and smart environments) and recent advancement in massive-MIMO field.

3.4 Single-cluster Scenario

To gain some insights in the structure of the problem being solved, a simplified single-cluster scenario is considered where data transmitted by nodes is the same and synchronisation among nodes is perfect. Translating this statement in mathematical equations yields:

- $L = 1$, allows for dropping double indices such that node nl can simply be denoted as node n and sink kl can be denoted as sink k ,
- $\phi_{nl} = \phi_n = 1$, thus $\Phi_l^{N \times N} = \Phi^{N \times N} = \text{diag}\{1, \dots, 1\}$, allows for omission on matrix Φ in all equations;
- $C_{m,n} = 1, \forall n, m$, allows for simplifying the following expressions $\mathbf{s}^{N \times 1} = \mathbf{1}^{N \times 1} s$ and subsequently $\mathbf{V}\mathbf{s} = \mathbf{v}s$, s being data transmitted by nodes and $\mathbf{v} = [v_1, \dots, v_N]^T$ being the precoding vector.

3.4.1 Energy Efficiency

Substituting (3.2.11) into (3.2.5) and using (3.2.4) and assumptions presented at the beginning of Section 3.4 one gets the expression for a received signal at sink k

$$y_k = \sqrt{p(1 - \epsilon^2)} \mathbf{h}_k^H \mathbf{\Lambda}^{-1/2} \mathbf{h}_k s + \sqrt{p(1 - \epsilon^2)} \mathbf{h}_k^H \mathbf{e} s + \sqrt{p(1 - \epsilon^2)} \sum_{i=1, i \neq k}^K \mathbf{h}_k^H \mathbf{\Lambda}^{-1/2} \mathbf{h}_i s + \epsilon \sqrt{p} \mathbf{h}_k^H \boldsymbol{\eta} + n_k. \quad (3.4.1)$$

In equation (3.4.1) there are five terms:

- $\sqrt{p(1 - \epsilon^2)} \mathbf{h}_k^H \mathbf{\Lambda}^{-1/2} \mathbf{h}_k s$ represents the useful signal;

- $\sqrt{p(1-\epsilon^2)}\mathbf{h}_k^H \mathbf{e}_s$ is the "noise" term due to imperfect channel estimation;
- $\sqrt{p(1-\epsilon^2)} \sum_{i=1, i \neq k}^K \mathbf{h}_k^H \mathbf{\Lambda}^{-1/2} \mathbf{h}_{i,s}$ is "interference" due to simple and sub-optimal beamforming-like precoder;
- $\epsilon\sqrt{p}\mathbf{h}_k^H \boldsymbol{\eta}$ is the "noise" term due to hardware impairments;
- n_k is the thermal noise.

Apart from the first term, all the others have a negative impact on communication and are either "interference" or "noise" by nature.

The achievable rate at sink k is [55, 56]

$$r_k = B \log_2(1 + \gamma_k) \quad (3.4.2)$$

where γ_k is Signal to Interference and Noise Ratio (SINR) given by (3.4.5) with \mathbf{D} being defined as $\mathbf{D} = \text{diag}\{|v_1|^2, \dots, |v_N|^2\}$. From (3.2.5), it turns out that

$$P_{\text{TX}} = \frac{1}{\mu_{\text{SEN}}} [p(1-\epsilon^2) \text{E}\{\hat{\mathbf{v}}^H \hat{\mathbf{v}}\} + p\epsilon^2 \text{E}\{\boldsymbol{\eta}^H \boldsymbol{\eta}\}] \quad (3.4.3)$$

where $\mu_{\text{SEN}} \in (0, 1]$ accounts for the transceiver efficiency of sensor nodes. Using simple calculus we obtain

$$P_{\text{TX}} = \frac{p}{\mu_{\text{SEN}}} \left(\mathbf{v}^H \mathbf{v} + \frac{\zeta^2}{\tau p_\tau} \text{tr}\{\boldsymbol{\Lambda}^{-1}\} \right). \quad (3.4.4)$$

Putting all the above results together, the expression for EE takes the form in (3.4.6).

3.4.2 Analysis and Optimisation

To gain some insights into the structure of the solution of the problem expressed in (3.3.3), it is assumed that the number of sensors N grows without bound while the

$$\gamma_k = \frac{p(1 - \epsilon^2) \left| \mathbf{h}_k^H \mathbf{\Lambda}^{-1/2} \mathbf{h}_k \right|^2}{p \frac{\zeta^2}{\tau p_\tau} \mathbf{h}_k^H \mathbf{\Lambda}^{-1/2} \mathbf{h}_k + p(1 - \epsilon^2) \left| \sum_{i \neq k} \mathbf{h}_k^H \mathbf{\Lambda}^{-1/2} \mathbf{h}_i \right|^2 + p\epsilon^2 \mathbf{h}_k^H \mathbf{D} \mathbf{h}_k + \sigma^2} \quad (3.4.5)$$

$$\text{EE} = \frac{(1 - \frac{\tau}{M}) B \sum_{k=1}^K \log_2(1 + \gamma_k)}{\frac{p}{\mu_{\text{SEN}}} (1 - \frac{\tau}{M}) \left(\mathbf{v}^H \mathbf{v} + \frac{\zeta^2}{\tau p_\tau} \text{tr} \{ \mathbf{\Lambda}^{-1} \} \right) + \frac{\tau}{M} \frac{p_\tau}{\mu_{\text{SINK}}} K + N P_{\text{SEN}} + K P_{\text{SINK}}} \quad (3.4.6)$$

number of sinks is kept fixed. For notational convenience, the following notation is used

$$\mathcal{A}_k = \mathbb{E} \left\{ \frac{d_k}{\sqrt{\sum_{i=1}^K d_i}} \right\} \quad \mathcal{B}_k = \mathbb{E} \left\{ \frac{d_k}{\sum_{i=1}^K d_i} \right\} \quad (3.4.7)$$

and

$$\mathcal{C}_k = \mathbb{E} \left\{ \frac{d_k^2}{\sum_{i=1}^K d_i} \right\} \quad \mathcal{D}_k = \sum_{\ell \neq k} \mathbb{E} \left\{ \frac{d_k d_\ell}{\sum_{i=1}^K d_i} \right\}. \quad (3.4.8)$$

Observe that the above coefficients depend only on the average channel attenuation. The following result can be easily proved.

Lemma 1. If N grows without bound, then $\frac{1}{N} \gamma_k - \bar{\gamma}_k \rightarrow 0$ almost surely with

$$\bar{\gamma}_k = \frac{p(1 - \epsilon^2) |\mathcal{A}_k|^2}{p \frac{\zeta^2}{\tau p_\tau} \mathcal{B}_k + p\epsilon^2 (2\mathcal{C}_k + \mathcal{D}_k)}, \quad (3.4.9)$$

and $\frac{1}{N} P_{\text{TX}} - \bar{P}_{\text{TX}} \rightarrow 0$ almost surely with

$$\bar{P}_{\text{TX}} = \frac{p}{\mu_{\text{SEN}}} \left(1 + \frac{\zeta^2}{\tau p_\tau} \mathbb{E} \left\{ \frac{1}{\sum_{i=1}^K d_i} \right\} \right). \quad (3.4.10)$$

Proof. The results easily follow using simple statistical arguments and from observing that $\mathbf{v}^H \mathbf{v} = \sum_{i=1}^K \mathbf{h}_i^H \mathbf{\Lambda}^{-1} \mathbf{h}_i$ from which using (3.2.1) and (3.2.4) it follows that $\frac{1}{N} \sum_{i=1}^K \mathbf{h}_i^H \mathbf{\Lambda}^{-1} \mathbf{h}_i - 1 \rightarrow 0$ almost surely. \square

Chapter 3. Cooperative Communications in Wireless Sensor Networks

Lemma 1 shows that SINR and the total transmit power on nodes increase linearly with N . Although valid for N growing without bounds, next this result is used for a system with a large but finite number of nodes. Using (3.4.9) and (3.4.10) into (3.4.6) leads to

$$\overline{\text{EE}} = \frac{(1 - \frac{\tau}{M}) B \sum_{k=1}^K \log_2(1 + \bar{\gamma}_k N)}{(1 - \frac{\tau}{M}) \alpha(\tau) N + \beta \tau + NP_{\text{SEN}} + KP_{\text{SINK}}} \quad (3.4.11)$$

where $\alpha(\tau)$ and β are introduced for compactness and defined as

$$\alpha(\tau) = \frac{p}{\mu_{\text{SEN}}} \left(1 + \frac{\zeta^2}{\tau p_\tau} \text{E} \left\{ \frac{1}{\sum_{i=1}^K d_i} \right\} \right) \quad (3.4.12)$$

and

$$\beta = \frac{K}{M} \frac{p_\tau}{\mu_{\text{SINK}}} \quad (3.4.13)$$

respectively.

Lemma 2. For N and K given, the value of τ maximising (3.4.11) is

$$\tau^* = \left[\frac{1}{M} \frac{1 \pm \sqrt{\frac{M^2}{cN} \left(\frac{NP_{\text{SEN}} + KP_{\text{SINK}}}{M} + \beta \right)}}{1 - \frac{M^2}{cN} \left(\frac{NP_{\text{SEN}} + KP_{\text{SINK}}}{M} + \beta \right)} \right] \quad (3.4.14)$$

with

$$c = \frac{p}{\mu_{\text{SEN}}} \frac{\zeta^2}{p_\tau} \text{E} \left\{ \frac{1}{\sum_{i=1}^K d_i} \right\}. \quad (3.4.15)$$

Proof. The result follows setting $\partial \overline{\text{EE}} / \partial \tau = 0$ and solving with respect to τ . \square

Finding the optimal N^* for a given τ is a cumbersome task due to the summing over sinks. A possible setting in which this can be easily accomplished is when the

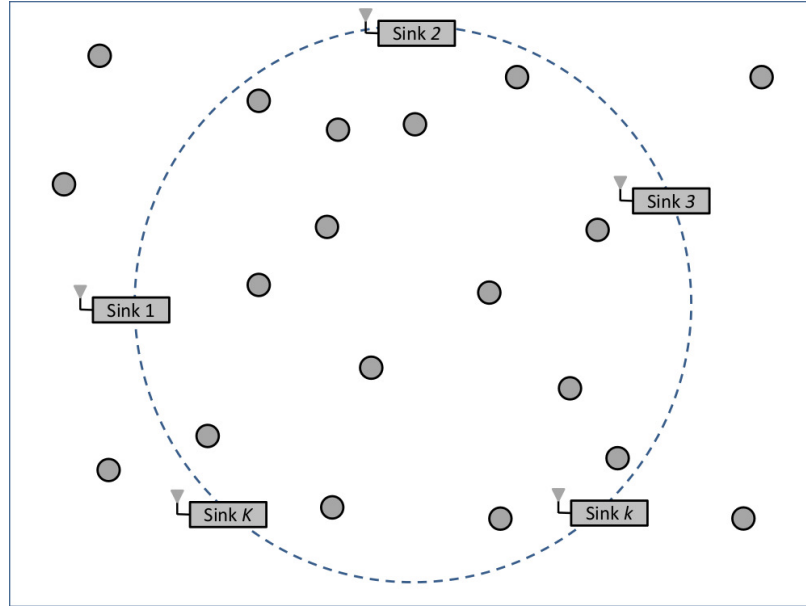


Figure 3.3: Symmetric scenario setting.

sinks are uniformly distributed over a circle (see Fig. 3.3). In these circumstances, the symmetry implies that $\bar{\gamma}_k = \bar{\gamma}, \forall k$ so that (3.4.11) reduces to

$$\overline{\text{EE}} = \frac{(1 - \frac{\tau}{M}) BK \log_2(1 + \bar{\gamma}N)}{\alpha N + \beta\tau + KP_{SINK}}. \quad (3.4.16)$$

Now the EE-optimal value of N , when τ is given, can be found.

Lemma 3. For τ given, the value of N maximising (3.4.16) is given by

$$N^* = \frac{e^{(z^*+1)} - 1}{\bar{\gamma}} \quad (3.4.17)$$

where

$$z^* = W\left(\frac{\bar{\gamma}(\beta\tau + KP_{SINK})}{\alpha e} - \frac{1}{e}\right) \quad (3.4.18)$$

and $W(x)$ is the Lambert function defined by the equation $t = W(t)e^{W(t)}$ for any $t \in \mathbb{C}$.

Chapter 3. Cooperative Communications in Wireless Sensor Networks

Proof. The proof relies on using the same arguments of Theorem 2 in [58]. Let $\overline{\text{EE}} = \frac{g \log(1+bN)}{c+dN}$ denote the objective function in (3.4.16). Note that $\partial \overline{\text{EE}} / \partial N = 0$ if and only if

$$\frac{1}{\ln(2)} \frac{b(c+dN)}{1+bN} - d \log(1+bN) = 0 \quad (3.4.19)$$

or, equivalently,

$$\frac{bc-d}{1+bN} = d(\ln(1+bN) - 1). \quad (3.4.20)$$

Plugging $z = \ln(1+bN) - 1$ into (3.4.20) yields

$$\frac{bc}{de} - \frac{1}{e} = ze^z \quad (3.4.21)$$

whose solution is eventually found to be $z^* = W(\frac{bc}{de} - \frac{1}{e})$ where $W(\cdot)$ is the Lambert function. Since $z^* = \ln(1+bN) - 1$, the result in (3.5.17) follows. \square

3.4.3 Numerical Results

The above presented model was implemented in Matlab. Sensor nodes and sinks are assumed to be uniformly distributed within the observation area, a square of side a . The results are obtained by averaging over 1000 realisations of positions and all the other random variables, such as noise, fading, etc. The network parameters are given in Table 3.1. Those related to the energy consumption are taken from the datasheet of a popular WSN device, TI CC2530 [59], while PHY layer parameters are inspired by the IEEE 802.15.4 standard [60].

Fig. 3.4 illustrates the energy efficiency as a function of N for different values of K when $\tau = 5$. As can be seen, increasing K improves energy efficiency but the optimal number of nodes N needs to be increased accordingly. Observe that the maximum region of the curve tends to become flat as K becomes large, meaning that

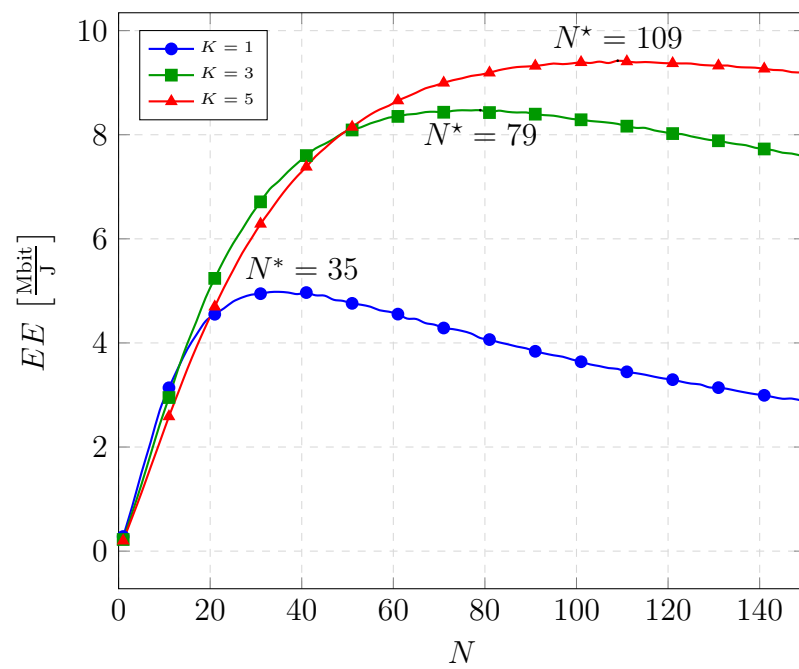


Figure 3.4: Energy efficiency as a function of N for $\tau = 5$.

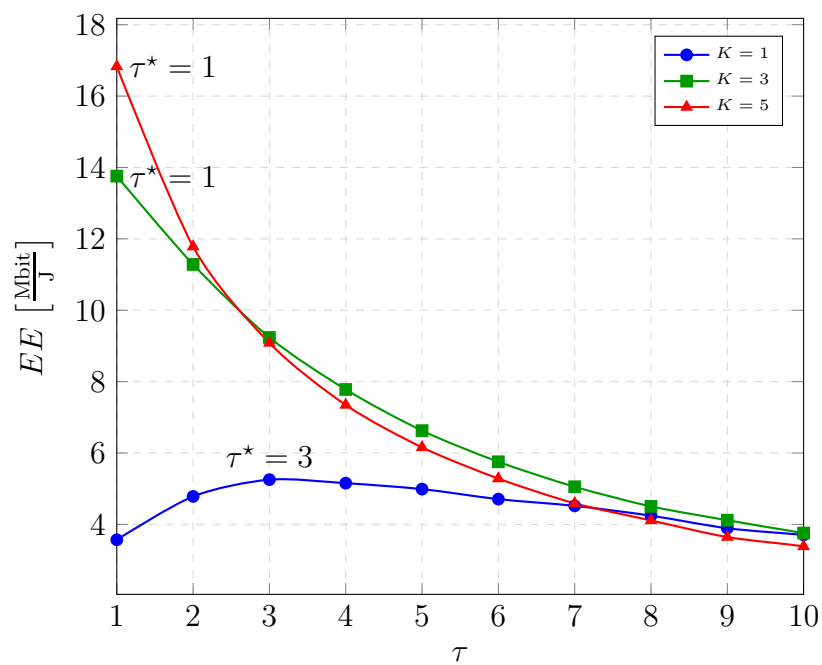


Figure 3.5: Energy efficiency as a function of τ for $N = 30$.

3.4 Single-cluster Scenario

Table 3.1: Single-cluster scenario simulation parameters.

Parameter	Value
Area side length: a	500 metre
Path-loss model: d_{nk}	$10^{-3.53} \text{distance}_{nk}^{-3.76}$
Sensor nodes transmit power: p	1 mW
Pilot transmit power: p_τ	100 mW
Circuit power sensor nodes: P_{SEN}	20 mW
Circuit power sinks: P_{SINK}	100 mW
Total noise power: $B\sigma^2$	-107 dBm
Transceiver efficiency sensor nodes: μ_{SEN}	0.08
Transceiver efficiency sinks: μ_{SINK}	0.3
Hardware impairments: ϵ^2	0.17
Bandwidth: B	5 MHz
Frame duration: T	8.25 ms
Number of symbols in a frame: M	256
Symbol time: T_s	32 μs

certain error in the computation of the optimal N can be allowed without losing in performance. This will prove useful later on in the discussing about the performance loss due to selection of sub-optimal N .

Fig. 3.5 illustrates the energy efficiency as a function of τ when $N = 30$ and $K = 1, 3$ and 5 . As it can be observed, the EE-optimal value of τ decreases when increasing K . This is due to the fact that the energy consumption of pilot transmission phase increases with K and becomes the dominant part of the overall energy consumption,

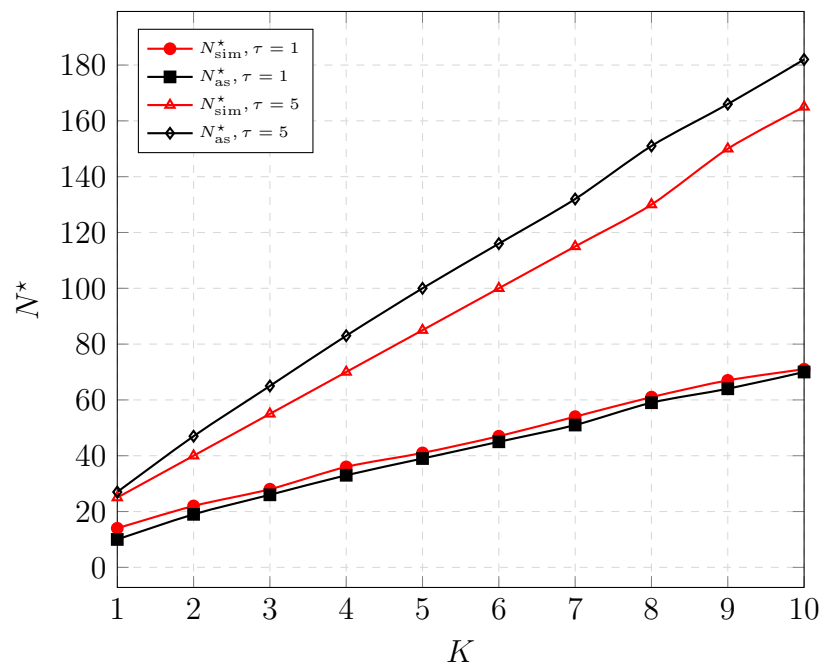
Chapter 3. Cooperative Communications in Wireless Sensor Networks

mostly because pilots are transmitted with high power. In this setting, the gain in terms of achievable rate obtained by increasing τ is counter-weighted by the increase in energy consumption.

The results of Figs. 3.6 and 3.7 refer to the asymptotic analysis. In particular, Fig. 3.6 shows the optimal number of sensor nodes, N^* , as a function of K for $\tau = 1$ and 5. It can be seen that N^* increases linearly with K with a slope that depends on τ . The difference between the values of N^* obtained by simulations, N_{sim}^* , and asymptotic analysis, N_{as}^* , does not exceed 10%. Fig. 3.7 illustrates the energy efficiency achieved by the optimal number of sensor nodes N_{sim}^* and N_{as}^* as a function of K for different τ . As it is seen, N_{as}^* achieves the same performance as N_{sim}^* , meaning that it is safe to use (3.4.17), instead of running simulations, in order to get the EE-optimal value of N .

From the analysis of a single-cluster scenario it is possible to some conclusions. The EE-optimal number of sensor nodes increases linearly with the number of sinks. The analysis shows that as the number of sinks increases, the energy consumption due to pilots transmission becomes dominant and, consequently, the EE-optimal duration of the channel estimation phase gets shorter. It can also shown that when all the sinks are symmetrically distributed within the observation area, the optimisation problem is simplified and asymptotic analysis provides a closed form solution for the optimal number of sensor nodes.

In the next section, a multi-cluster scenario with realistic aspects, such as imperfect synchronisation and data correlation, taken into account is analysed.

Figure 3.6: Optimal number of sensor nodes, N^* as a function of K .

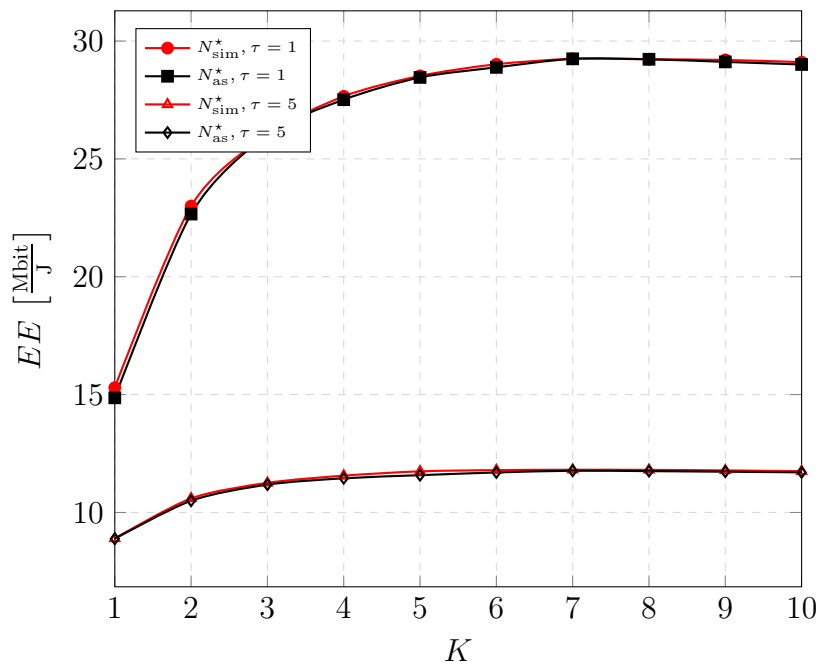


Figure 3.7: Energy efficiency achieved by N_{sim}^* and N_{as}^* , as a function of K .

3.5 Multi-cluster Scenario

In this section, a multi-cluster scenario is considered. This adds the inter-cluster interference to the analysis presented in the previous section. Nodes of the same cluster are assumed to be imperfectly synchronised (see Section 3.2.4) and data they are transmitting is considered to be correlated, with correlation matrix $\mathbf{C}^{N \times N}$ (see Section 3.2). The objective of the following analysis is to understand how the inter-cluster interference affects the EE-optimising number of sensor nodes and how the synchronisation error affects the overall performance of the system.

3.5.1 Wyner Model

To facilitate the analysis, the Wyner model [53] is employed (see Fig. 3.8):

- All the nodes within a cluster experience the same pathloss towards the sink antennas, $d_{nlkl} = d_{ll}, \forall nl, kl$;
- All the nodes from the neighbouring cluster experience the same pathloss towards the sink antennas in the observed cluster, $d_{nikl} = d_{il} = \alpha d_{ll}, \forall ni, kl$;
- All the nodes from the second neighbouring cluster experience the same pathloss towards the sink antennas in the observed cluster, $d_{n_jkl} = d_{jl} = \alpha^2 d_{ll}, \forall n_j, kl$;
- Interference from all the other clusters is neglected.

The parameter α is defined by the proximity between the clusters (see Fig. 3.8) and $0 < \alpha < 1$.

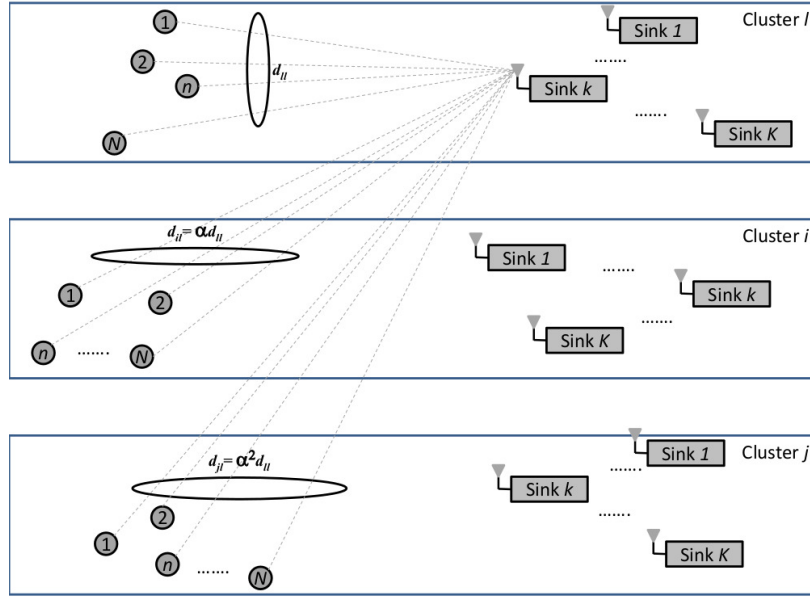


Figure 3.8: Wyner model.

3.5.2 Energy Efficiency

Plugging (3.2.4) and (3.2.11) into (3.2.5) and exploiting properties of Wyner model (described in Section 3.5.1) one gets

$$\begin{aligned}
 y_{kl} &= \sqrt{\frac{p(1-\epsilon^2)d_{ll}}{K}} \mathbf{w}_{lkl}^H \mathcal{R}\{\Phi_l\} \mathbf{W}_{lkl} \mathbf{s}_l \\
 &+ \sqrt{\frac{p(1-\epsilon^2)d_{ll}}{K}} \mathbf{w}_{lkl}^H \mathcal{I}\{\Phi_l\} \mathbf{W}_{lkl} \mathbf{s}_l \\
 &+ \sqrt{\frac{p(1-\epsilon^2)d_{ll}}{K}} \mathbf{w}_{lkl}^H \Phi_l \sum_{m=1, m \neq k}^K \mathbf{W}_{lml} \mathbf{s}_l \\
 &+ \sqrt{p(1-\epsilon^2)d_{ll}} \mathbf{w}_{lkl}^H \Phi_l \mathbf{E}_l \mathbf{s}_l \\
 &+ \epsilon \sqrt{pd_{ll}} \mathbf{w}_{lkl}^H \Phi_l \left(\sqrt{\frac{1}{K}} \sum_{m=1}^K \mathbf{W}_{lml} + \mathbf{E}_l \right) \boldsymbol{\xi}_l \\
 &+ y_{ikl} + y_{jkl} + n_{kl}.
 \end{aligned} \tag{3.5.1}$$

Note that y_{ikl} and y_{jkl} can be expanded in a similar way. However, this is omitted for the sake of conciseness. The achievable rate at sink kl is thus given by

$$r_{kl} = B \log_2(1 + \gamma_{kl}) \quad (3.5.2)$$

where γ_{kl} is computed as

$$\gamma_{kl} = \frac{\frac{p(1-\epsilon^2)d_{ll}}{K} \mathcal{A}}{\frac{p(1-\epsilon^2)d_{ll}}{K} \mathcal{B} + \frac{p(1-\epsilon^2)d_{ll}}{K} \mathcal{C}(\alpha) + \frac{p}{K} \frac{\zeta^2}{\tau p_\tau} \mathcal{D}(\alpha) + \frac{p\epsilon^2 d_{ll}}{K} \mathcal{E}(\alpha) + \sigma^2} \quad (3.5.3)$$

with

$$\mathcal{A} = \mathbf{w}_{lkl}^H \mathcal{R}\{\Phi_l\} \mathbf{W}_{lkl} \mathbf{C} \mathbf{W}_{lkl}^H \mathcal{R}\{\Phi_l\} \mathbf{w}_{lkl} \quad (3.5.4)$$

$$\mathcal{B} = \mathbf{w}_{lkl}^H \mathcal{I}\{\Phi_l\} \mathbf{W}_{lkl} \mathbf{C} \mathbf{W}_{lkl}^H \mathcal{I}\{\Phi_l\} \mathbf{w}_{lkl} \quad (3.5.5)$$

$$\begin{aligned} \mathcal{C}(\alpha) &= \mathbf{w}_{lkl}^H \Phi_l \sum_{m \neq k} \mathbf{W}_{lml} \mathbf{C} \sum_{m \neq k} \mathbf{W}_{lml}^H \Phi_l^H \mathbf{w}_{lkl} \\ &+ \alpha \mathbf{w}_{ikl}^H \Phi_i \sum_{k=1}^K \mathbf{W}_{iki} \mathbf{C} \sum_{k=1}^K \mathbf{W}_{iki}^H \Phi_i^H \mathbf{w}_{ikl} \\ &+ \alpha^2 \mathbf{w}_{jkl}^H \Phi_j \sum_{k=1}^K \mathbf{W}_{jkj} \mathbf{C} \sum_{k=1}^K \mathbf{W}_{jkj}^H \Phi_j^H \mathbf{w}_{jkl} \end{aligned} \quad (3.5.6)$$

$$\mathcal{D}(\alpha) = \mathbf{w}_{lkl}^H \mathbf{w}_{lkl} + \alpha \mathbf{w}_{ikl}^H \mathbf{w}_{ikl} + \alpha^2 \mathbf{w}_{jkl}^H \mathbf{w}_{jkl} \quad (3.5.7)$$

$$\begin{aligned} \mathcal{E}(\alpha) &= \mathbf{w}_{lkl}^H \sum_{k=1}^K \mathbf{W}_{lkl} \sum_{k=1}^K \mathbf{W}_{lkl}^H \mathbf{w}_{lkl} \\ &+ \alpha \mathbf{w}_{ikl}^H \sum_{k=1}^K \mathbf{W}_{iki} \sum_{k=1}^K \mathbf{W}_{iki}^H \mathbf{w}_{ikl} \\ &+ \alpha^2 \mathbf{w}_{jkl}^H \sum_{k=1}^K \mathbf{W}_{jkj} \sum_{k=1}^K \mathbf{W}_{jkj}^H \mathbf{w}_{jkl} \end{aligned} \quad (3.5.8)$$

being coefficients depending on fading and synchronisation error only. From (3.2.5), it turns out that

$$P_{TX_l} = \frac{1}{\mu_{SEN}} \left[p(1 - \epsilon^2) \mathbb{E} \left\{ \text{tr} \{ \hat{\mathbf{V}}_l^H \hat{\mathbf{V}}_l \} \right\} + p\epsilon^2 \mathbb{E} \{ \boldsymbol{\eta}_l^H \boldsymbol{\eta}_l \} \right] \quad (3.5.9)$$

where $0 < \mu_{SEN} \leq 1$ accounts for the transceiver efficiency of sensor nodes. Using simple calculus and assumptions from 3.5.1 we obtain

$$P_{TX_l} = \frac{p}{\mu_{SEN}} \frac{1}{K} \left(\text{tr} \left\{ \sum_{k=1}^K \mathbf{W}_{lkl}^H \sum_{k=1}^K \mathbf{W}_{lkl} \right\} + \frac{\zeta^2 N}{\tau p_\tau d_{ll}} \right). \quad (3.5.10)$$

Putting all the above results together, the expression for EE takes the form in (3.5.11).

$$EE_l = \frac{(1 - \frac{\tau}{M}) B \sum_{k=1}^K \log_2(1 + \gamma_{kl})}{(1 - \frac{\tau}{M}) \frac{p}{\mu_{SEN}} \frac{1}{K} \left(\text{tr} \left\{ \sum_{k=1}^K \mathbf{W}_{lkl}^H \sum_{k=1}^K \mathbf{W}_{lkl} \right\} + \frac{\zeta^2 N}{\tau p_\tau d_{ll}} \right) + \frac{\tau}{M} K \frac{p_\tau}{\mu_{SINK}} + NP_{SEN} + KP_{SINK}} \quad (3.5.11)$$

At this point EE-optimising N can be found by performing an exhaustive search over the integer set, i.e., performing Monte Carlo simulations of (3.5.11) for each possible value of N . However, to gain more intuitive insights in the structure of the solution of (3.3.3) the asymptotic analysis is performed, presented in the next section.

3.5.3 Analysis and Optimisation

The analysis is conducted in the regime in which the number of sensors N is infinitely large.

Lemma 4. If N grows without bound, then $\frac{1}{N} \gamma_l - \bar{\gamma}_l \rightarrow 0$ almost surely with

$$\bar{\gamma}_l(\alpha) = \frac{(1 - \epsilon^2) d_{ll} \text{sinc}^2(t_{\max})}{(1 - \epsilon^2) d_{ll} (1 - \text{sinc}(2t_{\max})) + \frac{\zeta^2}{\tau p_\tau} (1 + \alpha + \alpha^2) + \epsilon^2 d_{ll} (K + 1) + K d_{ll} (\alpha + \alpha^2)}. \quad (3.5.12)$$

Moreover, $\frac{1}{N}P_{\text{TX}_l} - \overline{P}_{\text{TX}_l} \rightarrow 0$ almost surely with

$$\overline{P}_{\text{TX}_l} = \frac{p}{\mu_{\text{SEN}}} \left(1 + \frac{\zeta^2}{\tau p_\tau} \frac{1}{K d_{ll}} \right). \quad (3.5.13)$$

Proof. The results easily follow using simple statistical arguments and asymptotic results. \square

Lemma 4 shows that the SINR and the transmit power increase linearly with N . Although valid for N growing without bounds, next we use this result for a system with a large but finite number of sensors. This yields

$$\overline{\text{EE}}_l = \frac{\left(1 - \frac{\tau}{M}\right) BK \log_2(1 + \overline{\gamma}_l(\alpha) N)}{\kappa + N\theta_l} \quad (3.5.14)$$

where θ_l and κ are introduced for compactness and defined as

$$\theta_l = \left(1 - \frac{\tau}{M}\right) \frac{p}{\mu_{\text{SEN}}} \left(1 + \frac{\zeta^2}{\tau p_\tau} \frac{1}{K d_{ll}}\right) + P_{\text{SEN}} \quad (3.5.15)$$

and

$$\kappa = KP_{\text{SINK}} + \frac{\tau}{M} K \frac{p_\tau}{\mu_{\text{SINK}}}. \quad (3.5.16)$$

Now, the EE-optimal value of N can be found is α is known.

Lemma 5. For α given, the value of N maximising (3.5.14) is given by

$$N^* = \frac{e^{(z^*+1)} - 1}{\overline{\gamma}_l} \quad (3.5.17)$$

where

$$z^* = W\left(\frac{\overline{\gamma}_l(\alpha) \kappa}{\theta_l e} - \frac{1}{e}\right) \quad (3.5.18)$$

and $W(x)$ is the Lambert function defined by the equation $t = W(t)e^{W(t)}$ for any $t \in \mathbb{C}$.

Table 3.2: Multi-cluster scenario simulation parameters

Parameter	Value
Intra-cluster distance: a	100 m
Pilot sequence length: τ	1
Data correlation factor: c	0.8
Maximum synchronisation error: t_{\max}	$0.5 T_s$

Proof. The proof relies on using the same arguments of Theorem 2 in [58] and it follows the same line of reasoning as the proof of Lemma 3. \square

A close inspection of (3.5.17) reveals that N^* increases with α . This is because higher interference level brings to lower SINR, with ensuing reduction of the achievable rate. This can only be compensated by increasing N^* . Another interesting observation is that N^* must increase with K . This is due to the fact that when K increases, the energy consumption of sinks becomes the dominant component of the overall energy consumption, due to the high transmit power of pilots and complex circuitry of sinks (P_{SINK}). In this setting, increasing N , while being beneficial for the achievable rate, does not affect the total energy consumption too much, implying that EE-optimal N should be higher.

3.5.4 Numerical Results

As with the case of single-cluster scenario, Monte Carlo simulations have been used to validate the analysis above. Results are obtained averaging over 1000 realisations of all the random variables, such as fading, noise, etc. The network parameters are

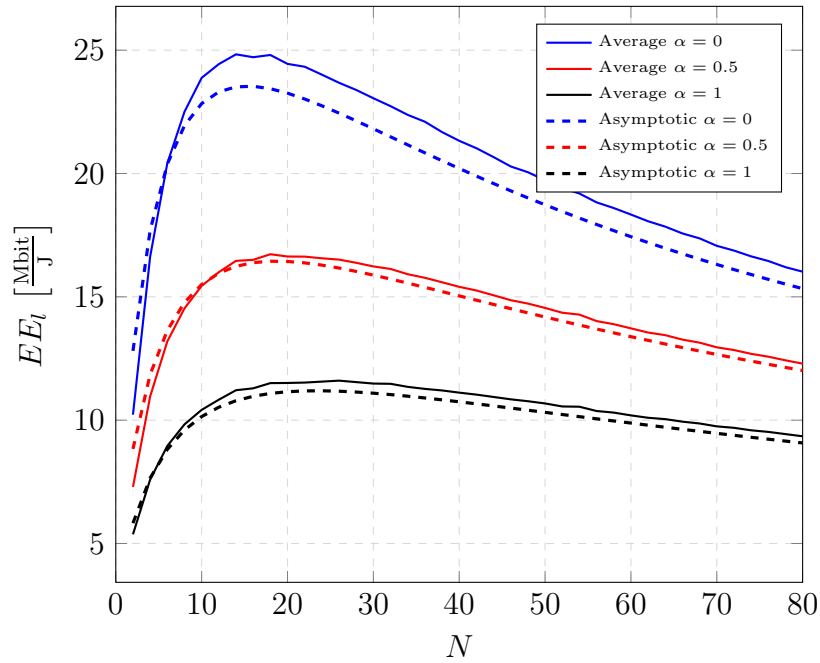


Figure 3.9: Energy efficiency vs. N for $K = 3$ and $\alpha = 0, 0.5$ and 1 .

given in Tables 3.1 (where applicable) and 3.2.

Fig. 3.9 plots the energy efficiency as a function of N for $K = 3$ and different values of α . The curves obtained from the asymptotic results of Lemma 4 closely follow the ones obtained through Monte Carlo simulations. This proves that the asymptotic analysis is accurate even for a relatively low number of sensor nodes. As expected, the energy efficiency decreases with α due to the higher level of interference.

Fig. 3.10 illustrates the EE-optimal value of sensor nodes as a function of α for $K = 1, 3$ and 5 . Firstly, notice that the closed form solution obtained through (3.5.17) is very close to the values obtained through simulations. The difference between the two is higher for higher values of K . However, for high values of K , i.e., $K \geq 5$, a wider range of values of N achieves similar energy efficiency (see Fig. 3.11) such that

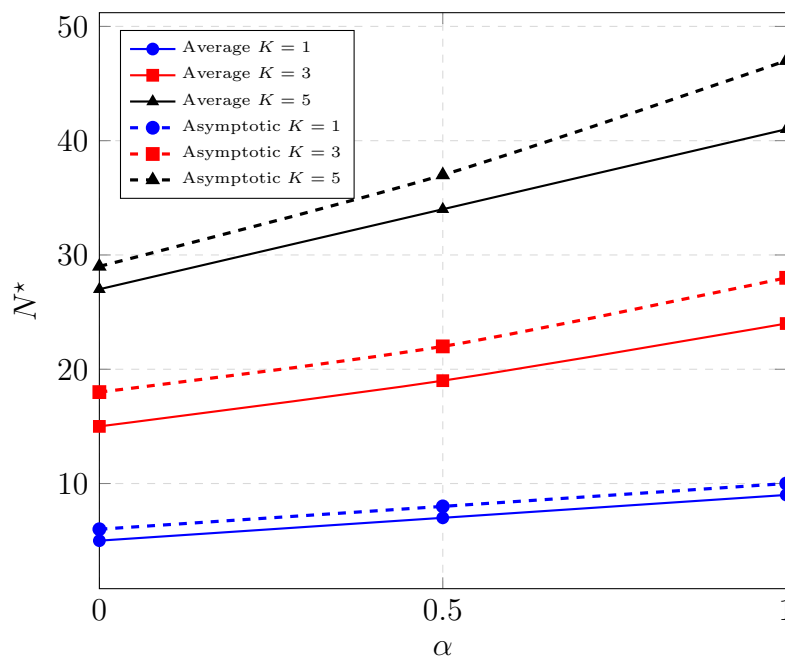


Figure 3.10: EE-optimal value of sensor nodes N^* vs. α for $K = 1, 3$ and 5 .

N^* computed by (3.5.17) achieves energy efficiency very close to the optimal one. Secondly, as predicted at the end of Section 3.5.3, N^* increases with α and K .

Fig. 3.11 reports energy efficiency as a function of N for $\alpha = 0.5$ and different values of K and t_{\max} . A large performance gap can be observed between the case where synchronisation is perfect, $t_{\max} = 0$, and the case where the maximum synchronisation error is $t_{\max} = 0.5$. The global maximum of the energy efficiency is obtained for $K = 1$, while the value of N^* depends on the level of de-synchronisation among nodes. Fig. 3.11 also gives an insight about the solution of the reverse problem: if N is given, find the EE-maximising value of K . These remarks would not change for other values of α and c .

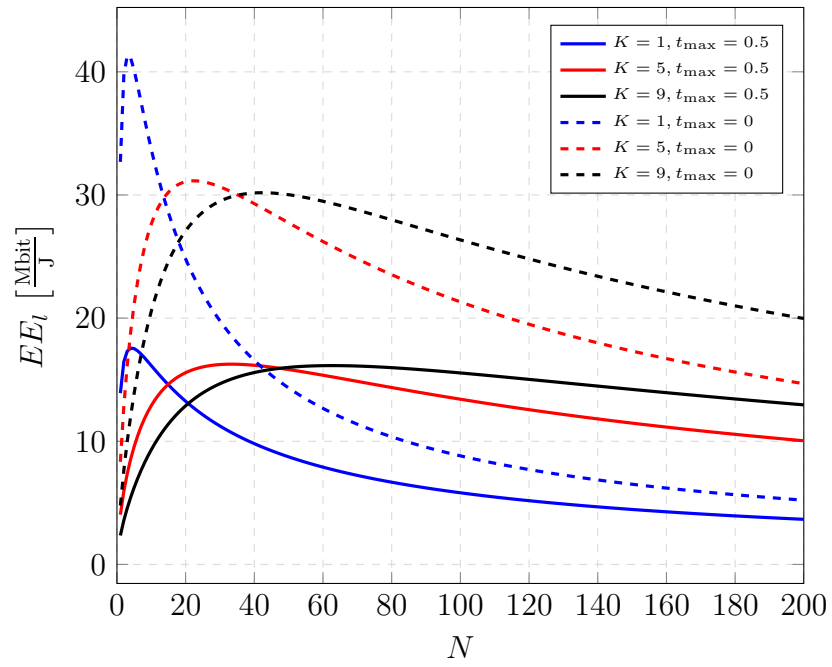


Figure 3.11: Energy efficiency vs. N , for $\alpha = 0.5$ and different K and t_{\max} .

3.6 Conclusions

In this chapter, a cooperative MIMO scheme for WSNs was presented. The scheme exploits the fact that sensor nodes are often employed to measure the same parameter, so that the data they are transmitting is correlated. Under such assumption, the proposed mechanism proves to be very energy efficient while maintaining low overhead. Data transmission phase is preceded by training phase in which sinks transmit pilot signals which are used by sensor nodes for channel estimation. In the subsequent analysis, nodes are assumed to have imperfect CSI, thus limiting the performance gain of cooperation. After the training phase, nodes of the same cluster transmit data together towards sinks using a simple beamforming-based precoding scheme. Considering cheap sensor nodes implies the necessity of taking into account certain realistic impairments from which this kind of devices are known to suffer from. "Distortion noise" is a well known performance hindrance, especially affecting devices with low-cost RF components (amplifiers, filters, Digital to Analog Converters (DACs), etc.). Another important aspect to take into account was synchronisation among nodes of the same cluster which proves to be greatly affecting the performance and requires special attention by the system designer. Finally, having in mind the future massive deployment of WSNs, external, i.e., inter-cluster, interference plays a major role in system performance and needs to be analysed carefully. Under previously described settings, the problem under investigation was: how many sensors should be deployed to maximise the energy efficiency?

Firstly, a simplified single-cluster scenario was considered. This analysis was useful

because it allows for obtaining the basic intuition of the optimisation problem by reducing system complexity. From this scenario it could be seen that the EE-optimising number of sensor nodes, N^* , increases with the number of sinks, K , because the overall energy consumption becomes dominated by sinks such that the "cost", in terms of energy consumption, of employing more nodes is not relevant. Monte Carlo simulations were used to validate the asymptotic analysis, which is proven to be accurate even for a relatively low number of sensor nodes and thus can be safely used for performance optimisation. Another important conclusion is drawn about the EE-optimising duration, τ , of the training phase. It is shown that τ depends on K and that if $K > 1$, τ should be kept at its minimum, i.e., $\tau = 1$. Some of these conclusions are later used when analysis is performed on a more complex model.

Secondly, the multi-cluster scenario, where inter-cluster interference plays a significant role, is considered. System model was extended, with respect to the single-cluster case, to include all the above mentioned realistic effects. Wyner model was employed for analytic tractability and the asymptotic analysis was used to compute a closed form expression for N^* . This allowed to get some insights on how N^* is affected by the network parameters. In particular, it turned out that N^* must increase with the inter-cluster interference level as well as with the number of sinks in each cluster. While the former conclusion is inherited from the single-cluster case, the latter is due to the need for compensating the decrease of SINR due to increasing interference. It is also shown that the imperfect synchronisation greatly affects the performance and that in the future deployment a lot of attention needs to be given to this problem.

Conclusions and Future Work

The general topics investigated in this thesis are related to the *body-centric communications* and *cooperative communications* paradigm.

Body-centric communications are characterised by the human presence defining their distinctive communication characteristics among other wireless systems. On one hand, the human body represents a unique propagation environment susceptible to different sources of channel variability. On the other hand, different application fields, especially healthcare and biomedical, require reliable and ultra-low power communication systems. To meet the requirements, improvements are necessary in several fields, one of which is protocol design.

This thesis presented a protocol architecture implemented for the purposes of the WiserBAN project. Given their huge impact on overall system performance, the spotlight was on the design of MAC protocols. To cope with heterogeneous use cases (wearable and implanted devices) two MAC modes were implemented: Superframe (SF)-based and Low Power Listening (LPL) MAC. SF-based MAC is a synchronous protocol intended for being used primarily in a high traffic scenario with multiple devices. On the other hand, LPL MAC is an asynchronous protocol

Conclusions and Future Work

which offers great energy efficiency in a low traffic setting, but suffers from the lack of proper collision avoidance techniques. To guarantee interoperability and varying traffic rates and topologies, seamless transition between the two modes is allowed. Presented protocol was implemented on a hardware platform, developed by project partner (CSEM), intended for WBANs. In order to validate that the developed protocol satisfies the application requirements, an experimental campaign was conducted. Performance was evaluated in terms of average packet delay, average PLR, average energy consumption and throughput. First, the two MAC modes were evaluated separately. The conclusions are drawn about performance tuning through protocol parameters. Trade-offs, such as average delay vs. average energy consumption, in the case of LPL, or PLR vs. average delay, in the case of SF-based MAC, are discussed and guidelines are given about how to favour one performance metric over the other. Once this was done, the two MAC modes were compared. The results provide insights about the suitability of the two MAC modes based on the use case. LPL mode should be used if the main objective is network lifetime, while if the main objective is high throughput, especially in larger networks, usage of the SF-based MAC is mandatory.

Some of the issues in WBANs cannot be properly solved only through the communication protocol. Body shadowing proves to be a major obstacle to reliable and efficient communication. Moreover, nodes of the same WBAN, may experience very different channel conditions. A method for solving this problem is cooperation: other nodes of a WBAN are used for transmitting data generated in a WBAN. However, if cooperating nodes are not properly selected, cooperation can lead to excessive interference and energy consumption.

This thesis presented B-MIMO, a cooperative beamforming scheme for WBANs.

An indoor scenario is considered where multiple WBANs are present and nodes of the same WBAN establish a VAAs to transmit data towards a sink. In B-MIMO, cooperating nodes are selected according to the channel conditions, thus avoiding transmissions which do not contribute sufficiently to the overall power received by sinks. Comparison between B-MIMO and a cooperative solution where all nodes in the BAN belong to the VAA demonstrates the advantage of the novel solution in terms of energy efficiency and also in terms of BLER, in interference-limited scenarios. The decreasing of the number of cooperating nodes decreases the energy consumption and the level of interference generated by WBANs.

As a future research direction, cooperative schemes involving body-to-body communication should be considered. It is not hard to imagine advantages offered by cooperation between WBANs (e.g., higher diversity, reduced interference, etc.) and, to benefit from it, advanced PHY and MAC layer mechanisms need to be studied.

Finally, the thesis presented a cooperative MIMO scheme for a broader scenario, that is a Wireless Sensor Network (WSN). In WSNs, sensor nodes are typically employed to measure the same parameter or the same set of parameters, meaning that the data nodes are transmitting is the same, or at least correlated. The previous assumption allows for the proposed cooperation scheme which greatly boosts energy efficiency. The scheme is characterised by simplicity and low overhead. Since sensor nodes are simple devices with limited hardware capabilities, a realistic analysis needed to take into account various, often disregarded, effects. These effects include CSI errors, hardware impairments and imperfect synchronisation. The contribution of this part of the thesis is the analysis and optimisation of multi-cluster WSN affected by the above mentioned issues. Having in mind future mass deployment of sensor nodes,

Conclusions and Future Work

asymptotic analysis, inspired by recent advances in massive MIMO field, is employed. It allows for derivation of closed form solution of the optimisation problem. Monte Carlo simulations were performed to prove the validity of the asymptotic assumption for a high but limited number of sensor nodes. The results show that the number of nodes needs to increase with the number of sinks and the level of inter-cluster interference.

To extend and further generalise the presented work, a stochastic geometry approach should be considered. Considering variable-structure clusters and geometrical distributions would allow for drawing general conclusions on the energy-efficiency of cooperative WSNs.

Although the *cooperative communications* concept is currently one of the hot topics in the field of telecommunications, the experimentation is not keeping up with the theory. There are few test-beds and even fewer commercial systems exploiting the advantages of cooperation. Further research should attempt to experimentally validate models used in this and many other works from the literature.

Bibliography

- [1] WiserBAN - Smart miniature low-power wireless microsystem for Body Area. <http://www.wiserban.eu/>, 2013.
- [2] Newcom# - Network of Excellence in Wireless Communications. <http://www.newcom-project.eu/>, 2012.
- [3] Benoît Latré, Bart Braem, Ingrid Moerman, Chris Blondia, and Piet Demeester. A Survey on Wireless Body Area Networks. *Wirel. Netw.*, 17(1):1–18, January 2011.
- [4] Sana Ullah, Henry Higgins, Bart Braem, Benoit Latre, Chris Blondia, Ingrid Moerman, Shahnaz Saleem, Ziaur Rahman, and Kyung Sup Kwak. A Comprehensive Survey of Wireless Body Area Networks. *J. Med. Syst.*, 36(3):1065–1094, June 2012.
- [5] A. Boulis, D. Smith, D. Miniutti, L. Libman, and Y. Tselishchev. Challenges in body area networks for healthcare: the MAC. *Communications Magazine, IEEE*, 50(5):100–106, May 2012.
- [6] Qinqing Zhang, Erwu Liu, and Kin K. Leung. Cooperative Communication and Networking. *Johns Hopkins APL Technical Digest*, 30(2), 2011.

Bibliography

- [7] D. Gesbert, S. Hanly, H. Huang, S. Shamai Shitz, O. Simeone, and Wei Yu. Multi-Cell MIMO Cooperative Networks: A New Look at Interference. *Selected Areas in Communications, IEEE Journal on*, 28(9):1380–1408, December 2010.
- [8] Yong Yuan, Zhihai He, and Min Chen. Virtual mimo-based cross-layer design for wireless sensor networks. *Vehicular Technology, IEEE Transactions on*, 55(3):856–864, May 2006.
- [9] Stefan Drude. Requirements and Application Scenarios for Body Area Networks. In *Mobile and Wireless Communications Summit, 2007. 16th IST*, pages 1–5, July 2007.
- [10] R. Cavallari, F. Martelli, R. Rosini, C. Buratti, and R. Verdone. A survey on wireless body area networks: Technologies and design challenges. *Communications Surveys Tutorials, IEEE*, 16(3):1635–1657, Third 2014.
- [11] A. Rahim, N. Javaid, M. Aslam, Z. Rahman, U. Qasim, and Z.A. Khan. A Comprehensive Survey of MAC Protocols for Wireless Body Area Networks. In *Seventh International Conference on Broadband, Wireless Computing, Communication and Applications (BWCCA), 2012*, pages 434–439, Nov 2012.
- [12] S.A. Gopalan and Jong-Tae Park. Energy-efficient MAC protocols for wireless body area networks: Survey. In *International Congress on Ultra Modern Telecommunications and Control Systems and Workshops (ICUMT), 2010*, pages 739–744, Oct 2010.
- [13] P.K. Tiwary, Woon-Sung Baek, Dong-Min Kim, and Jae-Young Pyun. A study on ultra low power MAC protocols over Wireless Body Area Network. In *TENCON 2012 - 2012 IEEE Region 10 Conference*, pages 1–6, Nov 2012.
- [14] Wei Ye, John Heidemann, and Deborah Estrin. An energy-efficient mac protocol for wireless sensor networks. In *INFOCOM 2002. Twenty-First Annual Joint*

- Conference of the IEEE Computer and Communications Societies. Proceedings. IEEE*, volume 3, pages 1567–1576. IEEE, 2002.
- [15] Tijs van Dam and Koen Langendoen. An adaptive energy-efficient mac protocol for wireless sensor networks. In *Proceedings of the 1st international conference on Embedded networked sensor systems*, SenSys '03, pages 171–180, New York, NY, USA, 2003. ACM.
- [16] Joseph Polastre, Jason Hill, and David Culler. Versatile low power media access for wireless sensor networks. In *Proceedings of the 2nd international conference on Embedded networked sensor systems*, SenSys '04, pages 95–107, New York, NY, USA, 2004. ACM.
- [17] Amre El-Hoiydi and Jean-Dominique Decotignie. Low power downlink mac protocols for infrastructure wireless sensor networks. *Mob. Netw. Appl.*, 10(5):675–690, October 2005.
- [18] Michael Buettner, Gary V. Yee, Eric Anderson, and Richard Han. X-mac: a short preamble mac protocol for duty-cycled wireless sensor networks. In *Proceedings of the 4th international conference on Embedded networked sensor systems*, SenSys '06, pages 307–320, New York, NY, USA, 2006. ACM.
- [19] Kyung Sup Kwak Sana Ullah. Throughput and delay limits of iee 802.15.6. pages 1–5, South Korea, 2011. IEEE, IEEE.
- [20] R. Rosini, F. Martelli, M. Maman, R. D'Errico, C. Buratti, and R. Verdone. On-body area networks: from channel measurements to mac layer performance evaluation. In *Proceedings of European Wireless 2012 - 18th European Wireless Conference 2012*, Poznan, Poland, April 2012.

Bibliography

- [21] Vojislav Misić Saeed Rashwand, Jelena Misić. Mac performance modeling of ieee 802.15.6 -based wban over rician-faded channels. pages 1–6, University of Manitoba, 2012. IEEE.
- [22] Jelena Misić Saeed Rashwand. Performance evaluation of ieee 802.15.6 under non-saturation condition. pages 1–6, 2011.
- [23] W.G. Scanlon N.F. Timmons. Improving the ultra-low-power performance of ieee 802.15.6 by adaptive synchronisation. *IET Wirel. Sens. Syst*, 1:161–170, October 2011.
- [24] IEEE standard 802.15.4 2003: part 15.4: Wireless medium access control (MAC) and physical layer (PHY) specifications for low-rate wireless personal area networks (LR-WPANs).
- [25] IEEE Standard for Local and metropolitan area networks - Part 15.6: Wireless Body Area Networks. *IEEE Std 802.15.6-2012*, pages 1–271, February 2012.
- [26] CSEM - icycom platform. <http://www.csem.ch/docs/Show.aspx?id=12228>, 2010.
- [27] C. Arm, S. Gyger, J.-M. Masgonty, M. Morgan, J.-L. Nagel, C. Piguet, F. Rampogna, and P. Volet. Low-power 32-bit dual-mac 120 w/mhz 1.0 v icyflex1 dsp/mcu core. *Solid-State Circuits, IEEE Journal of*, 44(7):2055–2064, july 2009.
- [28] S. Alamouti. A simple transmit diversity technique for wireless communications. *Selected Areas in Communications, IEEE Journal on*, 16(8):1451–1458, Oct 1998.
- [29] Vahid Tarokh, N. Seshadri, and A.R. Calderbank. Space-time codes for high data rate wireless communication: performance criterion and code construction. *Information Theory, IEEE Transactions on*, 44(2):744–765, Mar 1998.

- [30] Xiangyi Li, Guixia Kang, Xidong Zhang, and Dongyan Huang. An energy-efficient cooperative MIMO strategy for Wireless Sensor Networks with intra-body channel. In *International Symposium on Communications and Information Technologies (ISCIT), 2012*, pages 679–684, 2012.
- [31] Yuehui Ouyang, D.J. Love, and W.J. Chappell. Body-Worn Distributed MIMO System. *IEEE Transactions on Vehicular Technology*, 58(4):1752–1765, 2009.
- [32] I. Khan, P.S. Hall, Y.I. Nechayev, and L. Akhoondzadeh-Asl. Multiple antenna systems for increasing on-body channel capacity and reducing BAN-to-BAN interference. In *International Workshop on Antenna Technology (iWAT), 2010*, pages 1–4, 2010.
- [33] Jie Ding, Eryk Dutkiewicz, and Xiaojing Huang. Performance evaluation of virtual MIMO for UWB based body area networks. In *7th International Symposium on Medical Information and Communication Technology (ISMICT), 2013*, pages 28–32, 2013.
- [34] Pengkai Zhao and B. Daneshrad. Net-eigen MAC: A new MIMO MAC solution for interference-oriented concurrent link communications. In *MILITARY COMMUNICATIONS CONFERENCE, 2011 - MILCOM 2011*, pages 248–253, Nov 2011.
- [35] Pengkai Zhao, You Lu, B. Daneshrad, and M. Gerla. Cooperative spatial scheduling in distributed MIMO MAC with interference/concurrency awareness. In *MILITARY COMMUNICATIONS CONFERENCE, 2012 - MILCOM 2012*, pages 1–6, Oct 2012.
- [36] P. Castiglione, S. Savazzi, M. Nicoli, and T. Zemen. Partner Selection in Indoor-to-Outdoor Cooperative Networks: An Experimental Study. *IEEE Journal on Selected Areas in Communications*, 31(8):1559–1571, August 2013.

Bibliography

- [37] A. Antonopoulos and C. Verikoukis. Network-Coding-Based Cooperative ARQ Medium Access Control Protocol for Wireless Sensor Networks. *International Journal of Distributed Sensor Networks*, 2012, 2012.
- [38] R.A.M. Khan and H. Karl. MAC Protocols for Cooperative Diversity in Wireless LANs and Wireless Sensor Networks. *IEEE Communications Surveys Tutorials*, 16(1):46–63, First 2014.
- [39] Xiayu Zheng, Yao Xie, Jian Li, and Petre Stoica. MIMO Transmit Beamforming Under Uniform Elemental Power Constraint. *IEEE Transactions on Signal Processing*, 55(11):5395–5406, 2007.
- [40] R. Rosini and R. D’Errico. Off-Body channel modelling at 2.45 GHz for two different antennas. In *6th European Conference on Antennas and Propagation (EUCAP), 2012*, pages 3378–3382, 2012.
- [41] K. Shashi Prabh and Jan-Hinrich Hauer. Opportunistic Packet Scheduling in Body Area Networks. In *Proceedings of the 8th European Conference on Wireless Sensor Networks, EWSN’11*, pages 114–129, Berlin, Heidelberg, 2011. Springer-Verlag.
- [42] K.S. Prabh, F. Royo, S. Tennina, and T. Olivares. BANMAC: An Opportunistic MAC Protocol for Reliable Communications in Body Area Networks. In *IEEE 8th International Conference on Distributed Computing in Sensor Systems (DCOSS), 2012*, pages 166–175, May 2012.
- [43] P.A. Dighe, R.K. Mallik, and S.S. Jamuar. Analysis of transmit-receive diversity in Rayleigh fading. *IEEE Transactions on Communications*, 51(4):694–703, April 2003.

- [44] Raj K. Jain. *The Art of Computer Systems Performance Analysis: Techniques for Experimental Design, Measurement, Simulation, and Modeling*. Wiley, 1 edition, April 1991.
- [45] Emre Telatar. Capacity of Multi-antenna Gaussian Channels. *European Transactions on Telecommunications*, 10(2):585-595, Autumn 1999.
- [46] M. Dohler, A. Gkelias, and H. Aghvami. A resource allocation strategy for distributed MIMO multi-hop communication systems. *IEEE Communications Letters*, 8(2):99-101, Feb 2004.
- [47] A. Del Coso, U. Spagnolini, and C. Ibars. Cooperative distributed mimo channels in wireless sensor networks. *Selected Areas in Communications, IEEE Journal on*, 25(2):402-414, 2007.
- [48] G. Barriac, R. Mudumbai, and U. Madhow. Distributed beamforming for information transfer in sensor networks. In *Third International Symposium on Information Processing in Sensor Networks*, pages 81-88, April 2004.
- [49] N.M. Tessema, X. Lian, and H. Nikoogar. Distributed beamforming with close to optimal number of nodes for green wireless sensor networks. In *Online Conference on Green Communications (GreenCom), 2012 IEEE*, pages 139-144, Sept 2012.
- [50] H. Abusaimh and Shuang-Hua Yang. Energy-aware optimization of the number of clusters and cluster-heads in wsn. In *Innovations in Information Technology (IIT), 2012 International Conference on*, pages 178-183, March 2012.
- [51] Kyungseop Shin, Woo-Chan Kim, Sung-Jin Park, and Dong-Ho Cho. Cooperative communication with joint optimization of cluster size and resource allocation in wireless sensor networks. In *MILITARY COMMUNICATIONS CONFERENCE, 2012 - MILCOM 2012*, pages 1-5, Oct 2012.

Bibliography

- [52] J. Agrakhed, G.S. Biradar, and V.D. Mytri. Cluster based energy efficient qos routing in multi-sink wireless multimedia sensor networks. In *Industrial Electronics and Applications (ICIEA), 2012 7th IEEE Conference on*, pages 731–736, July 2012.
- [53] A.D. Wyner. Shannon-theoretic approach to a Gaussian cellular multiple-access channel. *Information Theory, IEEE Transactions on*, 40(6):1713–1727, Nov 1994.
- [54] Wenyi Zhang. A General Framework for Transmission with Transceiver Distortion and Some Applications. *IEEE Transactions on Communications*, 60(2):384–399, Feb. 2012.
- [55] E. Bjornson, P. Zetterberg, M. Bengtsson, and B. Ottersten. Capacity Limits and Multiplexing Gains of MIMO Channels with Transceiver Impairments. *IEEE Communications Letters*, 17(1):91–94, Jan. 2013.
- [56] E. Björnson, J. Hoydis, M. Kountouris, and M. Debbah. Massive MIMO Systems With Non-Ideal Hardware: Energy Efficiency, Estimation, and Capacity Limits. *IEEE Transactions on Information Theory*, 60(11):7112 – 7139, Nov 2014.
- [57] H.V. Balan, R. Rogalin, A. Michaloliakos, K. Psounis, and G. Caire. AirSync: Enabling Distributed Multiuser MIMO With Full Spatial Multiplexing. *IEEE/ACM Transactions on Networking*, 21(6):1681–1695, Dec 2013.
- [58] E. Bjornson, L. Sanguinetti, J. Hoydis, and M. Debbah. Optimal Design of Energy-Efficient Multi-User MIMO Systems: Is Massive MIMO the Answer? *IEEE Transactions on Wireless Communications*, To appear, 2015.
- [59] Texas Instruments CC2530 - Second Generation System-on-Chip Solution for 2.4 GHz IEEE 802.15.4 / RF4CE / ZigBee . <http://www.ti.com/product/cc2530>.

- [60] IEEE Standard for Local and metropolitan area networks-Part 15.4: Low-Rate Wireless Personal Area Networks (LR-WPANs). <http://standards.ieee.org/getieee802/download/802.15.4-2011.pdf>, 2011.

Publications

Reported research resulted in publications at international conferences and journals. They are summarised below.

- Journals

- Stefan Mijovic, Andrea Stajkic, Riccardo Cavallari, and Chiara Buratti, *Low Power Listening in BAN: Experimental Characterisation*, International Journal of E-Health and Medical Communications (IJEHMC), 5:52–66, May 2015.
- Chiara Buratti, Andrea Stajkic, Gordana Gardasevic, Sebastiano Milardo, M. Danilo Abrignani, Stefan Mijovic, Giacomo Morabito, and Roberto Verdone, *Testing Protocols for the Internet of Things on the EuWin Platform*, IEEE Journal of Internet of Things, May 2015.

- Conferences:

- Alfonso Panunzio, Marco Pietro Caria, Stefan Mijovic, Riccardo Cavallari, and Chiara Buratti, *Experimental Characterisation of an IEEE 802.15.6-based Body Area Network*, 8th International Conference on Body Area

Publications

- Networks (BodyNets'13), Sep 2013;
- Stefan Mijovic, Andrea Stajkic, Riccardo Cavallari, and Chiara Buratti, *Experimental Characterization of Low Power Listening in BAN*, IEEE 15th International Conference on e-Health Networking, Applications and Services (Healthcom'13), Oct 2013;
 - Stefan Mijovic, Chiara Buratti, Alberto Zanella, and Roberto Verdone, *Co-operative Beamforming and Scheduling Strategies for Body Area Networks*, European Conference on Networks and Communications (EuCNC'14), June 2014;
 - Stefan Mijovic, Chiara Buratti, Alberto Zanella, and Roberto Verdone, *A Cooperative Beamforming Technique for Body Area Networks*, Fourth International Conference on Selected Topics in Mobile and Wireless Networking (MoWNet'14), Sep 2014.
 - Stefan Mijovic, Luca Sanguinetti, Chiara Buratti, and Merouane Debbah, *Optimal Design of Energy-Efficient Cooperative WSNs: How many sensors are needed?*, 16th IEEE International Workshop on Signal Processing Advances in Wireless Communications (SPAWC'15), Jun, 2015.
 - Gordana Gardasevic, Stefan Mijovic, Andrea Stajkic, and Chiara Buratti, *On the Performance of 6LoWPAN Through Experimentation*, International Wireless Communications and Mobile Computing Conference (IWCMC'15), Aug 2015.
 - Stefan Mijovic, Riccardo Cavallari, and Chiara Buratti, *Experimental Characterisation of Energy Consumption in Body Area Networks*, IEEE World Forum on Internet of Things (WF-IoT'15), Dec 2015.

- Stefan Mijovic, Luca Sanguinetti, Chiara Buratti, and Merouane Debbah, *On the Optimum Number of Cooperating Nodes in Interfered Cluster-Based Sensor Networks*, IEEE ICC 2016 Ad-Hoc and Sensor Networks Symposium (ICC'16 AHSN), May 2016.

Acknowledgements

I would like to thank my supervisors, Dott.Ing. Chiara Buratti and Prof. Roberto Verdone for all the lessons they taught me throughout the years. Acknowledgements are also due to Dott.Ing. Alberto Zanella for the valuable inputs to the presented research. Many thanks to Prof. Luca Sanguinetti and Prof. Mérouane Debbah of CentraleSupélec for making my period abroad fun and productive and Prof. Claude Oestges of UCL for helping me improve my thesis.

I would also like to thank all my colleagues from Radio Networks group. It was the greatest crew (ever :)) one could assemble to work and have fun with. Thank you Andrea for bearing with me.

Finally, I would like to thank my family, especially my parents, for the support and motivation they gave me.